UNIVERSITÀ DEGLI STUDI DI NAPOLI

FEDERICO II

PHD IN CHEMICAL SCIENCES

XXXVI Cycle (2020 - 2024)

Coordinator: Prof. Angelina Lombardi

Synthesis and characterization of new drugs inspired by natural products.

Rita Pagano

Tutor

Prof. Giovanni Di Fabio

Prof. Armando Zarrelli

Examiner

Prof. Emiliano Bedini

Index

Curcumin Mimics

Abbreviations

A549	Human Lung Carcinoma
AAPH	2,2′-Azobis(2-methylpropionamidine) dihydrochloride
AChE	Acetylcholinesterase
ACN	Acetonitrile
AcOH	Acetic acid
AD	Alzheimer's Disease
AKT	Protein kinase 3
ALP	alkaline phosphatase
API	Active Pharmaceutical Ingredient
APP	Amyloid Precursor Protein
Ar	Adenosine
ATP	Adenosine triphosphate
AUC	Area Under the kinetic Curve
Aβ	Amyloid β
BACE	β-secretase
BChE	Butyrylcholinesterase
Bcl-2	B-cell lymphoma 2
Bz	Benzoyl
CE	2-Cyanoethyl
ChT-L	Chymotrypsin-like
COX-2	Cyclooxygenase-2
CP	Core particle
DCA	Dichloroacetic acid

DCI	4,5-Dicyanoimidazole
DCM	Dichloromethane
DHS	2,3-dehydro-silybin
DHSA	2,3-dehydro-silybin A
DHSB	2,3-dehydro-silybin B
DIAD	Diisopropyl azodicarboxylate
DIC	N,N′-Diisopropylcarbodiimide
DIEA	N,N-Diisopropylethylamine
DMF	Dimethylformamide
DMSO	Dimethyl sulfoxide
DMT	4,4′-dimethoxytrityl
DNA	Deoxyribonucleic Acid
DPPH	2,2-diphenyl-1-picrylhydrazyl
EMT	Epithelial-to-mesenchymal transition
EtOAc	Ethyl acetate
FBS	fetal bovine serum
FDA	Food and Drug Administration
Fer-1	Ferroptosis inhibitors
GABA	Gamma-aminobutyric acid
GPX4	Glutathione peroxidase 4
GPX4	Glutathione peroxidase 4
HDFs	Human dermal fibroblasts
HeLa	Human Cervix Adenocarcinoma
HI	heat-inactivated

HPLC	High Performance Liquid Chromatography
HTS	High Throughput screening
*i*bu	isobutyryl
IC_{50}	half maximal inhibitory concentration
Im	Imidazole
KOAc	Potassium acetate
Lys	Lysine
MDA-MB-231	breast cancer cells
MeOH	Methanol
MS	Mass spectrometry
MSNT	1-mesitylenesulfonyl-3-nitro-1,2,4-triazole
NADPH	Nicotinamide adenine dinucleotide phosphate
NF-kB	Nuclear Factor kB
NFTs	Neurofibrillary tangles
NH_4OAc	Ammonium acetate
NMR	Nuclear Magnetic Resonance
NPs	Natural products
ORAC	Oxygen Radical Absorption Capacity
p53	Tumor protein 53
PANC	Human Pancreatic Cancer
PANC1	human pancreatic cancer cells
PBS	Phosphate Buffered Saline
PC-3	Prostate cancer cells
PCDs	Protein Conformational Diseases

PD	Parkinson Disease
PGPH	Peptidylglutamyl-peptide hydrolyzing
PI	propidium iodide
PI3Ks	Phosphoinositide 3-kinase
Py	Pyridine
Q-VD	Apoptosis inhibitors
RA	trans-retinoic acid
RNA	Ribonucleic acid
RNase 1	Human pancreatic ribonuclease
RNase A	Bovine pancreatic ribonuclease
RNS	Reactive nitrogen species
ROS	Reactive oxygen species
RP	Reverse Phase
RT	Room temperature
SA	Systemic amyloidosis
SAR	structure-activity relationships
SE	Standard error
SEM	Standard error of the mean
sGF	simulated Gastric Fluid
SH-SY5Y	Human Neuroblastoma Cell Line
sIF	simulated Intestinal Fluid
Sil	Silibinin
SilA	Silybin A
SilB	Silybin B

SW480	colorectal cancer cells
T2DM	Type II diabetes mellitus
TBDMS	*tert*-butyldimethylsilyl
*t*ButOOH	*tert*-butyl hydroperoxide
TE	Trolox equivalents
TEA	triethylamine
TFA	Trifluoroacetic acid
THF	Tetrahydrofuran
T-L	Trypsin-like
TLC	Thin layer chromatography
TPP	Triphenylphosphine
U87	Human Glioblastoma
Ub	Ubiquitin
UPS	Ubiquitin-Proteasome System
Ur	Uridine
UV	Ultra Violet

Abstract

Natural products (NPs) have always been a source of lead compounds that promote pharmacological advances to treat different health problems, mainly related to cancer, infectious diseases, inflammation, neurodegeneration and cardiovascular disorders.[1]

Among NPs, plant polyphenols are gaining increasing recognition thanks to their potent antioxidant properties, and their therapeutic advantages in the modulation of cell signaling, anti-inflammatory effects and neuroprotection.[2] Despite their widespread distribution and different benefits, the poor bioavailability of flavonoids may significantly impact their therapeutic effects. For these reasons, the research is active in identifying more common or easily synthetic flavonoids with enhanced absorption, better therapeutic efficacy and fewer side effects.[3]

During my PhD I focused my attention on two natural products, silibinin and curcumin, both of plant origin which simultaneously suffer from very low solubility in water and poor bioavailability.

Silibinin is the main component of the silymarin extracted from milk thistle seeds and consists of an approximately equimolar mixture of two diastereoisomers: silybin A (Sil A) and silybin B (Sil B) (Figure 1).[4] Silibinin, known above all for its hepatoprotective activity, has a wide range of biological and pharmacological activities, but it's limited by its low solubility in water and bioavailability.[5] In many cases the optical pure aspect of this two diastereoisomers has been largely neglected, but some studies have demonstrated that stereochemistry matters when describing their biological effects.[6] A recent study, indeed, investigated the silybins ability to inhibit Aβ amyloid growth and toxicity, and demonstrated that only Sil B was able to significantly inhibit Aβ aggregation in aqueous solutions and counteract Aβ proteotoxicity in worms (*Caenorhabditis elegans*) expressing human Aβ.[7] Conversely, in the case of human 20S proteasome (h20S) Sil A demonstrated a higher affinity and more efficient activation than Sil B.[8]

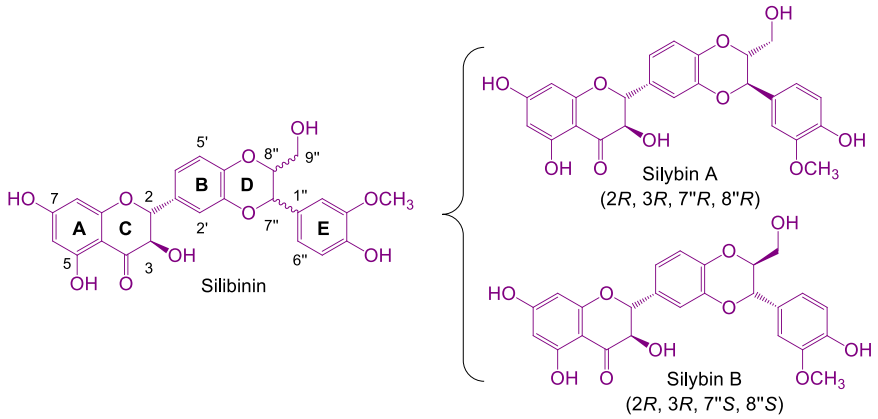

Figure 1 Silibinin and its diastereoisomers, Silybin A and Silybin B

Curcumin is the bioactive compound of *Curcuma longa* (Figure 2).[9] Its pharmacological action has been mainly attributed to its antioxidant and anticancer activities, ability to chelate bio-metals and to inhibit the aggregation of the Aβ peptide.[10] Despite such potential, curcumin suffer of low bioavailability and poor chemical stability that limit its pharmacological applications.[11] Several strategies were developed to overcome these disadvantages, such as nanoparticle and formulations in liposomal complex.[12] One of the most common strategies is the design and synthesis of new curcumin mimics with better therapeutic properties and bioavailability.[13]

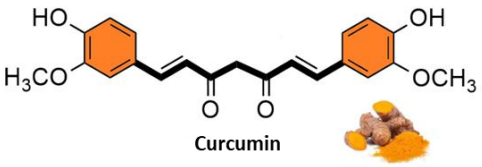

Figure 2 Curcumin: bioactive compound of Curcuma longa

In this frame, during my PhD I was involved in the synthesis, characterization and evaluation of different biological activities of new silybin derivatives and curcumin mimics.

Silybin derivatives

To increase water solubility of silybins, new prodrugs were designed (Figure 3).[14] A mini-library of 9″-silybins conjugated with 3′-ribonucleotide units through phosphodiester junctions was synthesized with an efficient regioselective solid-phase synthetic approach.

The new prodrugs showed greater solubility in water (3.7 mM and 6 mM for uridine and adenosine conjugates, respectively) compared to silybins (1 μM)[5].

Investigations performed to validate the effective timed-release of new prodrugs have revealed that uridine-silybin derivatives were quickly cleaved by RNase A, releasing the active silybin drugs even at low RNase concentrations. MTT assays confirmed the lack of toxicity of the new compounds on neuronal cancer cells.

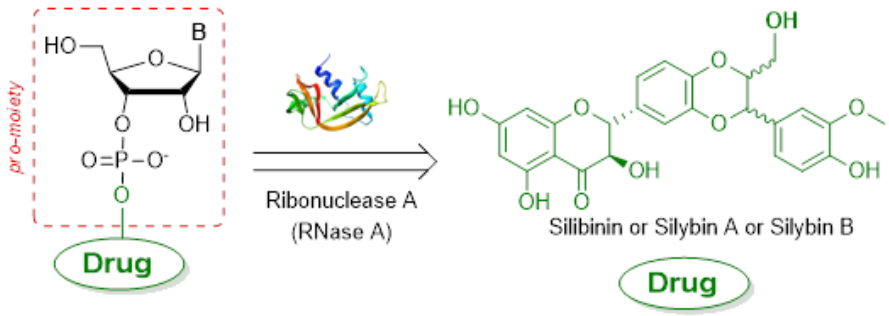

Figure 3 Silybins prodrugs

A recent study reported the synthesis and antioxidant activity of *bi*-flavonoids based on silibinin.[15] The new dimers, linked through a phosphodiester bond in position 3-3, 3-9" and 9"-9", have displayed high ability to scavenge ROS, comparable to the value reported for known potent antioxidants such as quercetin.

In this regard, during my PhD I investigate the structure–activity relationships of dimer 9"-9", which turned out to be the best one (Figure 4).[16] Starting from diastereoisomerically pure silybin monomers (Sil A and Sil B), employing orthogonal protection of various hydroxyl groups and the phosphoramidite chemistry, novel 9"-

9" dimers of silybin A and silybin B (**7aa**, **7ab**, and **7bb**) were successfully synthesized.

They showed a higher ability to scavenge reactive oxygen species (ROS), specifically the hydroxyl radical (HO•), comparable to quercetin. Investigations on the anticancer activity of new dimers, reveal that both monomers and dimers display selective anti-proliferative activity against leukemia cells at the concentrations employed, and low activity on normal cells. However, the cytotoxic mechanisms is not apoptosis for everyone, underlighting the pivotal role of stereochemistry.

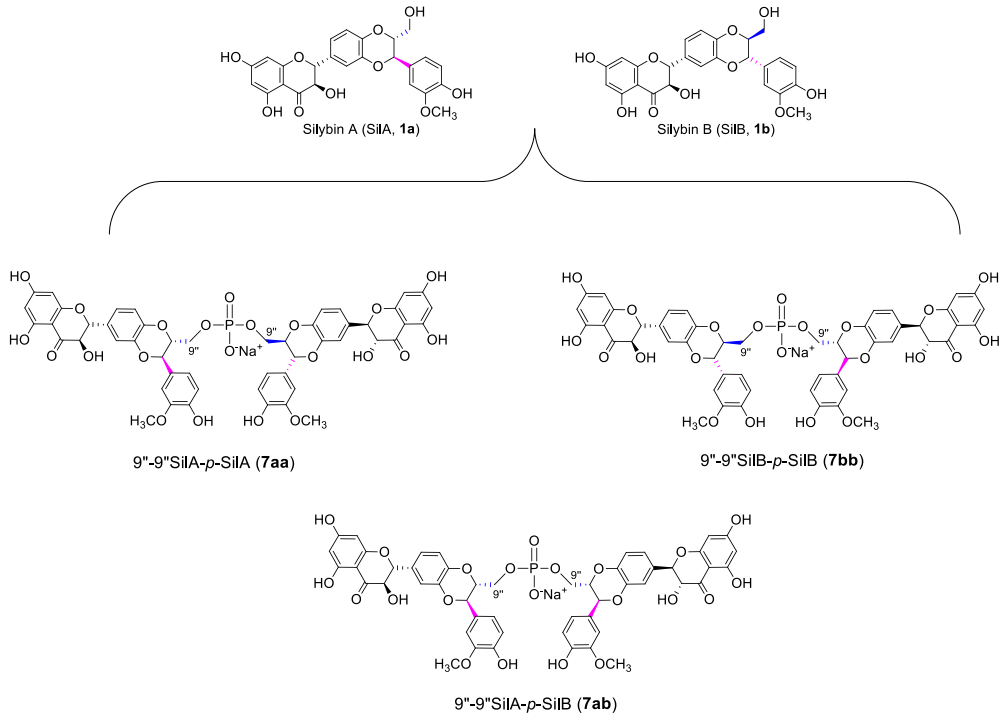

Figure 4 New silybins dimers

Considering the inhibitory effects on various cancer cells of silibinin and its oxidation product 2,3-dehydrosilybin (DHS), [17,18] chemical modification studies could enhance their bioavailability and antiproliferative activity against prostate cancer cell lines.[19] For this reason, it was developed a regioselective synthesis of new 7-*O*-alkyl

derivatives aims to combine the pharmacological properties of silybins and DHS with tyrosol-based metabolites, potentially yielding compounds with improved antioxidant and anticancer activities (Figure 5). While in the ORAC assay there was no significant variation in antioxidant activity, in the DPPH assays, the new derivatives exhibited pronounced activity due to the role of tyrosolic counterpart.

From the study on PC-3 prostate cancer cells emerged that the compounds **DHS-HTYR, DHSA-HTYR** and **DHSB-HTYR** inhibit cell proliferation and induce cell death in PC-3 cells.

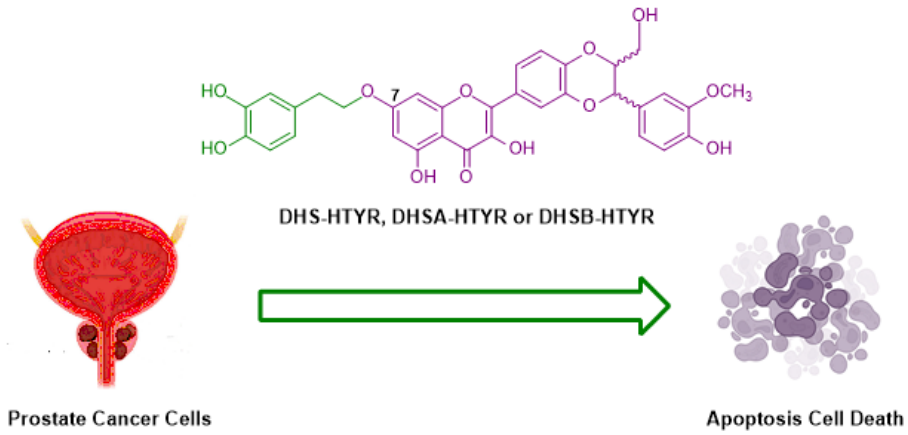

Figure 5 New 7-*O*-alkyl derivatives: inhibitors of prostate cancer.

Curcumin mimics

With the aim of synthesizing curcumin mimics with broad molecular diversity, it has been carried out a rapid solid-phase synthetic strategy to obtain tyrosol-based phosphodiester mimics which retain the two aromatic rings with distinct hydroxyl substituents and a distance between them comparable to that of curcumin (Figure 6).[20] The phosphodiester linker was chosen with the aim of increasing the water solubility and the stability of the new mimics.

From the study emerged that all new mimics exhibited high stability in simulated intestinal fluid, simulated gastric fluid, alkaline phosphatase, and serum buffers. The phosphodiester dimers potent growth inhibition and cell death efficacy in PC-3 prostate cancer cells for the compound tyrosol with a homovanillil substitution, demonstrating a substantial effectiveness in cell growth inhibition and in inducing significant cell death.

Figure 6 Phosphodiester curcumin mimics

To expand this first library, new tyrosol-based ethyl phosphonates curcumin mimics were synthesized (Figure 7). The new mimics retain the phenolic moieties based on tyrosol, homovanillil and hydroxytyrosol alcohols, in addition to the 5-methoxy tryptophol. The linker was replaced with an uncharged ethyl phosphonate with a length of seven atoms. The mimics **EP2** and **EP4** resulted the most interesting. **EP2** displayed strong antioxidant activity and potent inhibitory effect on ferroptosis, representing a potential candidate for neurodegenerative disorders. Conversely, **EP4** is a very potent anticancer agent against different human cancer cell lines (HeLa,

A375, WM266, MDA-MB-231) and no cytotoxic on normal cell (HDF). Mechanistic investigation suggested that **EP4**-induced cell death occurs primarily by apoptosis.

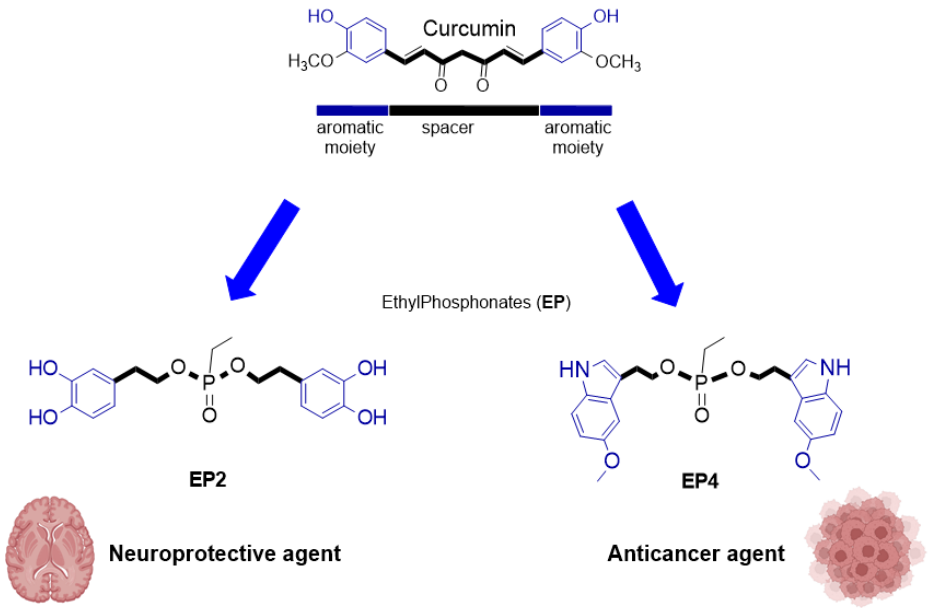

Figure 7 New curcumin mimics: **EP2** potential neuroprotective candidate, **EP4** anticancer agent

Bibliography

1. Coy-Barrera, E., Ogungbe, I. V. & Schmidt, T. J. Natural Products for Drug Discovery in the 21st Century: Innovations for Novel Therapeutics. *Molecules* **28**, 3690 (2023).
2. Wang, T., Li, Q. & Bi, K. Bioactive flavonoids in medicinal plants: Structure, activity and biological fate. *Asian J. Pharm. Sci.* **13**, 12–23 (2018).
3. Molino, S. *et al.* Polyphenols in dementia: From molecular basis to clinical trials. *Life Sci.* **161**, 69–77 (2016).
4. Bijak, M. Silybin, a Major Bioactive Component of Milk Thistle (Silybum

marianum L. Gaernt.)—Chemistry, Bioavailability, and Metabolism. *Molecules* **22**, 1942 (2017).

5. Romanucci, V. *et al.* Phosphate-Linked Silibinin Dimers (PLSd): New Promising Modified Metabolites. *Molecules* **22**, 1323 (2017).

6. Křen, V. Chirality Matters: Biological Activity of Optically Pure Silybin and Its Congeners. *Int. J. Mol. Sci.* **22**, 7885 (2021).

7. Sciacca, M. F. M. *et al.* Inhibition of Aβ Amyloid Growth and Toxicity by Silybins: The Crucial Role of Stereochemistry. *ACS Chem. Neurosci.* **8**, 1767–1778 (2017).

8. Persico, M. *et al.* Silybins are stereospecific regulators of the 20S proteasome. *Bioorg. Med. Chem.* **66**, 116813 (2022).

9. Nelson, K. M. *et al.* The Essential Medicinal Chemistry of Curcumin. *J. Med. Chem.* **60**, 1620–1637 (2017).

10. Noureddin, S. A., El-Shishtawy, R. M. & Al-Footy, K. O. Curcumin analogues and their hybrid molecules as multifunctional drugs. *Eur. J. Med. Chem.* **182**, 111631 (2019).

11. Anand, P., Kunnumakkara, A. B., Newman, R. A. & Aggarwal, B. B. Bioavailability of curcumin: Problems and promises. *Mol. Pharm.* **4**, 807–818 (2007).

12. Moreira, J., Saraiva, L., Pinto, M. M. & Cidade, H. Diarylpentanoids with antitumor activity: A critical review of structure-activity relationship studies. *Eur. J. Med. Chem.* **192**, 112177 (2020).

13. Reinke, A. A. & Gestwicki, J. E. Structure–activity Relationships of Amyloid Beta-aggregation Inhibitors Based on Curcumin: Influence of Linker Length and Flexibility. *Chem. Biol. Drug Des.* **70**, 206–215 (2007).

14. Romanucci, V. *et al.* Investigation on the solid-phase synthesis of silybin prodrugs and their timed-release. *Bioorg. Med. Chem.* **50**, 116478 (2021).

15. Romanucci, V., Di Fabio, G. & Zarrelli, A. A New Class of Synthetic Flavonolignan-Like Dimers: Still Few Molecules, but with Attractive Properties.

Molecules **24**, 108 (2018).

16. Romanucci, V. *et al.* Phosphodiester Silybin Dimers Powerful Radical Scavengers: A Antiproliferative Activity on Different Cancer Cell Lines. *Molecules* **27**, 1702 (2022).
17. Gažák, R. *et al.* Oxidised derivatives of silybin and their antiradical and antioxidant activity. *Bioorg. Med. Chem.* **12**, 5677–5687 (2004).
18. Agarwal, C. *et al.* Anti-Cancer Efficacy of Silybin Derivatives - A Structure-Activity Relationship. *PLoS One* **8**, e60074 (2013).
19. Polachi, N. *et al.* Modulatory effects of silibinin in various cell signaling pathways against liver disorders and cancer – A comprehensive review. *Eur. J. Med. Chem.* **123**, 577–595 (2016).
20. Romanucci, V. *et al.* Solid-phase synthesis of curcumin mimics and their anticancer activity against human pancreatic, prostate, and colorectal cancer cell lines. *Bioorg. Med. Chem.* **42**, 116249 (2021).

Results discussed in the coming chapters have been published in the papers listed below:

1. Romanucci, V.; Giordano, M.; Pagano, R.; Agarwal, C.; Agarwal, R.; Zarrelli, A; Di Fabio, G. Solid-phase synthesis of curcumin mimics and their anticancer activity against human pancreatic, prostate, and colorectal cancer cell lines. *Bioorganic & Medicinal Chemistry* **2021**, *42* (March), 116249. https://doi.org/10.1016/j.bmc.2021.116249.

2. Romanucci, V.; Giordano, M.; Pagano, R.; Zimbone, S.; Giuffrida, M.L.; Milardi, D.; Zarrelli, A; Di Fabio, G. Investigation on the solid-phase synthesis of silybin prodrugs and their timed-release. *Bioorganic & Medicinal Chemistry* **2021**, *50* (October), 116478. https://doi.org/10.1016/j.bmc.2021.116478.

3. Romanucci, V.; Pagano, R.; Lembo, A.; Capasso, D.; Di Gaetano, S.; Zarrelli, A; Di Fabio, G. Phosphodiester Silybin Dimers Powerful Radical Scavengers: A Antiproliferative Activity on Different Cancer Cell Lines. *Molecules* **2022**, *27* (5), 1702. https://doi.org/10.3390/molecules27051702.

Natural Products in Drug Discovery

1 Introduction

Natural products (NPs) represent a large family of different chemical entities originated from bacterial, fungal, plant, and marine animal sources, with a wide variety of biological activities that have found multiple uses, notably in human and veterinary medicine and in agriculture.[1]

The first written documents on the use of NPs in medicinal applications date back to 2600 BC and report the existence of a sophisticated medicinal system in Mesopotamia, including about 1000 plant-derived medicines.[2] The knowledge of the medicinal application of plants in the Western world is mainly based on the Greek and Roman culture. In particular, there are the compendia written by the Greek physician Dioscorides (1st century AD), and by the Romans Pliny the Elder (1st century AD) and Galen (2nd century AD). During all that time, medicinal plants were only applied on an empirical basis, without mechanistic knowledge of their pharmacological activities or active constituents. Rational drug discovery from plants started at the beginning of the 19th century, when the German apothecary assistant Friedrich Sertürner succeeded in isolating the analgesic and sleep-inducing agent from opium which he named morphium (morphine) in honor of the Greek god of dreams, Morpheus. He published a comprehensive paper on its isolation, crystallization, crystal structure, and pharmacological properties, which he studied first in stray dogs and then in self-experiments. This triggered the examination of other medicinal herbs, and during the following decades of the 19th century, many bioactive natural products, primarily alkaloids (e.g., quinine, caffeine, nicotine, codeine, atropine, colchicine,

cocaine, capsaicin) could be isolated from their natural sources.[3,4] Subsequently, efforts were undertaken to produce natural products by chemical synthesis in order to facilitate production at higher quality and lower costs. Salicylic acid was the first natural compound produced by chemical synthesis in 1853. After the discovery of penicillin (1928), an era of drug discovery from microbial sources was initiated in the 1930s, that laid the scientific and financial foundation of the modern pharmaceutical industry after World War II. At that time, the therapeutic use of extracts and partly purified natural products was increasingly replaced by the use of pure compounds.[5] Despite the advent of combinatorial chemistry and HTS campaigns during the last decades, the impact of NPs for drug discovery is still very high.[6]

Of the 1394 new chemical entities belonging to the group of small molecules that had been approved between 1981 and 2019, only 33.3% were purely synthetic, while more than half were derived or inspired by nature.[6] NPs hold out the best options for finding novel agents/active templates, which when worked on in conjunction with synthetic chemists and biologists, offer the potential to discover novel structures that can lead to effective agents in a variety of human diseases for which no effective treatment exists or available yet. Due to their vast natural chemodiversity and structural complexity, research into NPs has uncovered bioactive agents, hits, and lead compounds which promote pharmacological advances to treat different health problems, mainly related to cancer, infectious diseases, inflammation, pain, and metabolic and cardiovascular disorders.[7] In recent decades, NP-inspired drug discovery has experienced a leap in progress due to several innovations overcoming crucial barriers and limitations to developing NP-derived drugs. In addition, the innovations are also oriented toward expanding NP chemical space by identifying more NPs and derivatives, designing and optimizing bioactive NP-based libraries to find novel therapeutic agents with low toxicity and improved physicochemical, pharmacokinetic, and pharmacodynamics properties.[8]

1.1 Polyphenols

One of the most studied class of NPs derived from plants are polyphenols.[9] They vary from simple, low molecular weight molecules to large complex tannins and derived.

According to a common classification, the polyphenols are divided into several sub-classes, based on the number of phenolic rings present in their structure, the structural elements that bind these rings between them and to the substituents bound on the rings. On this basis, they can be identified two major groups: flavonoids and non-flavonoids polyphenols (Figure 1.1).[10]

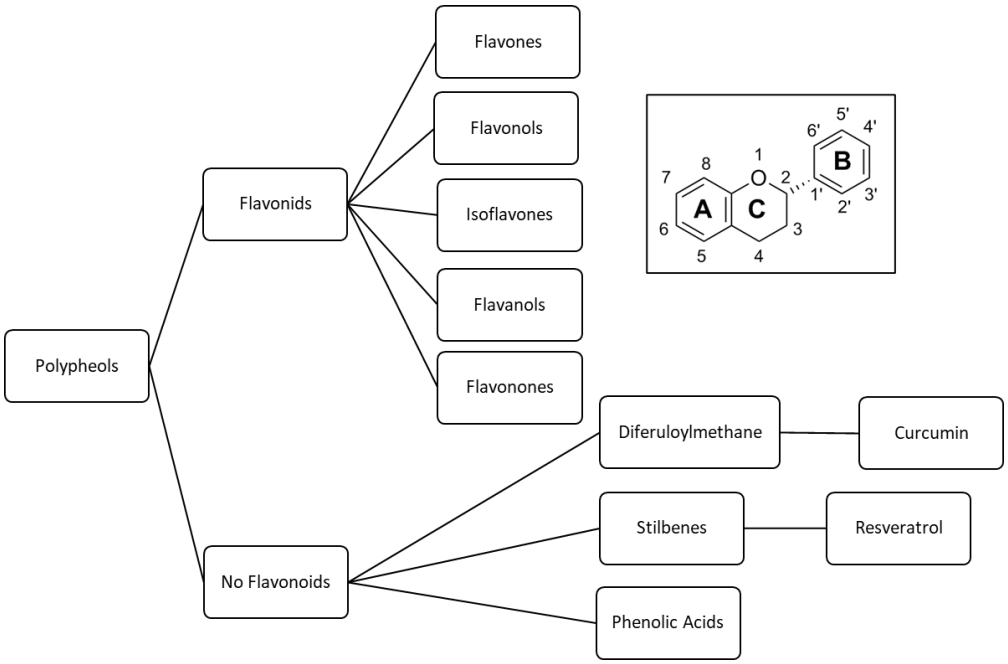

Figure 1.1 Subclasses of polyphenols.

The flavonoids, share a structure formed by two aromatic rings, indicated as A and B, linked together by three carbon atoms that form oxygenated heterocycle, the ring

C (Figure 1.1). They can be further divided into several subclasses, depending on the type of involved heterocycle: flavones, flavonols, isoflavones, flavanols, and flavonones. Among the non-flavonoid polyphenols are identified: diferuloylmethane, stilbenes, and phenolic acids..

Nowadays, plant polyphenols enjoy an ever-increasing recognition not only by the scientific community but also, and most remarkably, by the general public because of their presence and abundance in fruits, seeds, vegetables, and derived foodstuffs and beverages, whose regular consumption has been claimed to be beneficial for human health.[9,11] It has been demonstrated that polyphenolic compounds exert a strong antioxidant activity, and therapeutic benefits also derive from their modulatory role in cell signaling and anti-inflammatory activity. In addition, it is thought that polyphenols may be important in the prevention of multiple diseases, i.e. cardiovascular and neurodegenerative diseases, atherosclerosis, type II diabetes, and cancer.[12,13] Although wide distribution and broad benefits, bioavailability of flavonoids is poor which may significantly influence the impact of nutritional effects. Pharmacokinetic profile of flavonoids with certain functional groups remains systematically elusive, which is important for screening out more common/easily synthetic flavonoids with better absorption and higher nutritional/ therapeutic or less side effects.[10]

1.2 Natural Products in Cancer Therapy

A cancerous tumor refers to a colony of cells proliferating more frequently than normal tissue, with invasive and metastatic properties.[14] According to the newest information, although the mortality caused by cancer has decreased over the past decade in both males and females, it is still the second most common cause of mortality in the United States following cardiovascular disease.[15] Generally, the cause of cancer development is a genetic defect in one or more proteins that regulate the cell

cycle. In some cases, the defective gene is inherited, in some other cases mutations occur in response to environmental carcinogens. Generally, both hereditary and environmental factors coexist, and for the development of cancer an accumulation of mutations is required.[16] When affected by environmental factors such as oxidative stress or UV radiation, the DNA of the cell is damaged and repair mechanisms are activated. If they are not able to adequately repair the damage, cell death signals are activated.[17] However, if these mechanisms are disrupted, the mutated cells can proliferate and, even over time and with accumulation of mutations, form a cancerous tumor (Figure 1.2).

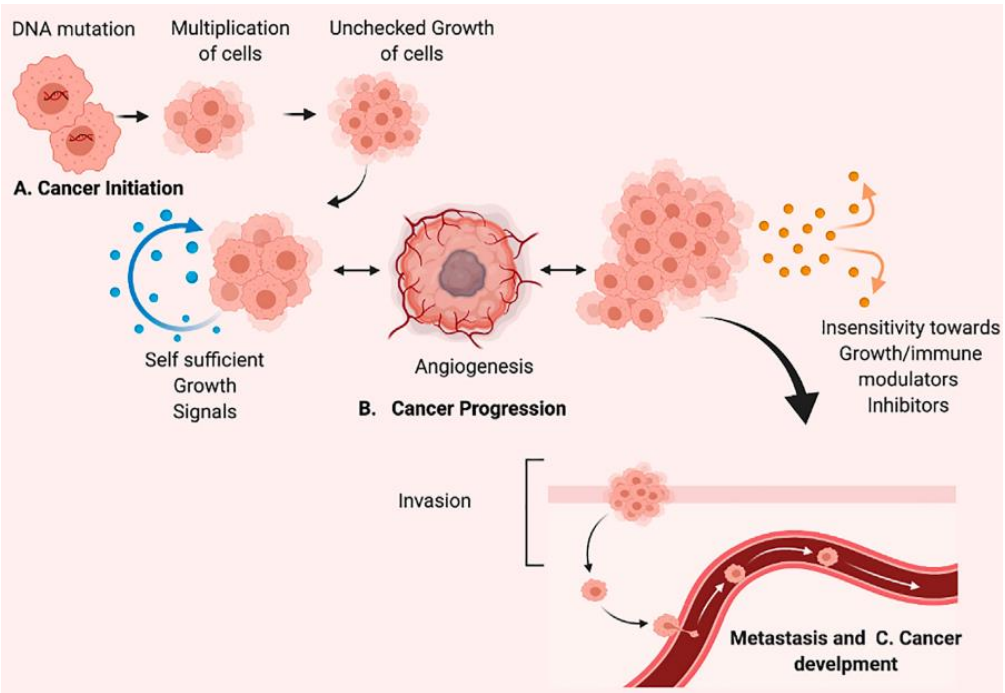

Figure 1.2 Process of cancer development/carcinogenesis, (A) Cancer initiation (B). Cancer Progression (C). Metastasis and Cancer development.

Resistance to the effects of cell death signals and immortality is one of the major characteristics of cancerous cells. There are four main categories of programmed cell death: apoptosis, autophagic cell death, necrosis, and ferroptosis; they may jointly determine the fate of the cancer cell.[18] Apoptosis has a particular importance, and studies on cancer treatment have focused on ways to induce apoptosis in cancer cells. In terms of function, the genes involved in the development and progression of cancer can be categorized into oncogenes and tumor suppressor genes. Oncogenes encode proteins that stimulate tumorigenesis. On the other hand, tumor suppressor genes inhibit the development of tumors. p53 is among the most important tumor suppressor genes involved in controlling the cell cycle and induction of apoptosis.[19] Ferroptosis is an iron-dependent, novel cell death mode, which is significantly different from apoptosis, cell necrosis, and autophagy.[20] The main mechanism is that, under the action of ferrous iron or lipoxygenase, iron catalyzes liposomal peroxidation of highly expressed unsaturated fatty acids on cell membranes, thereby inducing cell death. Numerous studies have shown that ferroptosis is also related to a reduction in the expression of glutathione and glutathione peroxidase 4 (GPX4) in the antioxidant system of cells.[21,22] Lipid peroxides cannot be metabolized by the reduction reaction catalyzed by GPX4, and lipids are oxidized by ferrous iron in Fenton reaction to generate a large amount of reactive oxygen species (ROS) that promote ferroptosis.[23] Ferroptosis is considered a key mechanism in the development of various diseases such as atherosclerosis, Alzheimer, diabetes, cancer, and renal failure. The redox status of cells, such as the balance between intracellular oxidants (lipid peroxides, reactive oxygen species, free iron ions) and antioxidants (glutathione, GPX4), plays a major role in ferroptosis regulation and constitutes its principal biomarkers.[24]

Various signaling pathways are involved in tumorigenesis, one of these is oxidative stress. Oxidative stress refers to conditions when the balance between the production of oxidizing species and the ability of antioxidant system for clearing them is

impaired. Oxidizing species are compounds that are highly reactive. These compounds are produced both in normal and pathological conditions in cells, the main source of production is the respiratory chain of the mitochondria. NADPH oxidases are other source of oxidizing species production.[25] These compounds are involved in the pathogenesis of many diseases including cancer, diabetes, cardiovascular disease, inflammatory bowel disease, etc. Furthermore, some therapeutic approaches have focused on neutralizing these harmful compounds by antioxidants.[26] Usage of some antioxidant compounds has been proposed as a therapeutic approach for the treatment of some types of cancer.[27] In addition, some antioxidant compounds appear to have beneficial effects in preventing cancer and reducing cancer mortality.[28]

Nowadays, the most effective treatment for cancer is chemotherapy. Chemotherapeutic drugs kill rapidly proliferating cancer cells, but these drugs also damage normal cells and result in a high incidence of complications.[29] Despite significant advancements, the survival rates remain unsatisfactory mainly because of drug resistance, which impedes the progress of patient prognosis. Therefore, in the last years, phytochemicals were considered suitable candidates for anti-cancer drug development, due to their multiple actions on several targets with different mechanisms of action.[30] Several NPs derived from plant, such as alkaloids, flavonoids, lignans, saponins, terpenes and other primary and secondary metabolites, play significant roles in either inhibiting cancer cell activating proteins, enzymes and signaling pathways (Figure 1.3). For instance, terpenoids exert their anti-cancer activity by activating proapoptotic members Bax and Bak, activating p53 and causing a down-regulation of signaling transduction of antiapoptotic protein Bcl-2. By far, different mechanisms have highlighted the role of flavonoids in cancer-therapy, including induction of apoptosis, proteasome inhibition, nuclear factor signaling inhibition, differentiation induction, cell cycle arrest induction, receptor interaction, or interaction with carcinogenic associated enzymes.[11] Notably, many reports have

provided evidences about influences of hydroxylation on tumor modulation. Specific hydroxylated flavonoids possess stronger inhibitory activity on cancer cells than permethoxylated counterparts. Ring B substitution such as a catechol moiety with vital influences has been proposed, and additional hydroxyl group substitution in ring B does not alter the activity. In the case of ring C, 3-hydroxylation has been considered as a highly decisive moiety for improving biological effects.

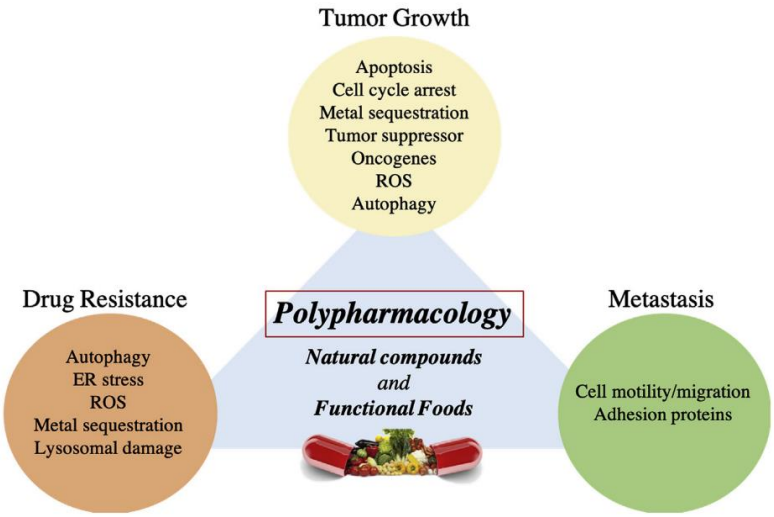

Figure 1.3 Natural products and their anticancer activities.

For example, flavonoids like quercetin, kaempferol, luteolin, epi-catechin, catechin, cyanidin exert their anti-cancer activity on several cancer cell lines with different mechanisms of actions: decreasing phosphorylation of epidermal growth factor receptor; increasing DNA fragmentation; counteracting angiogenesis in cancer cells; inhibiting enzymes such as xanthine oxidase, COX-2, lipo-oxygenases, and ornithine decarboxylase; inhibiting signal transduction enzymes such protein kinase C, PI3K, AKT.

1.3 Natural Products in Neurodegenerative Diseases

In the last two decades, a large number of evidences points to the misfolding, aggregation and accumulation of structurally abnormal proteins, termed amyloids, as a common pathogenic mechanism of several diseases known as Protein Conformational Diseases (PCDs) and including Alzheimer's Disease (AD), Parkinson Disease (PD), type II diabetes mellitus (T2DM) and systemic amyloidosis (SA).[31]

Alzheimer's disease is one of the most common neurodegenerative disorders and accounts for more than 80% of dementia cases worldwide in elderly people. It leads to the progressive loss of mental, behavioral, functional decline and ability to learn.[32] Pharmacologic treatments employ medication to slow or stop an illness or treat its symptoms. Five drugs have been approved by the U.S. Food and Drug Administration (FDA) that temporarily improve symptoms of Alzheimer's disease by increasing the amount of chemicals called neurotransmitters in the brain (Figure 1.4).[33]

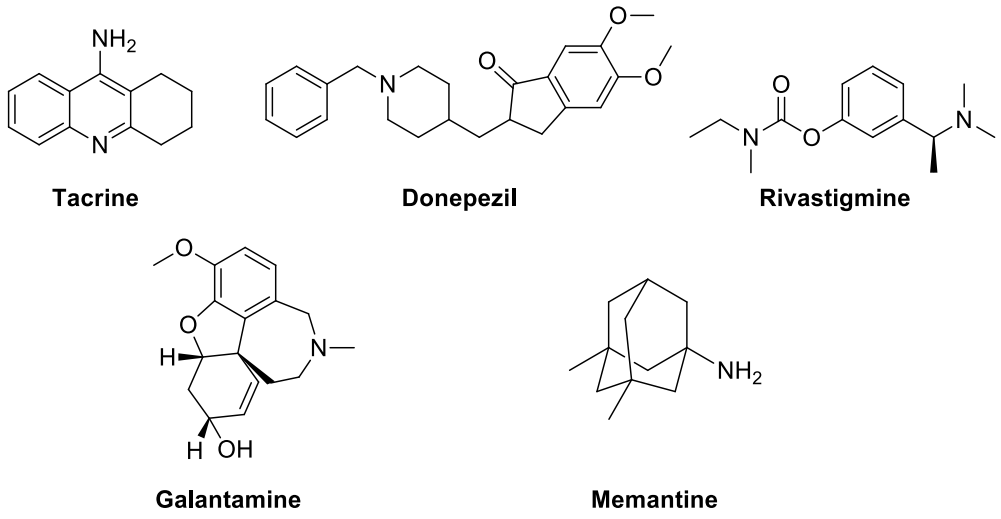

Figure 1.4 Drugs approved by FDA for the treatment of AD.

The effectiveness of these drugs varies from person to person. However, none of the treatments available today for Alzheimer's disease slows or stops the damage to neurons that causes Alzheimer's symptoms and eventually makes the disease fatal.[34] Accumulation of misfolded protein deposits as amyloid β (Aβ) plaques and tau-dependent neurofibrillary tangles represents the hallmarks of AD, but recent results have demonstrated that drugs designed to inhibit protein aggregation are mostly ineffective; therefore, the development of successful AD therapies needs a more comprehensive understanding of the biochemical pathways supervising excess protein clearance.

Aβ peptide is originated by the cleavage of a transmembrane protein called amyloid precursor protein (APP) by β- and γ-secretases. Different isoforms can be found, from 36 to 43 amino acids, but $A\beta_{1-40}$ and $A\beta_{1-42}$ are the most common isoforms; the first of them is the most abundant while the second is the most fibrillogenic. These insoluble aggregates were initially considered as the real cause of those disorders but, in the last years, the scientific community agrees that the real neurotoxic species are not amyloid aggregates but, rather, small-sized oligomeric species.[35] In the early steps of aggregation, amyloidogenic peptides form clusters that retain the structure of the monomeric state. These clusters are unstable, and an internal reorganization undergoes to form stable species having a β-sheet rich structure. The oligomers can aggregate by self-association to form well structurally defined fibrils with cross-β structure, the mature fibrils, that are inert species. Amyloid oligomers are thought to be toxic to the cell because they can interact and damage cell membranes causing disturbances in the homeostasis of small molecules and ions. Furthermore, the surface of the lipidic bilayer can act as nucleation site catalyzing amyloid growth.[36] Aβ is a cationic peptide and interacts through electrostatic interactions with the anionic head-groups of the lipidic bilayer, enhancing the local protein concentration in the membrane surface and fostering protein aggregation. The most important

mechanisms of membrane disruption are the pore formation, where amyloids are inserted into the membrane forming ion-channel structures, and the detergent-like mechanisms where amyloid fibrils interact with the lipid bilayer surface *via* non-specific bindings, induces membrane thinning and disruption (Figure 1.5). Both mechanisms are possible to occur *in vivo* and are not mutually exclusive.

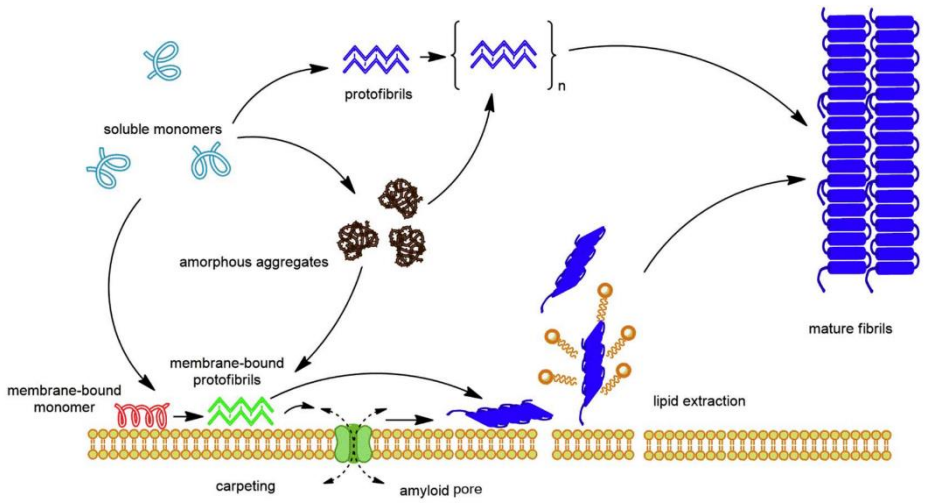

Figure 1.5 Amyloid formation and membrane disruption process.

Furthermore, amyloid aggregates can impair and ultimately block the protein degradation machinery, resulting in the collapse of protein quality control, compromising cellular function and survival. It is reported that aggregated β-sheet-rich proteins inhibit the ubiquitin-proteasome system (UPS) by jamming the entry site of the catalytic core.

The UPS is the main cytosolic proteolytic pathway responsible for the hydrolysis of misfolded or damaged proteins (Figure 1.6).[37] The UPS is ignited by a sequential process controlled by three enzymes, E1, E2 and E3 which couple ubiquitin (Ub) polymers to a protein substrate. In the first step, an ATP-dependent E1 ubiquitin-activating enzyme forms a high-energy thioester bond with Ub. Next, activated Ub is

moved to the E2 ubiquitin-conjugating enzymes which promote the growth of Lys-linked poly-ubiquitin chains that are, eventually, conjugated to the substrate by an E3-ligase. The endpoint of the UPS is the proteasome, a 2.5 MDa multimeric assembly that degrades the Ub-tagged proteins. The proteasome is composed by a catalytic unit termed core particle (CP) or 20S, coupled with one (26S) or two (30S) 19S regulatory particles (RPs).[38] The 20S unit has a barrel-like shape, made of 28 subunits arranged in four heptameric rings, stacked in an α-β-β-α form. The two inner β-rings include six proteolytic sites endowed with peptidylglutamyl-peptide hydrolyzing (PGPH), trypsin-like (T-L), and chymotrypsin-like (ChT-L) activities and located in the β1, β2, and β5 subunits, respectively.

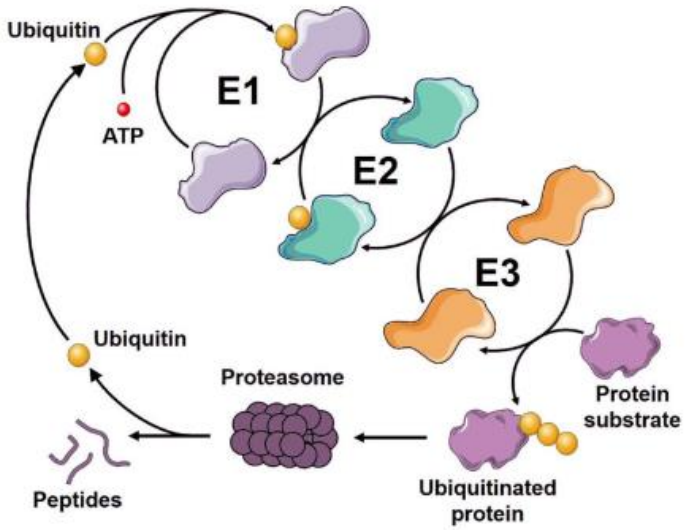

Figure 1.6 Ubiquitin-proteasome system: mechanism of action.

Another important target of neurodegeneration is oxidative stress.[39] Experimental evidence indicates that a dysregulation of the redox state strongly participates in an early stage of AD, inducing and activating multiple cell signaling pathways that contribute to the initial progression of the neurodegenerative process. Indeed, constant

evidence of reactive oxygen species (ROS) and reactive nitrogen species (RNS) mediated injury is observed in AD brain. Oxidative stress can influence Aβ formation by increasing APP levels or, indirectly, Aβ processing by modulating the activity and levels of key enzymes such as β-secretase (BACE) and γ-secretase. Aβ itself has oxidant ability by inducing more oxidative stress, sustained inflammatory responses, which ultimately will translate into irreversible cell damage, slow degeneration and eventual cell death.[40]

In the last decade, many investigations have focused on small natural molecules, rich in aromatic groups for the treatment of AD. The attractiveness of these compounds resides in the fact that they are normal biological molecules found in food or herbal extracts, and thus usually exhibit high availability, stability, low side effects, and convenience. Historically bioactivity of flavonoids against neurodegeneration is attributed to classical antioxidant effects, however, emerging evidences now have been attaching importance to interactions on acetylcholinesterase (AChE)/ butyrylcholinesterase (BChE), GABA-receptor, mitochondrial dysfunction, or through chelation of transition metal ions.[10] Furthermore, recent studies indicate that natural phenolic compounds, especially polyphenols, are potent inhibitors of amyloidogenesis. Some polyphenols have been shown to directly target the process of protein misfolding and aggregation of various amyloidogenic proteins.[41] Others have shown to act downstream of protein aggregation to prevent the toxic consequences of the accumulation of misfolded proteins. Interestingly, many polyphenols have been shown to have simultaneously two or more beneficial activities in combating AD.[42] However, despite extensive testing *in vitro* and *in vivo* models, polyphenols are yet to be used as a treatment for AD, a reluctance attributed to their poor metabolic stability and low bioavailability at the needed pharmacological concentrations.

1.4 Silibinin

Silibinin is the main component of the silymarin extracted from milk thistle seeds (*Silybum marianum* L. Gaernt.) and consists of an approximately equimolar mixture of two diastereoisomers: silybin A (Sil A) and silybin B (Sil B) (Figure 1.7).[43]

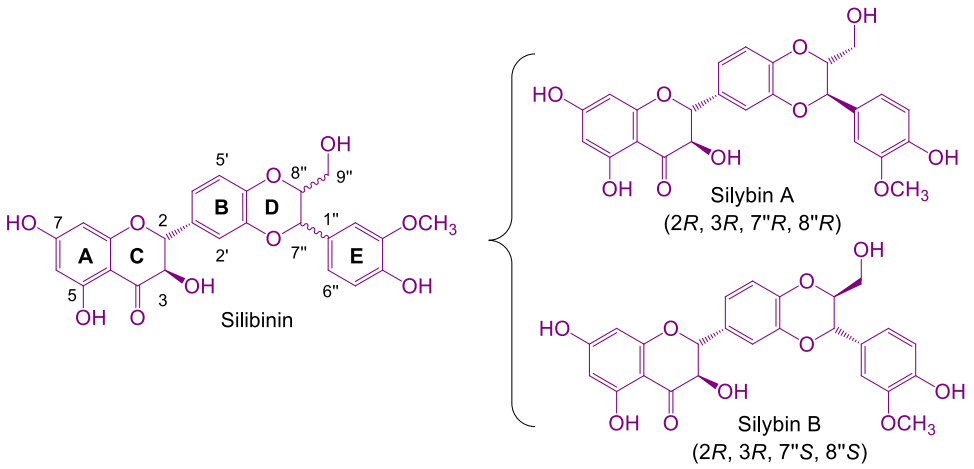

Figure 1.7 Chemical structure of silibinin and the two diastereoisomers silybin A and silybin B.

Silymarin has a long history of use in folk medicine and is now frequently employed for the prevention and/or treatment of liver disorders including viral hepatitis, liver cirrhosis associated with alcohol abuse, liver damage from drugs and industrial toxins. Silibinin is also considered an effective antidote against poisoning by death cap mushroom (*Amanita phalloides*). In the past two decades, in addition to hepatoprotective, silybin has demonstrated remarkable anticancer as well as cancer chemopreventive efficacy in preclinical cell culture and animal models of several epithelial cancers including skin, bladder, colon, prostate, lung, etc (Figure 1.8).

Silibinin has effects on multiple cancer cell signaling pathways, including growth inhibition, inhibition of angiogenesis, regulation of epithelial-to-mesenchymal transition (EMT), adhesion, and motility invasiveness, thereby inhibiting metastasis.[44]

It is also likely that the hepatoprotective and anticancer effects of silibinin are largely due to inhibition of abnormal cell proliferation and apoptosis induction through cell cycle arrest and interference of intrinsic and extrinsic mitochondrial pathways.

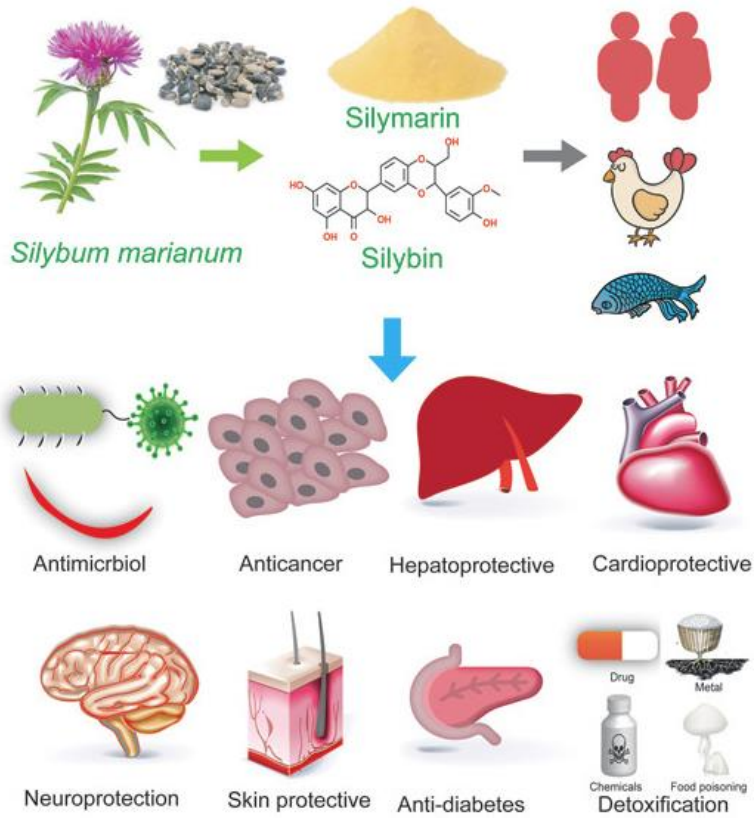

Figure 1.8 Biological activities of silibinin.

For a long time silibinin was studied and tested only as a mixture of the two diastereoisomers, but in the last decade many reports underline that the chirality is a very important feature to be not underestimate, indeed Sil A and Sil B possess different biological activities.[45] This aspect is highlighted regarding to the neuroprotective activities of silibinin.

Considering the interaction with Aβ peptide, Sil A slow down the aggregation process of $A\beta_{1-40}$, whereas Sil B fully abolished amyloid aggregation.[46] Also *in vivo* Sil B significantly protects transgenic *C. elegans* from the toxicity induced by Aβ suggesting that it is able to interact with toxic oligomers. Sil B has a specific affinity to the C-terminal domain of the peptide which, in the presence of the compound, remains unstructured throughout the entire simulation. By contrast, Sil A binds preferentially the aromatic residues and has a lower affinity with the C-terminal residues of the peptide. This different behavior has to be mainly ascribed to the methoxyphenol group which, in Sil A is free to rotate around the C−C bond linking it with the dioxane moiety, whereas in Sil B is blocked because of steric hindrance.

Conversely, in the case of human 20S proteasome (h20S), a higher affinity and more efficient activation is observed for Sil A.[47] The taxifolin group of both diastereoisomers plays a crucial role in their anchoring to the α5/α6 groove of the outer α-ring. However, due to the different stereochemistry at C-7" and C-8" of ring D, only Sil A was able to reproduce the interactions responsible for h20S proteasome activation induced by their cognate regulatory particles. Sil A is a more effective h20S enhancer than Sil B, and, accordingly, it showed a more favorable binding energy for the open than the closed h20S conformation, while the opposite result has been obtained in the case of Sil B.

Due to its highly hydrophobic and non-ionizable chemical structure, silibinin displays poor water solubility of less than 0.4 mg/L, and this has a great influence on its bioavailability.[48] After oral administration, silibinin is rapidly absorbed in the stomach (with a $t_{1/2}$ of about 6 – 8 h). However, the absorption efficiency is rather low: studies performed on rat models have shown that the absolute oral bioavailability of the pure form of silibinin is at a level of 0.95%. It has been established that 3 – 8% of orally administrated silibinin is excreted in an unchanged form in the urine. About 80% of silibinin is excreted as glucuronide and sulfate conjugates with bile (silibinin

concentration in bile is 60 – 100 times higher than in serum and attains a level of even 0.1 mM). It is assumed that 20 – 40% of bile silibinin is recovered, whereas the remaining part is excreted via feces. Silibinin monoglucuronides and diglucuronides, as well as silibinin monosulfates and silibinin diglucuronides sulfate, are all formed during phase II of silibinin's biotransformation.[49]

To overcome these limits, synthetic efforts have been aimed to derivatize silibinin to discover new biological activities of the derivatives and to make its biological activities more pronounced and selective.[50]

1.5 Curcumin

Curcumin, is a polyphenolic compound derived from dietary spice turmeric.[51] Chemically, curcumin is a bis-α,β-unsaturated β-diketone of two ferulic acid units, connected through a methylene group. Curcumin exists mostly in a hydrogen-bond-stabilized keto–enol state. Tautomeric equilibrium is partly dependent upon the polarity and the pH value of the solvent. In non-polar solvents, curcumin exists in the enol form, because of intramolecular hydrogen bond formation, whereas in polar solvents it exists in the diketo form. In acidic and neutral media, the keto form of curcumin dominates and acts as a proton donor, whereas at pH values above 8 the enol form predominates and serves as an electron donor (Figure 1.9).

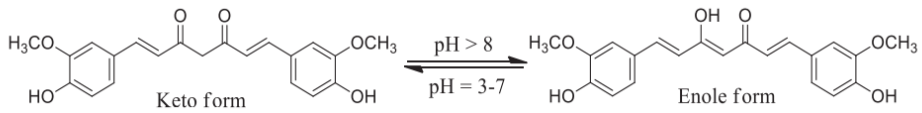

Figure 1.9 Keto and enol form of curcumin depending on pH.

Curcumin is a powerful antioxidant, and it has been found that curcumin can directly scavenge various free radicals, ROS and RNS, inhibit ROS-generating enzymes such as lipoxygenase/cyclooxygenase and xanthine dehydrogenase/oxidase, and upregulate antioxidant defense enzymes such as superoxide dismutase and glutathione peroxidase.[52] Curcumin can be metabolized through both conjugation and reduction pathways in humans and rodents. Curcumin given orally undergoes conjugation, resulting in curcumin glucuronide and sulfates.

Several studies have highlighted the role of the thiol-reactive α,ß unsaturated carbonyl groups of curcumin paying attention to the structure activity relationships.[53] A key role for the methoxy group has also been proposed. Curcumin has been considered as modulators of apoptosis.[54] Recent evidence supports that other less-

investigated pathways of cell death, i.e., necroptosis and ferroptosis may play a role in cellular response to curcumin and related compound action. Curcumin has been proposed as potential therapeutic agents in selected cancer types such as prostate, colon, breast and thyroid cancer and its anticancer effects have been tested *in vitro* and *in vivo* in combination with chemotherapeutic agents and radiotherapy.[54] Curcumin has shown to amplify the anticancer effects of drugs (e.g., doxorubicin, cisplatin, gefitinib) and radiotherapy.[55] For instance, curcumin displays a synergistic effect with some chemotherapeutic agents such as 5-fluorouracil and oxaliplatin while protecting normal tissues from cell death, and therefore without side effects. Curcumin inhibits the pathway of Nuclear Factor kB (NF-kB), a transcription factor that besides being involved in immune responses and inflammation, acts in regulating genes implicated in cancer development and progression. Inhibition of cell proliferation by curcumin has been reported in a variety of cancer cell lines, including non-small cell lung cancer cells, in which curcumin-induced ferroptosis was observed.[56] In gastric carcinoma cells, curcumin-induced proliferation inhibition was associated with the inhibition of the Wnt/β-catenin signaling pathway.

In the context of neurodegenerative diseases, *in vitro* studies have shown that curcumin can bind Aβ, thus influencing the peptide aggregation and inhibiting fibrils formation and elongation.[57] Moreover, curcumin can enhance Aβ cellular uptake avoiding plaques deposition and preventing cellular insults induced by the peptide and it can also downregulate Aβ production through BACE-1 (beta-site APP-cleaving enzyme) expression. *In vivo*, curcumin is able to rescue the distorted neuritic morphology near Aβ plaques, to decrease Aβ serum level as well as Aβ burden in the brain, especially in the neocortex and in the hippocampus, and to attenuate inflammation and microglia activation in AD mouse models.[58] Furthermore, curcumin can modulate tau protein processing and phosphorylation avoiding NFTs formation.

Phase I clinical trials have shown that curcumin is safe even at high doses (12 g/day) in humans but exhibit poor bioavailability. Major reasons contributing to the low plasma and tissue levels of curcumin appear to be due to poor absorption, rapid metabolism, and rapid systemic elimination. Furthermore, the stability of curcumin in aqueous solution is pH dependent. Curcumin is most stable at pH 1 – 6, for example, in the stomach or small intestine, where its degradation is very slow. However, its solubility in aqueous solution is poor in this pH range. Curcumin becomes unstable at pH >7 and, as such, 90% of curcumin is degraded within 30 min in in vitro preparations under physiological pH conditions (0.1 mM phosphate buffer solution, 37 °C, pH 7.2) (Figure 1.10).[52]

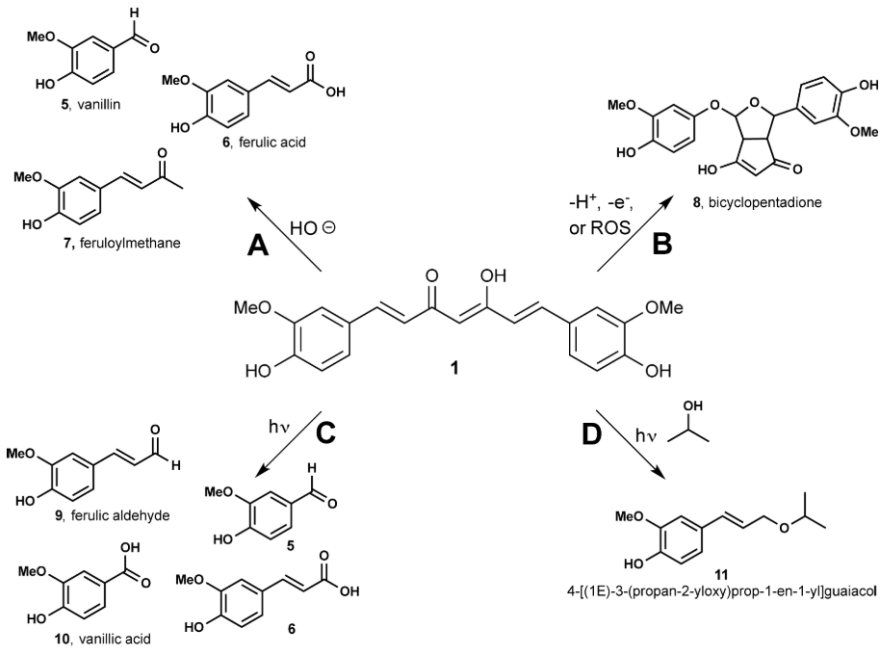

Figure 1.10 Chemical structures of degradation products of curcumin.

Curcumin degrades by two main pathways: solvolysis and oxidative degradation. The solvolysis (nucleophilic substitution or elimination by solvent molecules) of the heptadienedione chain in aqueous alkaline buffer results in 90% compound degradation leading to vanillin, ferulic acid, and feruloylmethane.[51] The major chemical degradation product is a bicyclopentadione that is produced by autoxidation. The spontaneous, free-radical-driven incorporation of O_2 leads to oxygenation and double cyclization of the heptadienedione chain connecting the two methoxyphenol rings. Crystalline curcumin is degraded by exposure to sunlight to give primarily vanillin, ferulic acid, ferulic aldehyde, and vanillic acid. The same degradation pattern is observed in organic solvents when it is exposed to light. Several solvent-dependent products are also formed. Isopropanol can also behave as a reactive substrate, leading to the formation of a guaiacol derivative.

To improve the bioavailability and stability of curcumin, numerous approaches have been undertaken. These approaches involve the use of adjuvant like piperine that interferes with glucuronidation; the use of liposomal curcumin, curcumin nanoparticles, curcumin phospholipid complex; and the use of structural analogues of curcumin.[59] Research is active in the design and synthesis of new curcumin-based mimics which allow to overcome the biological problems, intensifying the antioxidant, anticancer and anti-aggregating properties of curcumin and focusing on the cellular target of the drug.[53]

Various structural parameters need to be taken into account in the design of new molecules to derive a structure-activity relationships (SAR): the modification of each structural feature can vary one or more effects brought by the molecule (antioxidant power, anti-aggregating power, chelating capacity, solubility, etc.).[60]

It is believed that four structural parameters come into play in determining the effectiveness of the bond with β-amyloids and therefore the anti-aggregating properties (Figure 1.11).[61]

These parameters are:

- the number of aromatic rings at the ends of the chain (called linker);
- the substituents on the aromatic rings;
- the length of the linker;
- the conformational mobility of the linker.

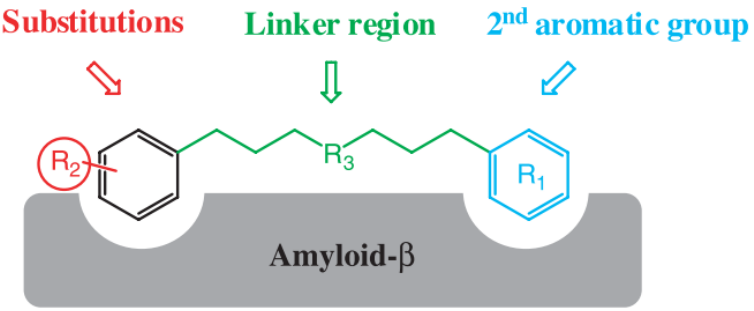

Figure 1.11. The structural elements common to curcumin-like amyloid ligands.

Molecules containing only one aromatic ring have demonstrated significantly lower anti-aggregating activity than molecules with both aromatic rings at the ends. The presence of a substituent on the aromatic rings capable of establishing hydrogen bonds (hydroxyl, carboxylic acid, sulfonic acid) is essential to preserve the anti-aggregating activity of the molecule; replacing this group with a methoxy makes the derivative less active. The active molecule, however, will also interact through hydrophobic interactions with the pocket of the amyloid fibril, exploiting the two aromatic rings. The absence of double bonds conjugated to the aromatic rings does not appear to affect the neuroprotective activity.[62]

The linker must have a length that falls within a well-defined range of values for which the derivatives have been found to be effective: it is believed that the length of the chain should not fall below 8 Å nor exceed 16 Å (from approximately 4 to 10 atoms).

The number of curcumin derivatives and analogues synthesized to date is very high and the pool of molecules is extremely heterogeneous. In some cases the curcumin analogues were obtained by combining portions of two already existing natural molecules, such as curcumin and melatonin (a, Figure 1.12), in other cases, however, a functionalization of curcumin with other bioactive molecules such as thalidomide (b, Figure 1.12) was carried out, obtaining actual conjugates of curcumin, in still others the linker between the two aromatic rings (c, Figure 1.12) was modified, using, for example, an isosteric pyrazole ring.[63]

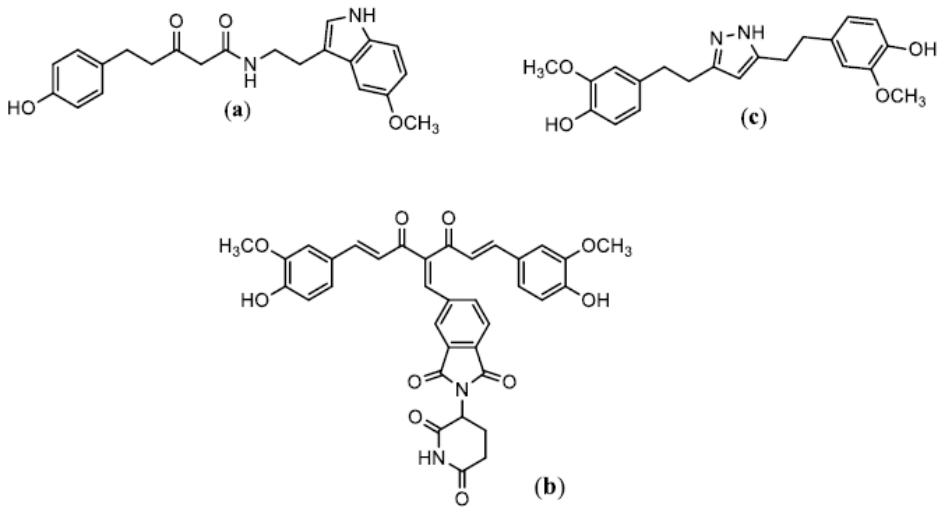

Figure 1.12 Synthetic hybrid molecules that reproduce the structure of curcumin.

The effects obtained (or intensified) through the production of curcumin derivatives are of different types, for example the hybrid compound (a) was synthesized with the aim of combining a notable neuroprotective action against Aβ to

the regulation of circadian rhythms, which appear to be altered in patients suffering from AD, the latter presenting low levels of melatonin. Compound (c) has an activity accentuated antioxidant, both due to the lack of double bonds on the linker and the presence of a pyrazole heterocycle. It is interesting to specify how the study of curcumin derivatives is not limited only to AD, but they also find a potential application as anticancer, an example is the compound (b), which was produced based on the logic that curcumin makes myeloma cells more sensitive to thalidomide; in this case the effect obtained is exactly the opposite of anti-Alzheimer drugs, in fact the curcumin-thalidomide hybrid generates a high quantity of ROS which will induce cellular apoptosis.

Bibliography

(1) Katz, L.; Baltz, R. H. Natural Product Discovery: Past, Present, and Future. *J Ind Microbiol Biotechnol* **2016**, *43* (2–3), 155–176. https://doi.org/10.1007/s10295-015-1723-5.

(2) Atanasov, A. G.; Waltenberger, B.; Pferschy-Wenzig, E.-M.; Linder, T.; Wawrosch, C.; Uhrin, P.; Temml, V.; Wang, L.; Schwaiger, S.; Heiss, E. H.; Rollinger, J. M.; Schuster, D.; Breuss, J. M.; Bochkov, V.; Mihovilovic, M. D.; Kopp, B.; Bauer, R.; Dirsch, V. M.; Stuppner, H. Discovery and Resupply of Pharmacologically Active Plant-Derived Natural Products: A Review. *Biotechnol Adv* **2015**, *33* (8), 1582–1614. https://doi.org/10.1016/j.biotechadv.2015.08.001.

(3) Corson, T. W.; Crews, C. M. Molecular Understanding and Modern Application of Traditional Medicines: Triumphs and Trials. *Cell* **2007**, *130* (5), 769–774. https://doi.org/10.1016/j.cell.2007.08.021.

(4) Zenk, M. H.; Juenger, M. Evolution and Current Status of the Phytochemistry of Nitrogenous Compounds. *Phytochemistry* **2007**, *68* (22–24), 2757–2772. https://doi.org/10.1016/j.phytochem.2007.07.009.

(5) David, B.; Wolfender, J.-L.; Dias, D. A. The Pharmaceutical Industry and Natural Products: Historical Status and New Trends. *Phytochemistry Reviews* **2015**, *14* (2), 299–315. https://doi.org/10.1007/s11101-014-9367-z.

(6) Newman, D. J.; Cragg, G. M. Natural Products as Sources of New Drugs over the Nearly Four Decades from 01/1981 to 09/2019. *J Nat Prod* **2020**, *83* (3), 770–803. https://doi.org/10.1021/acs.jnatprod.9b01285.

(7) Coy-Barrera, E.; Ogungbe, I. V.; Schmidt, T. J. Natural Products for Drug Discovery in the 21st Century: Innovations for Novel Therapeutics. *Molecules* **2023**, *28* (9), 3690. https://doi.org/10.3390/molecules28093690.

(8) Chopra, B.; Dhingra, A. K. Natural Products: A Lead for Drug Discovery and Development. *Phytotherapy Research* **2021**, *35* (9), 4660–4702. https://doi.org/10.1002/ptr.7099.

(9) Quideau, S.; Deffieux, D.; Douat-Casassus, C.; Pouységu, L. Plant Polyphenols: Chemical Properties, Biological Activities, and Synthesis. *Angewandte Chemie International Edition* **2011**, *50* (3), 586–621. https://doi.org/10.1002/anie.201000044.

(10) Molino, S.; Dossena, M.; Buonocore, D.; Ferrari, F.; Venturini, L.; Ricevuti, G.; Verri, M. Polyphenols in Dementia: From Molecular Basis to Clinical Trials. *Life Sci* **2016**, *161*, 69–77. https://doi.org/10.1016/j.lfs.2016.07.021.

(11) Wang, T.; Li, Q.; Bi, K. Bioactive Flavonoids in Medicinal Plants: Structure, Activity and Biological Fate. *Asian J Pharm Sci* **2018**, *13* (1), 12–23. https://doi.org/10.1016/j.ajps.2017.08.004.

(12) Heo, H. J.; Kim, D.-O.; Shin, S. C.; Kim, M. J.; Kim, B. G.; Shin, D.-H. Effect of Antioxidant Flavanone, Naringenin, from Citrus Junos on Neuroprotection. *J Agric Food Chem* **2004**, *52* (6), 1520–1525. https://doi.org/10.1021/jf035079g.

(13) Brasnyó, P.; Molnár, G. A.; Mohás, M.; Markó, L.; Laczy, B.; Cseh, J.; Mikolás, E.; Szijártó, I. A.; Mérei, Á.; Halmai, R.; Mészáros, L. G.; Sümegi, B.; Wittmann, I. Resveratrol Improves Insulin Sensitivity, Reduces Oxidative Stress and Activates the Akt Pathway in Type 2 Diabetic Patients. *British Journal of Nutrition* **2011**, *106* (3), 383–389. https://doi.org/10.1017/S0007114511000316.

(14) Vaghari-Tabari, M.; Ferns, G. A.; Qujeq, D.; Andevari, A. N.; Sabahi, Z.; Moein, S. Signaling, Metabolism, and Cancer: An Important Relationship for Therapeutic Intervention. *J Cell Physiol* **2021**, *236* (8), 5512–5532. https://doi.org/10.1002/jcp.30276.

(15) Siegel, R. L.; Miller, K. D.; Jemal, A. Cancer Statistics, 2018. *CA Cancer J Clin* **2018**, *68* (1), 7–30. https://doi.org/10.3322/caac.21442.

(16) Iranzo, J.; Martincorena, I.; Koonin, E. V. Cancer-Mutation Network and the Number and Specificity of Driver Mutations. *Proceedings of the National Academy of Sciences* **2018**, *115* (26), E6010–E6019. https://doi.org/10.1073/pnas.1803155115.

(17) Chaudhry, G.-S.; Md Akim, A.; Sung, Y. Y.; Sifzizul, T. M. T. Cancer and Apoptosis: The Apoptotic Activity of Plant and Marine Natural Products and Their Potential as Targeted Cancer Therapeutics. *Front Pharmacol* **2022**, *13* (August), 1–24. https://doi.org/10.3389/fphar.2022.842376.

(18) Jain, M. V.; Paczulla, A. M.; Klonisch, T.; Dimgba, F. N.; Rao, S. B.; Roberg, K.; Schweizer, F.; Lengerke, C.; Davoodpour, P.; Palicharla, V. R.; Maddika, S.; Łos, M. Interconnections between Apoptotic, Autophagic and Necrotic Pathways: Implications for Cancer Therapy Development. *J Cell Mol Med* **2013**, *17* (1), 12–29. https://doi.org/10.1111/jcmm.12001.

(19) Zhao, M.; Sun, J.; Zhao, Z. Distinct and Competitive Regulatory Patterns of Tumor Suppressor Genes and Oncogenes in Ovarian Cancer. *PLoS One* **2012**, *7* (8), e44175. https://doi.org/10.1371/journal.pone.0044175.

(20) Dixon, S. J.; Lemberg, K. M.; Lamprecht, M. R.; Skouta, R.; Zaitsev, E. M.; Gleason, C. E.; Patel, D. N.; Bauer, A. J.; Cantley, A. M.; Yang, W. S.; Morrison, B.; Stockwell, B. R. Ferroptosis: An Iron-Dependent Form of Nonapoptotic Cell Death. *Cell* **2012**, *149* (5), 1060–1072. https://doi.org/10.1016/j.cell.2012.03.042.

(21) Zhao, Y.-Y.; Yang, Y.-Q.; Sheng, H.-H.; Tang, Q.; Han, L.; Wang, S.-M.; Wu, W.-Y. GPX4 Plays a Crucial Role in Fuzheng Kang'ai Decoction-Induced Non-Small Cell Lung Cancer Cell Ferroptosis. *Front Pharmacol* **2022**, *13* (April), 1–12. https://doi.org/10.3389/fphar.2022.851680.

(22) Zhan, S.; Lu, L.; Pan, S.; Wei, X.; Miao, R.; Liu, X.; Xue, M.; Lin, X.; Xu, H. Targeting NQO1/GPX4-Mediated Ferroptosis by Plumbagin Suppresses

in Vitro and in Vivo Glioma Growth. *Br J Cancer* **2022**, *127* (2), 364–376. https://doi.org/10.1038/s41416-022-01800-y.

(23) Alborzinia, H.; Ignashkova, T. I.; Dejure, F. R.; Gendarme, M.; Theobald, J.; Wölfl, S.; Lindemann, R. K.; Reiling, J. H. Golgi Stress Mediates Redox Imbalance and Ferroptosis in Human Cells. *Commun Biol* **2018**, *1* (1), 210. https://doi.org/10.1038/s42003-018-0212-6.

(24) El Hajj, S.; Canabady-Rochelle, L.; Gaucher, C. Nature-Inspired Bioactive Compounds: A Promising Approach for Ferroptosis-Linked Human Diseases? *Molecules* **2023**, *28* (6), 2636. https://doi.org/10.3390/molecules28062636.

(25) Moradi-Marjaneh, R.; Hassanian, S. M.; Mehramiz, M.; Rezayi, M.; Ferns, G. A.; Khazaei, M.; Avan, A. Reactive Oxygen Species in Colorectal Cancer: The Therapeutic Impact and Its Potential Roles in Tumor Progression via Perturbation of Cellular and Physiological Dysregulated Pathways. *J Cell Physiol* **2019**, *234* (7), 10072–10079. https://doi.org/10.1002/jcp.27881.

(26) Rouzbehan, S.; Moein, S.; Homaei, A.; Moein, M. R. Kinetics of α-Glucosidase Inhibition by Different Fractions of Three Species of Labiatae Extracts: A New Diabetes Treatment Model. *Pharm Biol* **2017**, *55* (1), 1483–1488. https://doi.org/10.1080/13880209.2017.1306569.

(27) Koolivand, M.; Ansari, M.; Piroozian, F.; Moein, S.; MalekZadeh, K. Alleviating the Progression of Acute Myeloid Leukemia (AML) by Sulforaphane through Controlling MiR-155 Levels. *Mol Biol Rep* **2018**, *45* (6), 2491–2499. https://doi.org/10.1007/s11033-018-4416-0.

(28) Mazidi, M.; Ferns, G. A.; Banach, M. A High Consumption of Tomato and Lycopene Is Associated with a Lower Risk of Cancer Mortality: Results from a Multi-Ethnic Cohort. *Public Health Nutr* **2020**, *23* (9), 1569–1575. https://doi.org/10.1017/S1368980019003227.

(29) Yuan, R.; Hou, Y.; Sun, W.; Yu, J.; Liu, X.; Niu, Y.; Lu, J.; Chen, X. Natural Products to Prevent Drug Resistance in Cancer Chemotherapy: A Review. *Ann N Y Acad Sci* **2017**, *1401* (1), 19–27. https://doi.org/10.1111/nyas.13387.

(30) Maruca, A.; Catalano, R.; Bagetta, D.; Mesiti, F.; Ambrosio, F. A.; Romeo, I.; Moraca, F.; Rocca, R.; Ortuso, F.; Artese, A.; Costa, G.; Alcaro, S.; Lupia, A. The Mediterranean Diet as Source of Bioactive Compounds with Multi-

Targeting Anti-Cancer Profile. *Eur J Med Chem* **2019**, *181*, 111579. https://doi.org/10.1016/j.ejmech.2019.111579.

(31) Chiti, F.; Dobson, C. M. Protein Misfolding, Amyloid Formation, and Human Disease: A Summary of Progress Over the Last Decade. *Annu Rev Biochem* **2017**, *86* (1), 27–68. https://doi.org/10.1146/annurev-biochem-061516-045115.

(32) Kumar, A.; Singh, A.; Ekavali. A Review on Alzheimer's Disease Pathophysiology and Its Management: An Update. *Pharmacological Reports* **2015**, *67* (2), 195–203. https://doi.org/10.1016/j.pharep.2014.09.004.

(33) Cummings, J. L.; Morstorf, T.; Zhong, K. Cummings, Jeffrey L_Alzheimer's_drug Development Candidates Failures_2014. *Alzheimers Res Ther* **2014**, *6* (37), 1–7.

(34) Association, A. Alzheimer ' s Disease Facts and Figures. **2013**, *11*, 332–384.

(35) Willbold, D.; Strodel, B.; Schröder, G. F.; Hoyer, W.; Heise, H. Amyloid-Type Protein Aggregation and Prion-like Properties of Amyloids. *Chem Rev* **2021**, *121* (13), 8285–8307. https://doi.org/10.1021/acs.chemrev.1c00196.

(36) Sciacca, M. F. M.; Tempra, C.; Scollo, F.; Milardi, D.; La Rosa, C. Amyloid Growth and Membrane Damage: Current Themes and Emerging Perspectives from Theory and Experiments on Aβ and HIAPP. *Biochimica et Biophysica Acta (BBA) - Biomembranes* **2018**, *1860* (9), 1625–1638. https://doi.org/10.1016/j.bbamem.2018.02.022.

(37) Dikic, I. Proteasomal and Autophagic Degradation Systems. *Annu Rev Biochem* **2017**, *86* (1), 193–224. https://doi.org/10.1146/annurev-biochem-061516-044908.

(38) Tundo, G. R.; Sbardella, D.; Santoro, A. M.; Coletta, A.; Oddone, F.; Grasso, G.; Milardi, D.; Lacal, P. M.; Marini, S.; Purrello, R.; Graziani, G.; Coletta, M. The Proteasome as a Druggable Target with Multiple Therapeutic Potentialities: Cutting and Non-Cutting Edges. *Pharmacol Ther* **2020**, *213*, 107579. https://doi.org/10.1016/j.pharmthera.2020.107579.

(39) Praticò, D. Oxidative Stress Hypothesis in Alzheimer's Disease: A Reappraisal. https://doi.org/10.1016/j.tips.2008.09.001.

(40) Cheignon, C.; Tomas, M.; Bonnefont-Rousselot, D.; Faller, P.; Hureau, C.; Collin, F. Oxidative Stress and the Amyloid Beta Peptide in Alzheimer's

Disease. *Redox Biol* **2018**, *14* (September 2017), 450–464. https://doi.org/10.1016/j.redox.2017.10.014.

(41) Pagano, K.; Tomaselli, S.; Molinari, H.; Ragona, L. Natural Compounds as Inhibitors of Aβ Peptide Aggregation: Chemical Requirements and Molecular Mechanisms. *Front Neurosci* **2020**, *14* (December), 1–18. https://doi.org/10.3389/fnins.2020.619667.

(42) Dhouafli, Z.; Cuanalo-Contreras, K.; Hayouni, E. A.; Mays, C. E.; Soto, C.; Moreno-Gonzalez, I. Inhibition of Protein Misfolding and Aggregation by Natural Phenolic Compounds. *Cellular and Molecular Life Sciences* **2018**, *75* (19), 3521–3538. https://doi.org/10.1007/s00018-018-2872-2.

(43) Wang, X.; Zhang, Z.; Wu, S.-C. Health Benefits of Silybum Marianum : Phytochemistry, Pharmacology, and Applications. *J Agric Food Chem* **2020**, *68* (42), 11644–11664. https://doi.org/10.1021/acs.jafc.0c04791.

(44) Polachi, N.; Bai, G.; Li, T.; Chu, Y.; Wang, X.; Li, S.; Gu, N.; Wu, J.; Li, W.; Zhang, Y.; Zhou, S.; Sun, H.; Liu, C. Modulatory Effects of Silibinin in Various Cell Signaling Pathways against Liver Disorders and Cancer – A Comprehensive Review. *Eur J Med Chem* **2016**, *123*, 577–595. https://doi.org/10.1016/j.ejmech.2016.07.070.

(45) Křen, V. Chirality Matters: Biological Activity of Optically Pure Silybin and Its Congeners. *Int J Mol Sci* **2021**, *22* (15), 7885. https://doi.org/10.3390/ijms22157885.

(46) Sciacca, Michele. F. M.; Romanucci, V.; Zarrelli, A.; Monaco, I.; Lolicato, F.; Spinella, N.; Galati, C.; Grasso, G.; D'Urso, L.; Romeo, M.; Diomede, L.; Salmona, M.; Bongiorno, C.; Di Fabio, G.; La Rosa, C.; Milardi, D. Inhibition of Aβ Amyloid Growth and Toxicity by Silybins: The Crucial Role of Stereochemistry. *ACS Chem Neurosci* **2017**, *8* (8), 1767–1778. https://doi.org/10.1021/acschemneuro.7b00110.

(47) Persico, M.; García-Viñuales, S.; Santoro, A. M.; Lanza, V.; Tundo, G. R.; Sbardella, D.; Coletta, M.; Romanucci, V.; Zarrelli, A.; Di Fabio, G.; Fattorusso, C.; Milardi, D. Silybins Are Stereospecific Regulators of the 20S Proteasome. *Bioorg Med Chem* **2022**, *66* (February), 116813. https://doi.org/10.1016/j.bmc.2022.116813.

(48) Romanucci, V.; Gravante, R.; Cimafonte, M.; Marino, C. Di; Mailhot, G.; Brigante, M.; Zarrelli, A.; Fabio, G. Di. Phosphate-Linked Silibinin Dimers

(PLSd): New Promising Modified Metabolites. *Molecules* **2017**, *22* (8), 1323. https://doi.org/10.3390/molecules22081323.

(49) Bijak, M. Silybin, a Major Bioactive Component of Milk Thistle (Silybum Marianum L. Gaernt.)—Chemistry, Bioavailability, and Metabolism. *Molecules* **2017**, *22* (11), 1942. https://doi.org/10.3390/molecules22111942.

(50) Biedermann, D.; Vavříková, E.; Cvak, L.; Křen, V. Chemistry of Silybin. *Nat. Prod. Rep.* **2014**, *31* (9), 1138–1157. https://doi.org/10.1039/C3NP70122K.

(51) Nelson, K. M.; Dahlin, J. L.; Bisson, J.; Graham, J.; Pauli, G. F.; Walters, M. A. The Essential Medicinal Chemistry of Curcumin. *J Med Chem* **2017**, *60* (5), 1620–1637. https://doi.org/10.1021/acs.jmedchem.6b00975.

(52) Shen, L.; Ji, H.-F. The Pharmacology of Curcumin: Is It the Degradation Products? *Trends Mol Med* **2012**, *18* (3), 138–144. https://doi.org/10.1016/j.molmed.2012.01.004.

(53) Costantino, M.; Corno, C.; Colombo, D.; Perego, P. Curcumin and Related Compounds in Cancer Cells: New Avenues for Old Molecules. *Front Pharmacol* **2022**, *13* (May), 1–8. https://doi.org/10.3389/fphar.2022.889816.

(54) Reuter, S.; Eifes, S.; Dicato, M.; Aggarwal, B. B.; Diederich, M. Modulation of Anti-Apoptotic and Survival Pathways by Curcumin as a Strategy to Induce Apoptosis in Cancer Cells. *Biochem Pharmacol* **2008**, *76* (11), 1340–1351. https://doi.org/10.1016/j.bcp.2008.07.031.

(55) Ashrafizadeh, M.; Najafi, M.; Makvandi, P.; Zarrabi, A.; Farkhondeh, T.; Samarghandian, S. Versatile Role of Curcumin and Its Derivatives in Lung Cancer Therapy. *J Cell Physiol* **2020**, *235* (12), 9241–9268. https://doi.org/10.1002/jcp.29819.

(56) Tang, X.; Ding, H.; Liang, M.; Chen, X.; Yan, Y.; Wan, N.; Chen, Q.; Zhang, J.; Cao, J. Curcumin Induces Ferroptosis in Non-Small-Cell Lung Cancer via Activating Autophagy. *Thorac Cancer* **2021**, *12* (8), 1219–1230. https://doi.org/10.1111/1759-7714.13904.

(57) Serafini, M. M.; Catanzaro, M.; Rosini, M.; Racchi, M.; Lanni, C. Curcumin in Alzheimer's Disease: Can We Think to New Strategies and Perspectives for This Molecule? *Pharmacol Res* **2017**, *124*, 146–155. https://doi.org/10.1016/j.phrs.2017.08.004.

(58) Garcia-Alloza, M.; Borrelli, L. A.; Rozkalne, A.; Hyman, B. T.; Bacskai, B. J. Curcumin Labels Amyloid Pathology in Vivo, Disrupts Existing Plaques, and Partially Restores Distorted Neurites in an Alzheimer Mouse Model. *J Neurochem* **2007**, *102* (4), 1095–1104. https://doi.org/10.1111/j.1471-4159.2007.04613.x.

(59) Moreira, J.; Saraiva, L.; Pinto, M. M.; Cidade, H. Diarylpentanoids with Antitumor Activity: A Critical Review of Structure-Activity Relationship Studies. *Eur J Med Chem* **2020**, *192*, 112177. https://doi.org/10.1016/j.ejmech.2020.112177.

(60) Koeberle, A.; Muñoz, E.; Appendino, G. B.; Minassi, A.; Pace, S.; Rossi, A.; Weinigel, C.; Barz, D.; Sautebin, L.; Caprioglio, D.; Collado, J. A.; Werz, O. SAR Studies on Curcumin's pro-Inflammatory Targets: Discovery of Prenylated Pyrazolocurcuminoids as Potent and Selective Novel Inhibitors of 5-Lipoxygenase. *J Med Chem* **2014**, *57* (13), 5638–5648. https://doi.org/10.1021/jm500308c.

(61) Reinke, A. A.; Gestwicki, J. E. Structure–Activity Relationships of Amyloid Beta-aggregation Inhibitors Based on Curcumin: Influence of Linker Length and Flexibility. *Chem Biol Drug Des* **2007**, *70* (3), 206–215. https://doi.org/10.1111/j.1747-0285.2007.00557.x.

(62) Bisceglia, F.; Seghetti, F.; Serra, M.; Zusso, M.; Gervasoni, S.; Verga, L.; Vistoli, G.; Lanni, C.; Catanzaro, M.; De Lorenzi, E.; Belluti, F. Prenylated Curcumin Analogues as Multipotent Tools To Tackle Alzheimer's Disease. *ACS Chem Neurosci* **2019**, *10* (3), 1420–1433. https://doi.org/10.1021/acschemneuro.8b00463.

(63) Teiten, M.-H.; Dicato, M.; Diederich, M. Hybrid Curcumin Compounds: A New Strategy for Cancer Treatment. *Molecules* **2014**, *19* (12), 20839–20863. https://doi.org/10.3390/molecules191220839.

2 Silybins Prodrugs

When using a drug, it is necessary for the Active Pharmaceutical Ingredient (API), to reach its target site to perform its functions.[1] Furthermore, the active ingredient must reach the target within a specific time and be available for a defined duration. After parenteral administration of a drug, there is a peak in plasma concentration, followed by a slow decline as the drug is eliminated or metabolized, complicating maintenance of it in useful concentrations.

Timed-release prodrug technology provides a potential means to overcome this problem. Ideally, the timed release modulates near-toxic peaks or near-ineffective doses in the active plasma concentration. Developing prodrugs is now a well-established strategy to improve the chemical-physical and biological properties of pharmacologically active compounds. Prodrugs are bioreversible derivatives of the corresponding drugs, capable of undergoing an enzymatic and/or chemical transformation *in vivo*, to then release the drug, which can exert the desired pharmacological effect. The prodrug is composed by a pro-moiety linked to the drug and this complex is generally pharmacologically non-active.

Prodrugs offer the possibility of overcoming various problems in drug formulation and administration, such as poor aqueous solubility, chemical instability, insufficient oral absorption, rapid metabolism, and inadequate brain penetration. Some of the most common functional groups that are amenable to prodrug design include carboxyl, hydroxyl, amine, phosphate/phosphonate, and carbonyl groups. Prodrugs typically

produced through modification of these groups include esters, carbonates, carbamates, amides, phosphates, and oximes.

Meet criteria of inactivation of a parent drug but also of timed-release during catalysis by an endogenous plasma enzyme is difficult since few enzymes have adequate plasma concentrations and many of them have high specificity for a native substrate. Human pancreatic ribonuclease (RNase 1) is an exception. Contrary to its name, RNase 1 is expressed in pancreatic juice at a concentration of 6.4 mg/mL, in saliva (0.2 mg/mL) and circulates in human plasma at a concentration of 0.4 mg/L. Furthermore, like its homologue bovine pancreatic ribonuclease (RNase A), RNase 1 catalyzes RNA cleavage by a transphosphorylation reaction with little specificity for its leaving group. Timed-release prodrugs, such as drugs conjugated with 3′-ribonucleotides, are reported as good prodrugs for oral and parenteral administration.[2,3]

2.1 Aim of Research Work

In this context, to improve the low bioavailability mainly due to the poor solubility in water, it was designed the synthesis of silibinin, silybin A and B conjugates.

Here it's reported an efficient and regioselective solid phase approach for obtaining new prodrugs of 9″-silybins conjugated with 3′-ribonucleotide units (uridine and adenosine) as pro-moieties through a phosphodiester bond (Figure 2.1).

The ribonucleotide unit as a pro-moiety has two advantages: first, its conjugation increases the water solubility of the drug thanks to the phosphodiester group; second, it can be specifically recognized by human pancreatic ribonuclease (RNase 1), allowing an in vivo drug release over time and ensuring maintenance of the drug at a beneficial concentration.[4] The stability of new prodrugs in different biological media and their cytotoxicity on neuronal-derived cell line were evaluated.

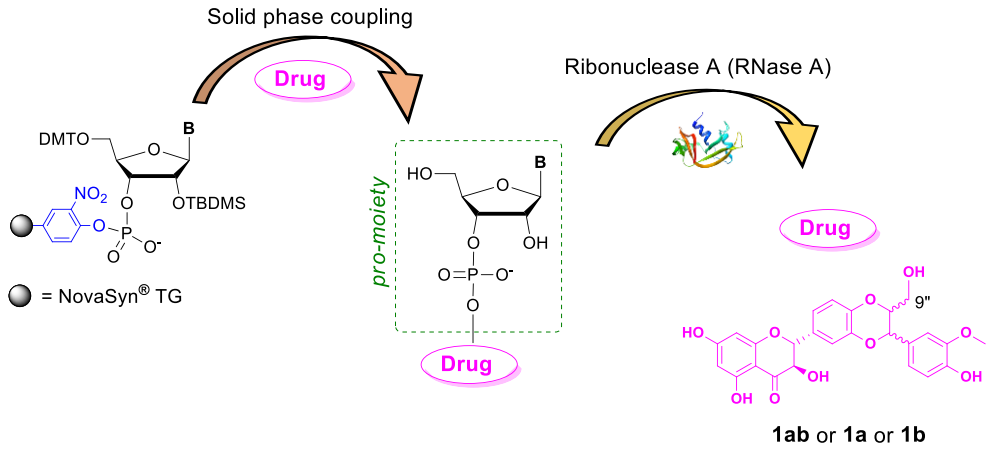

Figure 2.1. Synthesis of silybins prodrugs and evaluation of RNase A timed-release of silibinin (1ab), silybin A (1a) and silybin B (1b).

2.2 Results and Discussion

Silibinin (**1ab**) and silybins (**1a**, and **1b**) possess five hydroxyl functions that can be distinguished into three phenolic groups on C–5, C–7, and C–4″, one secondary group on C–3 and one primary alcoholic group on C–9″. Exploiting the greater nucleophilicity of 9″–OH, it's possible to obtain new silybins 9″-conjugates with natural 3′-ribonucleotide units without using protecting groups.

Initially, a NovaSyn® TG amino solid support (0.78 meq/g) was pre-derivatized with 4-hydroxy-3-nitrophenylacetic acid, resulting in the formation of a new support (**2**, Scheme 2.1). Subsequently, functionalization with 3′-phosphoramidite ribonucleotides **3** and **4** occurred using a classical phosphoramidite chemistry (step *i*). The conversion of phosphite to phosphate triester was accomplished by treatment with a widely used oxidizing reagent (0.02 M I_2 in a THF/H_2O/pyridine 66/12/22, v/v/v) and monitored by ^{31}P NMR spectroscopic analysis of the support suspended in $CDCl_3$. Two diagnostic signals of the phosphotriester group, centered at approximately −7.7 ppm, were observed. After capping with Ac_2O in pyridine 1:1 (v/v) (step *ii*) and

cyanoethyl removal through TEA/pyridine 1:1 (v/v), 50 °C, 1 h (step *iii*), the ribonucleotide loading was determined by quantifying the 4,4′-dimethoxytrityl (DMT) cation released from weighed amounts of supports **7** or **8** upon acidic treatment. The loading was found to be approximately 0.39 – 0.55 meq/g.

A classic phosphotriester chemistry was exploited to evaluate the efficiency of this support in the synthesis of 9″-silybin phosphodiesters. Hence, the functionalized supports **7** and **8** were reacted with 1-mesitylenesulfonyl-3-nitro-1,2,4-triazole (MSNT) for 30 min. Subsequently, flavonolignan (**1ab**, **1a** or **1b**) was added to the mixture at room temperature for 6 h (step iv).

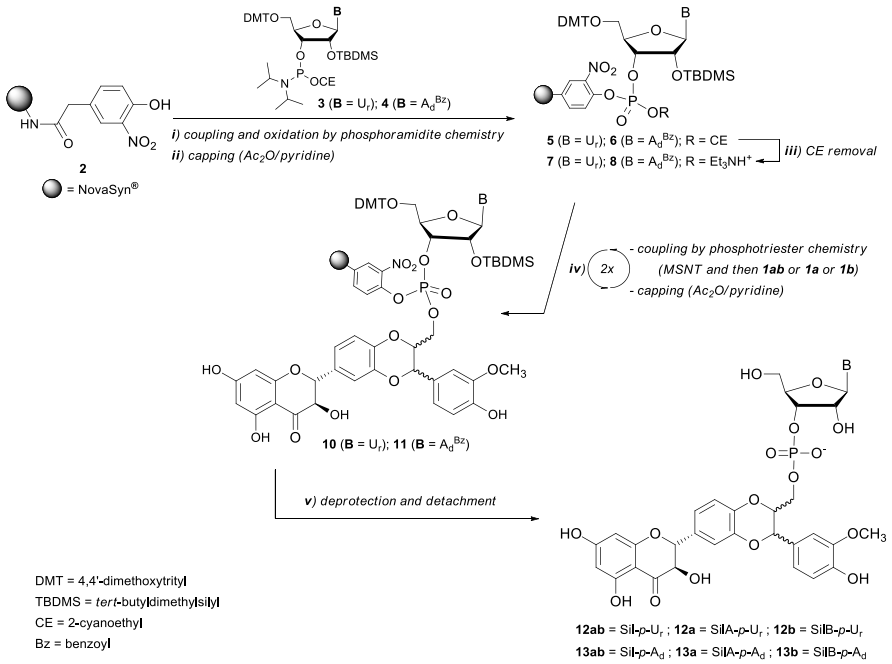

Scheme 2.1. Synthesis of prodrug **12** – **13**: reagents and conditions: *i*) **3** or **4**, DCI (10 eq.), ACN/DCM (1:1, v/v), RT., 15 min.; 0.02 M I_2 THF/H_2O/pyridine 66/12/22 (v/v/v); *ii*) Ac_2O/pyridine 1:1 (v/v), RT., 1 h; *iii*) TEA/pyridine 1:1 (v/v), 50 °C, 1 h; *iv*) MSNT (5 eq.), pyridine, RT. and then **1ab** or **1a** or **1b** (10 eq.), 6 h (2 times); *v*) 1% TFA in DCM; NH_4OH, 50 °C, 1 h; TEA·3HF (15 eq.), THF, rt., 2 h.

The supports underwent capping iterating the procedure twice, and the resin's ^{31}P NMR spectrum revealed only one peak centered at −7.1 ppm, confirming the complete conversion of the phosphodiester to a phosphotriester function. After washes with DMF, pyridine, DCM and Et_2O, the supports, dried under reduced pressure, were treated with concentrated aqueous ammonia (50 °C, 1 h). The resulting crude materials were then dried under reduced pressure and subjected to treatment at room temperature for 2 h with TEA·3HF in THF to remove the TBDMS group in the 2′ position. Final products were obtained through purification using RP-18 and Sep-Pak, to provide **12ab**, **12a**, **12b**, **13ab**, **13a**, and **13b** (Scheme 2.1) in overall good yields (41 – 50%). As expected, the HPLC profiles exhibited a single peak, typically constituting over 95% of the total integrated area. High purity was achieved as only the ribonucleotide conjugates linked to the support through a phosphodiester bond were easily detached. In contrast, the ribonucleotide anchored through a phosphodiester bond, representing the unreacted material, remained firmly attached to the resin after treatment with ammonia. The structures (**12ab**, **12a**, **12b**, **13ab**, **13a**, and **13b**) were confirmed by 1D/2D NMR as well as a MALDI-TOF-MS analysis.

The new conjugates were much more water soluble than silibinin, whose water solubility is approximately 1 μM, and concentrations of 3.7 mM and 6 mM could be achieved for uridine and adenosine conjugates, respectively.

2.2.1 Stability in Biological Media

To explore the potential for oral administration of the new conjugates, their stability was initially tested in simulated intestinal fluid (sIF) and simulated gastric fluid (sGF) (pH = 6.8 and pH = 1.1, respectively), as well as in the presence of alkaline phosphatase (ALP, pH = 7.4). Both uridine and adenosine conjugates exhibited robust stability in sIF ($t_{1/2} \gg 24$ h).

The uridine derivatives exhibited slightly lower stability than the adenosine derivatives in the more acidic pH media of sGF. Specifically, the adenosine derivatives (**13ab**, **13a**, and **13b**) showed degradation to the parent drugs of less than 5% after 24 h at 37 °C. In contrast, the uridine derivatives (**12ab**, **12a**, and **12b**) degraded by approximately 27% under the same conditions (Figure 2.2). All compounds demonstrated high stability in presence of ALP, with degradation of less than 2% after 48 h.

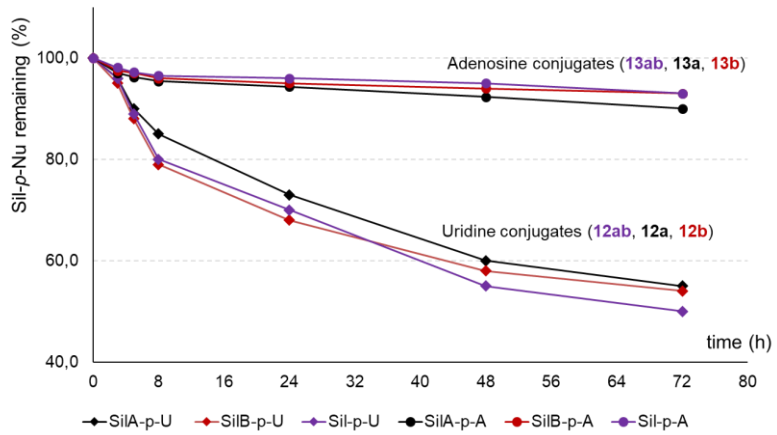

Figure 2.2. Profile of silybin conjugates remaining (%) over time in sGF (pH = 1.1); comparison of uridine and adenosine conjugates (**12** and **13** series).

2.2.2 Stability in presence of RNase A

For the development of an effective timed-release prodrug, it is essential for the pro-moiety to be recognized by the specific enzyme that releases the drug within a defined timeframe. Assuming pancreatic juice dilution in the intestine, RNase A was used at a concentration of 1.8 mg/L, a concentration quite close to that found in plasma (~0.4 mg/L). To evaluate the release rate of Sil (**1ab**), SilA (**1a**), and SilB (**1b**), the experiments were monitored by RP-HPLC analysis. The assays were performed with RNase A (final concentration: 1.8 mg/L) in a 50 mM imidazole (Im) buffer at pH 6.0,

containing NaCl (100 mM) and prodrugs (1 mM). The reaction mixture was incubated at 37 °C, and samples were collected at fixed intervals for the analysis.

The obtained data underline a rapid release of the drugs when modified with a uridine moiety, even at low RNase A concentrations (Table 2.1), affirming the high efficiency of uridine prodrugs (**12ab**, **12a**, and **12b**) and making them suitable for intravenous administration.

Table 2.1. Yields and RNase A stability of new ribonucleotide-silybin conjugates.

Compounds	yield (%)*	$t_{1/2}$ RNase A in Im buffer	$t_{1/2}$ RNase A in sIF
Sil-*p*-U_r (12ab)	41	100 min	20 h
SilA-*p*-U_r (12a)	45	87 min	13 h
SilB-*p*-U_r (12b)	46	50 min	11 h
Sil-*p*-A_d (13ab)	50	> 48 h	> 48 h
SilA-*p*-A_d (13a)	48	> 48 h	> 48 h
SilB-*p*-A_d (13b)	48	> 48 h	> 48 h
Sil (1ab)	–	–	–
SilA (1a)	–	–	–
SilB (1b)	–	–	–

As expected, uridine derivatives undergo cleavage much faster than compounds derivatized with adenosine due to the selectivity of RNase for pyrimidine nucleobases.[5] Consequently, the half-lives of compounds **13ab**, **13a**, and **13b** exceed 48 h. The cleavage of the **12b** derivative (SilB-*p*-Ur) is slightly faster than **12ab** and **12a**, with half-lives of 50 min compared to 87 and 100 min, respectively (Table 2.1), suggesting slightly better accessibility of the silybin B prodrug by RNase. RNase stability was also examined in simulated intestinal fluid (sIF), revealing slower

kinetics of prodrug cleavage compared to the imidazole buffer, with a highly efficient sustained release of the drug (approximately 13 h).

2.2.3 Evaluation of Cell Toxicity

The potential toxic effects of silybin ribonucleotide conjugates were assessed on fully differentiated neuroblastoma SH-SY5Y cells to obtain a neuronal-like phenotype (Figure 2.3). Cell viability was monitored after 48 h of treatment with increasing concentrations of **1ab**, **1a** and **1b**, with or without modifications. Toxic effects of the silibinin conjugates (**12ab** and 1**3ab**) were also evaluated. It was determined that not all the new compounds exhibited toxicity, and no significant difference was observed between the uridine and adenosine conjugates.

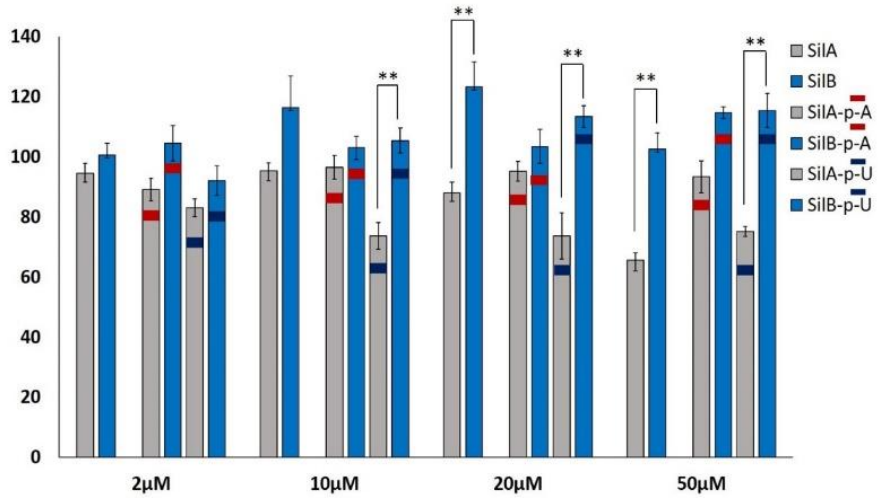

Figure 2.3. MTT assay of human differentiated SH-SY5Y after 48 h treatment with 2, 10, 20 and 50 µM of SilA, SilB, SilA-*p*-Ad/-pUr or SilB-*p*-Ad/-pUr. Bars represent the mean ± SEM of three independent experiments (n = 4). Values are expressed as percentage of viable cells, considering the untreated control cells as 100%. **P < 0.05 by One-way ANOVA + Tukey's Test.

2.3 Conclusions

Silibinin (Sil) is the main component of the silymarin extracted from milk thistle seeds and consists of an approximately equimolar mixture of two diastereoismers: silybin A (SilA) and silybin B (SilB). Silibinin has a wide range of biological and pharmacological activities, but it's limited by its low solubility in water and bioavailability.

To increase water solubility, in this study a versatile and efficient regioselective solid-phase synthetic approach was presented, obtaining new prodrugs with a 3'-ribonucleotide unit as a pro-moiety.

NovaSyn® TG support pre-derivatized with an appropriate linker, was anchored to the ribonucleotide units through the phosphate group, and using silybins (**1ab**, **1a** and **1b**), it was synthesized a mini-library of 9"-silybins conjugated with 3'-ribonucleotide units through phosphodiester bond in good yields. The new conjugates underwent comprehensive characterization through NMR and MALDI-TOF MS analyses. All new prodrugs exhibited a higher solubility in water compared to silibinin, with a solubility of approximately 3.7 mM and 6 mM for uridine and adenosine conjugates, respectively. They demonstrated stability in simulated intestinal fluid (sIF) and alkaline phosphatase (ALP), whereas the uridine conjugates (**12ab**, **12a**, and **12b**) displayed slightly reduced stability in simulated gastric fluid (sGF).

Further investigations into the efficacy of these compounds as timed-release prodrugs revealed that uridine-silybin prodrugs were rapidly cleaved by RNase A, releasing the active silybin drugs even at low RNase concentrations. Additionally, a small difference was observed between SilB and SilA uridine derivatives in RNase cleavage: SilB-*p*-Ur seemed to undergo hydrolysis faster than SilA-*p*-Ur, suggesting better accessibility of RNase to the SilB derivative. The cell viability assays confirmed the lack of toxicity of the new compounds. The found results encourage further

investigations of silybin-ribonucleotide conjugates as timed-release prodrugs for oral or parenteral administration.

2.4 Experimental Session

2.4.1 General Methods

NovaSyn® TG-NH_2 resin was purchased from Merck Milano-Italy. The functionalization of the solid support was performed in a short glass column (5 cm length, 1 cm i.d.) equipped with a sintered glass filter, a stopcock, and a cap. The coupling reaction to obtain supports **5** and **6** was performed using DMT-2′O-TBDMS-rU phosphoramidite (**3**) or DMT-2′O-TBDMS-rA(Bz) phosphoramidite (**4**) as the building blocks. The ribonucleotide, the activator solution (0.45 M tetrazole in ACN) and the oxidizer solution (0.02 M I_2 in THF/H_2O/pyridine 66/12/22, v/v/v) were all purchased from Merck Milano-Italy. The HPLC analyses were performed on a Shimadzu LC − 9A HPLC system equipped with a Shimadzu SPD − 6A VP UV − Vis detector, using a Phenomenex Luna RP18 column (5 μm particle size, 4.6 mm × 150 mm i.d.). HPLC purifications were performed on a Shimadzu LC − 8A HPLC system equipped with a Shimadzu SCL − 10A VP System control and a Shimadzu SPD − 10A VP UV − Vis detector on a Phenomenex RP Luna C18(2) semipreparative column (5 μm particle size, 250 mm × 10 mm i.d.). Mass spectrometric analyses were performed on AB SCIEX TOF/TOF 5800 in negative mode. The NMR spectra were recorded at 25 °C on an NMR spectrometer operating at 400 MHz (Bruker DRX, Bruker Advance, MA, USA).

2.4.2 Functionalization of the NovaSyn® TG support with Nucleotide units

500.0 mg of Aminomethyl NovaSyn® (0.78 meq/g, 0.39 mmol) underwent reaction at room temperature overnight with a mixture of 745.0 mg (3.78 mmol) of 4-hydroxy-3-nitrophenylacetic acid, 618 μL (3.9 mmol) of DIC, 690 μL (3.9 mmol) of DIEA,

and 611.5 mg (3.9 mmol) of N-hydroxybenzotriazole ($HOBt \cdot H_2O$) dissolved in 10 mL of anhydrous pyridine, pre-stirred for 30 min at room temperature. Following exhaustive washings with DMF, pyridine, DCM, and Et_2O, the support was dried under reduced pressure. The Kaiser test, performed on weighed samples of the dried support, estimated almost quantitative incorporation of the linker. After capping unreacted amino groups with Ac_2O/Py (1:1, v/v) for 1 h at room temperature, the support was treated with concentrated aqueous ammonia (28%) at 50 °C for 1 h.

Subsequently, 100.0 mg (0.78 meq/g, 0.078 mmol) of this support was suspended in 2.0 mL (0.9 mmol) of a commonly used "activator solution" (0.45 M tetrazole in ACN) and then added to a solution of 101 mg (0.12 mmol) of DMT-2′O-TBDMS-rU phosphoramidite (**3**) or 116 mg (0.12 mmol) DMT-2′O-TBDMS-rA (Bz) phosphoramidite (**4**). After 30 min, the support was thoroughly washed with ACN and treated (three times for 5 min) with 5 mL of a commonly used "oxidizer solution" (0.02 M I_2 in THF/H_2O/pyridine 66/12/22, v/v/v). After exhaustive washings with ACN, DCM, and Et_2O, the resulting supports were dried under reduced pressure. Complete oxidation of the phosphite triester to phosphate triester was monitored via ^{31}P NMR of the resin suspended in $CDCl_3$. Typically, a notable upfield shift was observed from 130 ppm to two signals centered at ca. −7.0 ppm. Ribonucleotide **3** or **4** incorporation yields onto resin **2** were consistently in the range of 50 – 70% (0.47 – 0.55 meq/g), as determined via quantitative DMT tests on dried and weighed samples of the supports. DMT removal was achieved through treatment with a 1% DCA solution in DCM. Following a standard capping procedure with Ac_2O/py 1:1 (v/v), phosphate deprotection from the 2-cyanoethyl group was conducted via treatment with a TEA/py solution (1:1, v/v) for 1 h at 50 °C, yielding supports **7** or **8**. Total deprotection was confirmed by a characteristic shift in the signal of the ^{31}P NMR spectrum of the solid support suspended in $CDCl_3$, from ca. δ = -7.7 ppm to δ = -5.8 ppm.

2.4.3 Synthesis and Purification of 12ab, 12a, 12b, 13ab, 13a and 13b

30 mg (0.39 meq/g, 0.012 mmol) of the dried support **7** or **8** underwent washing and swelling in anhydrous pyridine. Subsequently, it was reacted with 18 mg (0.06 mmol) of 1-mesitylenesulfonyl-3-nitro-1,2,4-triazole (MSNT) in 500 µL of anhydrous pyridine for 30 min at room temperature. 58 mg (0.12 mmol) of the selected silybins (**1ab** or **1a** or **1b**) was added, and the mixture was stirred for 6 h at room temperature. After thorough washing with pyridine, THF, and DCM, the capping procedure was conducted by treatment with Ac_2O/pyridine 1:1 (v/v) for 1 h. This procedure (coupling and capping) was repeated two times under the same conditions and for the same duration. After exhaustive washings with pyridine, THF, and DCM, the target prodrugs were detached from the support through treatment with concentrated aqueous ammonia at 50 °C for 1 h.

The crude released materials were analyzed using RP-HPLC on a Phenomenex Luna RP18 column (5 µm particle size, 4.6 mm × 150 mm i.d.) with a linear gradient of ACN in 0.1 M NH_4OAc in H_2O (pH 7.0) from 5% to 100% over 30 min with detection at 288 nm. The HPLC profiles of the detached prodrugs exhibited a single peak, typically constituting more than 85% of the total integrated area. The released material was then dried under reduced pressure and suspended in 300 mL of THF. Subsequently, 10 µL (0.06 mmol) of TEA·3HF in THF was added, and deprotection was completed in 2 h at room temperature. The crude materials were purified on a Sep-Pak RP-18 cartridge, resulting in products with a purity exceeding 95%, as confirmed by RP-HPLC analysis. In a typical experiment, starting from 30 mg of resins **7** or **8**, 5 – 7 mg of the pure compounds were obtained in good yields (41 – 50%). Finally, all compounds were converted into the corresponding sodium salts via cation exchange on a DOWEX (Na^+ form) resin.

To assess the effect of the prodrug moiety on the solubility of silybins, water solutions of prodrugs were prepared at different concentrations. The maximum concentration achieved for uridine and adenosine conjugates was 3.7 mM and 6 mM, respectively. All water solutions appeared clear and devoid of any solid particles. The absence of aggregation was confirmed through ^{1}H NMR experiments.

12ab ^{1}H NMR (400 MHz, DMSO, 25 °C, δ ppm, *J* Hz): 7.77 (1H, m, H-5 U_r); 7.15-6.75 (6H, overlapped signals, H-6', H-2'', H-2', H-5', H-6'' and H-5''); 5.95 (1H, s, H-6); 5.92 (1H, s, H-8); 5.85-5.75 (2H, overlapped signals, H-1' U_r, 3-OH); 5.70 (1H, d, *J* = 8.0, H-6 U_r); 5.11 (1H, d, *J* = 11.4, H-2); 4.92 (1H, m, H-7''); 4.64 (1H, m, H-3); 4.46-4.27 (2H, overlapped signals, H-3' U_r, H-8''); 4.11 (1H, m, H-2' U_r); 3.94 (1H, m, H-4' U_r); 3.83 (3H, s, OCH_3); 3.76-3.52 (4H, overlapped signals, H-9'' and H-5' U_r) ppm. ^{13}C NMR (100 MHz, DMSO, 25 °C, δ ppm): 198.2; 167.3; 163.7; 162.9; 151.2; 148.1; 147.5; 143.5; 140.8; 130.6; 127.5; 120.7; 117.1; 115.7; 112.0; 102.4; 100.9; 96.5; 95.5; 87.8; 84.4; 83.0; 77.0; 76.0; 73.8; 71.9; 63.8; 61.4 ppm. ^{31}P NMR (161.98 MHz, D_2O, 25 °C, δ ppm): 0.22 and 0.13 ppm. MALDI-MS (negative ions): m/z calculated for $C_{34}H_{32}N_2O_{18}P^-$ = 787.1393; found: 787.6533 [M-H]$^-$.

12a ^{1}H NMR (400 MHz, DMSO, 25 °C, δ ppm, *J* Hz): 7.86 (1H, d, *J* = 8.2, H-5 U_r); 7.10 (1H, d, *J* = 1.7, H-2'); 7.03-6.99 (2H, overlapped signals, H-2'' and H-6'); 6.95 (1H, d, *J* = 8.2, H-5'); 6.86 (1H, dd, *J* = 8.2, 1.6, H-6''); 6.79 (1H, d, *J* = 8.0, H-5''); 5.90 (1H, d, *J* = 2.0, H-6); 5.87 (1H, d, *J* = 2.0, H-8); 5.80-5.74 (2H, overlapped signals, H-1' Ur, 3-OH); 5.66 (1H, d, *J* = 8.1, H-6 U_r); 5.07 (1H, d, *J* = 11.3, H-2); 4.88 (1H, d, *J* = 7.5, H-7''); 4.60 (1H, m, H-3); 4.43-4.32 (2H, overlapped signals, H-2' Ur, H-8''); 4.10 (1H, t, *J* = 5.5, H-3' Ur); 3.94 (1H, m, H-4' Ur); 3.78 (3H, s, OCH_3); 3.71-3.52 ppm(4H, overlapped signals, H-9'' and H-5' Ur). ^{13}C NMR (100 MHz, DMSO, 25 °C, δ ppm): 198.2; 167.3; 163.7; 163.4; 162.9; 151.2; 148.1; 147.5; 143.7; 143.5; 140.8; 130.6; 127.6; 121.9; 120.8; 117.1; 116.7; 115.8; 112.1; 102.4; 100.9;

96.5; 95.5; 88.0; 84.4; 83.0; 77.0; 76.0; 73.8; 73.8; 71.8; 64.1; 61.4; 56.1 ppm. ^{31}P NMR (161.98 MHz, DMSO, 25 °C, δ ppm): 0.02 ppm. MALDI-MS (negative ions): m/z calculated for $C_{34}H_{32}N_2O_{18}P^-$ = 787.1393; found: 787.2769 $[M-H]^-$.

12b ^{1}H NMR (D_2O, 400 MHz, 25 °C, δ ppm, *J* Hz): δ = 7.77 (1H, d, *J* = 8.0, H-5 U_r), 7.00-6.75 (6H, overlapped signals, H-6', H-2'', H-2', H-5', H-6'' and H-5''), 5.95 (1H, s, H-6), 5.83-5.73 (3H, overlapped signals, H-8 SilB, H-1' and H-6 U_r), 4.87 (1H, m, H-2), 4.47-4.37 (2H, overlapped signals, H-7'' and H-3), 4.22-4.08 (3H, overlapped signals, H-2' and H-3' U_r, H-8''), 3.94 (1H, m, H-4' U_r), 3.75 (3H, s, OCH_3), 3.72-3.60 (4H, overlapped signals, H-9'' and H-5' U_r). ^{13}C NMR (D_2O, 100 MHz, 25 °C, δ ppm): δ = 196.7; 167.2; 165.8; 162.6; 162.5; 151.4; 147.7; 145.9; 143.5; 143.3; 141.6; 129.5; 127.7; 121.7; 120.8; 117.2; 116.7; 115.6; 111.5; 102.4; 101.0; 96.8; 95.6; 88.7; 83.6; 82.6; 76.5; 75.9; 73.3; 73.1; 71.8; 64.5; 60.6; 55.9 ppm. ^{31}P NMR (D_2O, 161.98 MHz, 25 °C, δ ppm): δ = – 0.93 ppm. MALDI-MS (negative ions): m/z calculated for $C_{34}H_{32}N_2O_{18}P^-$ = 787.1393; found: 787.3258 $[M-H]^-$.

13ab ^{1}H NMR (DMSO, 400 MHz, 25 °C, δ ppm, *J* Hz): δ = 8.33 (1H, s, H-2 A_d), 8.17 (1H, s, H-8 A_d), 7.13 (1H, bs, H-2'), 7.08 (1H, bs, H-2''), 7.04 (1H, complex signal, H-6'), 6.98 (1H, complex signal, H-5'), 6.90 (1H, complex signal, H-6''), 6.84 (1H, complex signal, H-5''), 5.95-5.89 (3H, overlapped signals, H-6 and H-8, H-1' A_d), 5.11 (1H, d, *J* = 11.6, H-2), 4.93 (1H, m, H-7''), 4.73-4.58 (3H, complex signals, H-2', H-3' A_d, H-3), 4.42 (1H, m, H-8''), 4.11 (1H, m, H-4' A_d), 3.80 (3H, s, OCH_3), 3.79-3.53 (4H, complex signals, H-9'' and H-5' A_d). ^{13}C NMR (DMSO, 100 MHz, 25 °C, δ ppm): δ = 198.3; 198.2; 167.2; 163.7; 162.9; 156.5; 152.7; 149.4; 148.1; 147.6; 147.5; 143.7; 143.6; 143.5; 130.7; 127.4; 122.0; 121.7; 120.8; 119.9; 117.1; 116.8; 115.8; 112.0; 100.9; 96.5; 95.5; 88.7; 88.5; 85.5; 82.9; 76.9; 76.0; 75.1; 73.5; 71.9; 64.3; 61.1; 56.0 ppm. ^{31}P NMR (DMSO, 161.98 MHz, 25 °C, δ ppm): δ = – 0.29 ppm. MALDI-MS (negative ions): m/z calculated for $C_{35}H_{33}N_5O_{16}P^-$ = 810.1665; found: 809.7322 $[M-H]^-$.

13a ^{1}H NMR (DMSO, 400 MHz, 25 °C, δ ppm, *J* Hz): δ = 8.33 (1H, s, H-2 A_d), 8.13 (1H, s, H-8 A_d), 7.06 (1H, d, *J* = 1.9, H-2'), 7.04 (1H, d, *J* = 1.7, H-2''), 6.98 (1H, dd, *J* = 8.5, 1.9, H-6'), 6.87 (1H, bs, H-6''), 6.85 (1H, bs, H-5'), 6.80 (1H, d, *J* = 8.1, H-5''), 5.84 (1H, d, *J* = 6.5, H-1' A_d), 5.77 (1H, d, *J* = 1.9, H-6), 5.74 (1H, d, *J* = 1.9, H-8), 5.02 (1H, d, *J* = 11.2, H-2), 4.88 (1H, d, *J* = 7.9, H-7''), 4.66-4.56 (2H, overlapped signals, H-2' and H-3' A_d), 4.52 (1H, d, *J* = 11.2, H-3),4.30 (1H, m, H-8''), 4.06 (1H, m, H-4' A_d), 3.78 (3H, s, OCH_3), 3.75-3.53 (4H, overlapped signals, H-9'' and H-5' A_d). ^{13}C NMR (DMSO, 100 MHz, 25 °C, δ ppm): δ = 196.8; 167.4; 163.7; 163.0; 156.1; 152.5; 149.0; 148.0; 147.2; 143.6; 143.5; 140.3; 130.7; 127.6; 121.7; 120.8; 119.6; 116.9; 116.7; 115.7; 112.0; 100.0; 96.9; 95.1; 88.7; 85.3; 82.8; 76.8; 76.0; 73.4; 72. 2; 71.7; 64.1; 61.8; 56.1 ppm. ^{31}P NMR (DMSO, 161.98 MHz, 25 °C, δ ppm): δ = 0.14 ppm. MALDI-MS (negative ions): m/z calculated for $C_{35}H_{33}N_5O_{16}P^-$ = 810.1665; found: 809.3420 $[M-H]^-$.

13b ^{1}H NMR (DMSO, 400 MHz, 25 °C, δ ppm, *J* Hz): δ = 8.36 (1H, s, H-2 A_d), 8.15 (1H, s, H-8 A_d), 7.11 (1H, d, *J* = 1.8, H-2'), 7.06 (1H, d, *J* = 1.7, H-2''), 7.03 (1H, dd, *J* = 8.6, 1.9, H-6'), 6.96 (1H, d, *J* = 8.4, H-5'), 6.89 (1H, dd, *J* = 8.3, 1.7, H-6''), 6.82 (1H, d, *J* = 8.1, H-5''), 5.91 (1H, d, *J* = 2.1, H-6), 5.88 (1H, d, *J* = 2.0, H-8), 5.87 (1H, d, *J* = 6.9, H-1' A_d), 5.07 (1H, d, *J* = 11.0, H-2), 4.91 (1H, d, *J* = 7.7, H-7''), 4.68 (1H, m, H-2' A_d), 4.63-4.57 (2H, overlapped signals, H-3 and H-3' A_d), 4.39 (1H, m, H-8''), 4.05 (1H, m, H-4' A_d), 3.78 (3H, s, OCH_3), 3.76-3.51 (4H, overlapped signals, H-9'' and H-5' A_d). ^{13}C NMR (DMSO, 100 MHz, 25 °C, δ ppm): δ = 198.2; 167.2; 163.7; 162.9; 156.5; 152.4; 149.4; 148.1; 147.5; 143.7; 143.5; 139.4; 130.7; 127.4; 121.7; 120.8; 119.8; 117.1; 116.8; 115.8; 112.0; 100.9; 96.5; 95.5; 88.4; 85.4; 82.9; 76.8; 76.0; 73.4; 72. 2; 71.9; 64.3; 62.1; 56.0 ppm. ^{31}PNMR (DMSO, 161.98 MHz, 25 °C, δ ppm): δ = – 0.29 ppm. MALDI-MS (negative ions): m/z calculated for $C_{35}H_{33}N_5O_{16}P^-$ = 810.1665; found: 809.5477 $[M-H]^-$.

2.4.4 Simulated Biological Fluid assays

For the preparation of simulated gastric fluid (sGF), sodium chloride was dissolved in bidistilled water, and the pH was adjusted to 1.2 by adding 37% aqueous HCl. Regarding simulated intestinal fluid (sIF), monopotassium phosphate was dissolved in bidistilled water, and the pH was adjusted to 6.8 by adding 0.2 M NaOH. The stability of each compound was assessed at 37 °C in both simulated fluids and monitored by RP-HPLC over time.

Each compound was dissolved to a final concentration of 1 mM in the sGF and sIF solutions. Stability was determined at 37 °C, with an aliquot of the reaction injected into the HPLC system for analysis. HPLC analyses were carried out on a Phenomenex Luna RP18 column (5 µm particle size, 4.6 mm × 150 mm i.d.), with elution in a gradient of B (ACN/A 95:5) in A (0.10 M NH_4OAc) from 20% to 100% over 10 min on a Phenomenex Luna RP18 column at a flow rate of 0.8 mL/min (λ = 288 nm).

2.4.5 Alkaline Phosphatase assay

All compounds were dissolved to a final concentration of 1 mM in 20 mM Tris-HCl (pH 7.4). The rate of hydrolysis in ALP solution was determined at 37 °C with the addition of 40 U of ALP (from bovine intestinal mucosa, 2.745 u/mg protein) to a prodrug solution (0.5 µmol) in 500 µL of the buffer solution. At each timepoint, an aliquot of the reaction (30 µL) was withdrawn, and 120 µL of MeOH was added to halt the enzymatic hydrolysis. After centrifugation (13000 rpm, 15 min), the samples (70 µL) were analyzed on a Shimadzu LC-9A HPLC system equipped with a Shimadzu SPD-6A UV/Vis detector. HPLC analyses were carried out on a Phenomenex Luna RP18 column (5 µm particle size, 4.6 mm × 150 mm i.d.) eluted in a gradient of solvent B (ACN/A 95:5) in solvent A (0.10 M NH_4OAc) from 20% to 100% over 15 min on a Phenomenex Luna RP18 column at 0.8 mL/min (λ = 288 nm).

2.4.6 RNase assay

All compounds were dissolved to a final concentration of 1 mM in a 50 mM imidazole (Im) buffer at pH 6.0, containing NaCl (0.10 M). RNase A was dissolved in Im buffer or simulated intestinal fluid (sIF) buffer to a final concentration of 1.3×10^{-4} mM (~2 mg/L) and added to a solution of samples (final concentration 1 mM) at 37 °C with a total volume of 500 µL. All samples were eluted in a gradient of solvent B in solvent A from 5% to 100% over 10 min on a Phenomenex Luna RP18 column (5 µm particle size, 4.6 mm × 150 mm i.d.) at 0.8 mL/min (λ = 288 nm) to record the retention time course of each prodrug before hydrolysis. Buffer A was 0.10 M NH_4OAc in H_2O, and buffer B was 0.10 M NH_4OAc in ACN/ NH_4OAc 95:5. At each timepoint, an aliquot of the reaction (30 µL) was withdrawn, and 120 µL of MeOH was added to stop enzymatic hydrolysis. After centrifugation (13000 rpm, 15 min), the samples (70 µL) were analyzed on a Shimadzu LC-9A HPLC system equipped with a Shimadzu SPD-6A UV/Vis detector. HPLC analyses were carried out on a Phenomenex Luna RP18 column (5 µm particle size, 4.6 mm × 150 mm i.d.). These experiments were repeated to analyze the stability of the prodrugs (1 mM) in the absence of RNase A in a 50 mM Im buffer, pH = 6.0.

2.4.7 MTT assay

Neuroblastoma cells, SH-SY5Y, were cultured in DMEM-F12 (Gibco, Thermofisher), supplemented with 10% heat-inactivated (HI) fetal calf serum (Gibco, Thermofisher), 100 mg/mL penicillin and streptomycin (Gibco, Thermofisher), and 2 mM L-glutamine at 37 °C and 5% CO_2. Two weeks before the experiments, 5×10^3 cells were seeded on 96-well plates in DMEM-F12 with 5% HI fetal calf serum. The percentage of serum gradually decreased until it reached 1% of the total. To induce neuronal differentiation, 5 µM all-trans-retinoic acid (RA) was used, and the medium containing RA was changed every 3 days. Treatments with Sil (**1ab**), SilA (**1a**), SilB (**1b**), and their ribonucleotide conjugates (**12ab**, **12a**, **12b**, **13ab**, **13a**, and **13b**) were

performed on fully differentiated cells at different concentrations. All compounds were dissolved in DMSO, maintaining the final DMSO concentration under 0.4%. After 48 h of treatment, the cell cultures were incubated with MTT (0.5 mg/mL) for 2 h at 37°C and then lysed with DMSO, and the formazan production was evaluated in a plate reader through absorbance at 570 nm.

3 Silybins Dimers

The main characteristic of flavonoids is the acclaimed ability to "capture" Reactive Oxygen Species (ROS), known to have deleterious effects on human health. Their antioxidant activity is frequently cited to be the key property underlying the prevention and/or reduction of oxidative stress-related chronic diseases and age-related disorders such as cardiovascular diseases, carcinogenesis, neurodegeneration, and many others. Today, however, there are many studies that suggest the implication of other properties in addition to the antioxidant capacity in their therapeutic activity.[6] In particular, the high structural diversity of polyphenols, as well as their different stereochemistry, can affect the binding mode with various target proteins.[7] In this frame, there has been an increasing interest in dimeric flavonoids (*bi*-flavonoids), characterized by the presence of two linked flavonoid units from an alkyl or alkoxy linker.[8] *Bi*-flavonoids of natural origin, present in many fruits, vegetables and plants, are associated with a multitude of biological properties (anti-cancer, anti-inflammatory, anti-microbial, anti-viral, anti- coagulants, anti-bacterial, anti-fungal and anti-oxidants) and in several cases their bioactivity is greater than their respective monomers.[9] Furthermore, it has been reported that *bi*-flavonoids of synthetic origin possess interesting biological activities, similar to those of products of natural origin.

3.1 Aim of Research Work

Recently, it was reported the synthesis and antioxidant activity of *bi*-flavonoids based on silibinin.[10] The new dimers, linked through a phosphodiester bond in position 3 – 3, 3 – 9" and 9" – 9", have displayed high ability to scavenge ROS, such as singlet oxygen ($^1O_2$) and hydroxyl radical (HO•), comparable to the value reported for known potent antioxidants such as quercetin. Given these results, it seemed interesting to investigate the structure–activity relationships of dimer 9" – 9", which turned out to

be the best one, starting from diastereoisomerically pure silybin monomers (SilA **1a** and SilB **1b**, Figure 3.1)

In this regard, this study reports the synthesis of new 9" – 9" phosphodiester dimers, obtained from pure silybins, and the investigation of their radical scavenger ability and the antiproliferative activity on different cell lines.

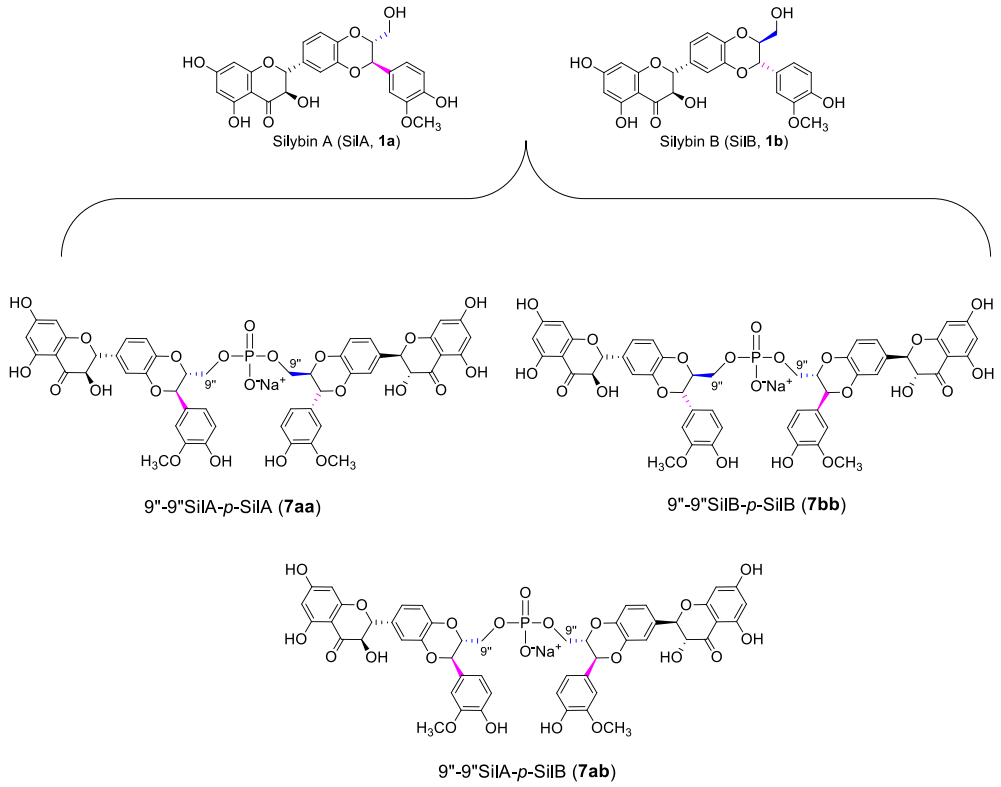

Figure 3.1. Synthesis of new silybins dimers.

3.2 Results and Discussion

Silybin (**1a** or **1b**) was initially converted into the corresponding 9"-dimethoxytriphenylmethylether (**2a** or **2b**, Scheme 3.1) by reaction with DMT-Cl, in dry pyridine, at room temperature, obtaining, after chromatographic purification, a yield of 88-94% (for **2a** and **2b**, respectively).

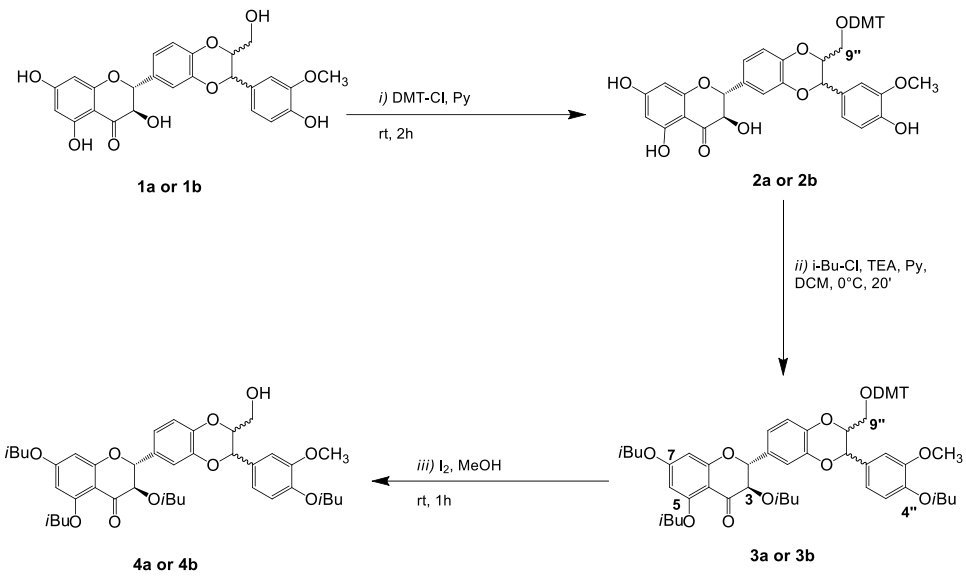

Scheme 3.1. Synthesis of silybins building blocks **4a** and **4b**.

Subsequently the remaining OH functions were protected with isobutyryl (*i*Bu) groups, orthogonal to DMT, using isobutyryl chloride, triethylamine (TEA) and pyridine, in dry dichloromethane (DCM) at 0 °C obtaining, after appropriate chromatographic purification, 3,5,7,4"-tetra-*O*-isobutyryl-9"-*O*-(4,4'-dimethoxytriphenyl)-silybin (**3a** or **3b**), in a yield of 92-86%, respectively. Compound **3a** (or **3b**) was therefore treated with a 1% (w/v) mixture of I_2 in MeOH in order to selectively remove the temporary DMT protecting group. The compound **4a** (or **4b**) was obtained with a yield of 78% (84% for **4b**) and the structures were confirmed by

^{1}H and ^{13}C NMR analysis. The 3,5,7,4"-tetra-*O*-isobutyryl-silybin-9"-phosphoramidite (**5a** or **5b**) (Scheme 3.2), a key intermediate for the synthesis of the new derivatives, was obtained starting from silybin building block **4a** or **4b** which was reacted, in an anhydrous conditions, with 2-cyanoethyl-N,N-diisopropylamino-chlorophosphoramidite and diisopropylethylamine (DIEA) in DCM, at room temperature.

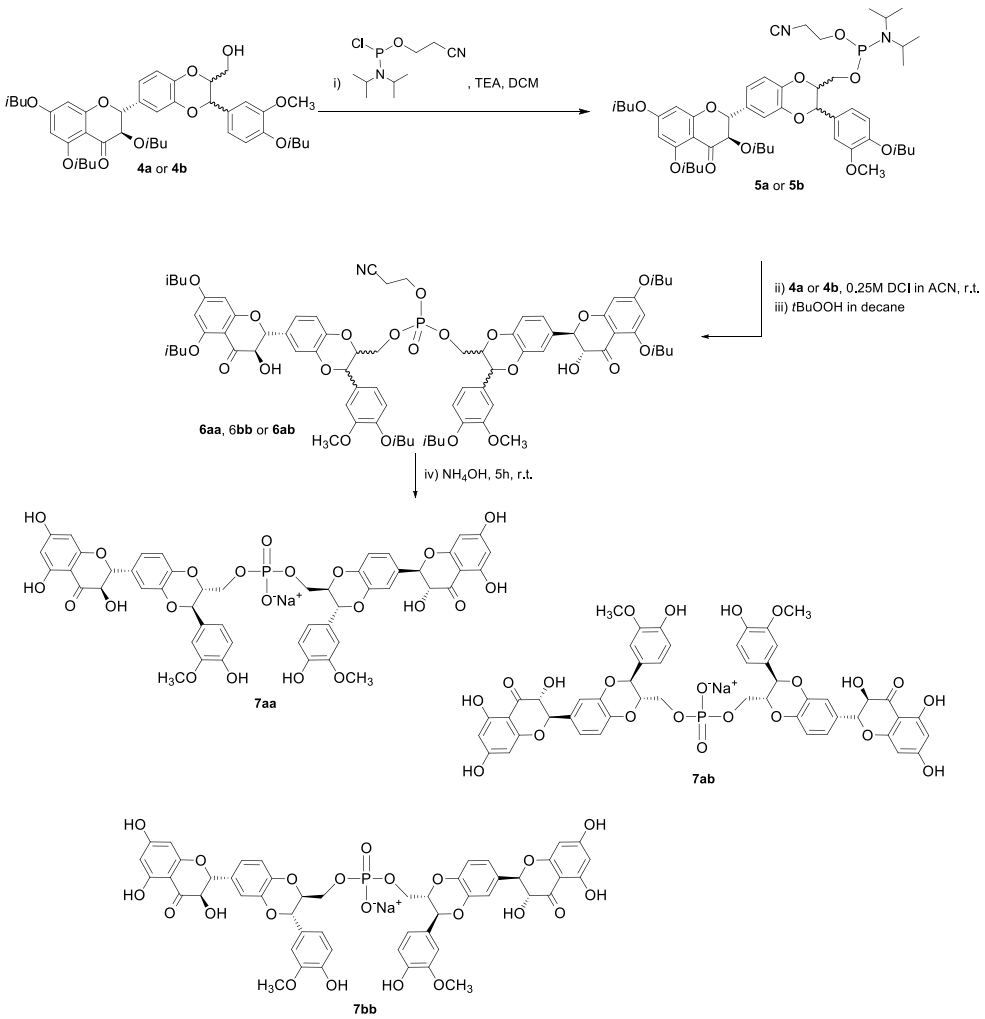

Scheme 3.2. Synthesis of 9"-9" linked-phosphate silybin dimers **7aa**, **7bb** and **7ab**.

The products were purified on silica gel, obtained with a yield of 86% (**5b**, 80%) and the structures were confirmed by ^{1}H and ^{13}C NMR analysis. These were then coupled with building blocks **4a** and **4b** in the presence of 4,5- dicyanoimidazole (DCI) in ACN. For the synthesis of the heterodimer SilA-*p*-SilB, the best yield was observed by coupling silybin A phosphoramidite **5a** and the protected silybin B (**4b**). After one-pot oxidation of the triester phosphite to phosphate with *t*ButOOH in decane, the phosphotriester dimers were purified and obtained in good yields (**6aa** 83%, **6bb** 80% and **6ab** 77%). Treatment with NH_4OH finally led to complete deprotection, and after RP-HPLC purification, dimers **7aa**, **7bb** and **7ab** were obtained in 77%, 82% and 80% yield, respectively.

3.2.1 Radical Scavenger Activities (OH·)

Biologically, the hydroxyl radical (HO•) is widely believed to be generated when hydrogen peroxide reacts with Fe(II) (Fenton reaction). The putative HO•·is an extremely reactive and short-lived species that can damage DNA, proteins, and lipids. However, the Fe(II)/H_2O_2 mixture has disadvantages in a scavenging assay because many flavonoids as well as flavonolignans are also metal chelators. When the sample is mixed with Fe(II), it may alter the activity of Fe(II) by chelation. As a result, it is impossible to distinguish if the antioxidants are simply good metal chelators or HO• scavengers.

In this study, the second-order rate constants for HO• reactions with silybin dimers (**7aa**, **7bb**, and **7ab**) have been determined by pulse photolysis method using hydrogen peroxide (H_2O_2) as ROS sources.[11] The reactivity towards HO• was determined to be in the same order of magnitude for dimers **7aa**, **7bb**, and **7ab** (Table 3.1), always remaining significantly greater than dimers 3-3 and 3-9". This could be explained considering that in dimers 9"-9" the 3, 5, and 4" OH functions, responsible for the radical scavenger activity, are not involved in any bond. In fact, the influence of the individual hydroxy groups of silibinin (**1ab**) on its antioxidant and radical scavenging

properties were studied in detail and the findings led to the conclusion that the 3, 5, and 4" phenolic moieties as well as the 3-OH group are essential for the compounds' radical-scavenging properties.[12,13]

Table 3.1. Second order rate constant $k^{II}_{HO^{\bullet},X}$ of silybin phosphodiester dimers **7aa**, **7bb** and **7ab**.

Compound	$k^{II}_{HO^{\bullet},X}$ ($M^{-1}\cdot s^{-1}$)[a]
7aa	$8.63 \pm 1.35 \times 10^{9}$
7bb	$1.01 \pm 0.16 \times 10^{10}$
7ab	$1.48 \pm 0.09 \times 10^{10}$

[a]: calculated in H_2O

3.2.2 In Vitro Antiproliferative Activity

The anti-cancer effectiveness of silibinin, primarily attributed to its impact on proliferation, apoptosis, inflammation, angiogenesis, and other cancer-modulating mechanisms, is evident from recent publications. Despite the considerable interest in the properties of this flavonolignan, notable for its non-toxic nature, there remains a need for pharmacological investigations on the two diastereoisomers, silybins A and B, to establish a comprehensive structure-activity profile.

To address this, the anti-proliferative effects of silibinin compounds were evaluated on various human tumor cell lines with distinct histological origins and metastatic potentials. Human dermal fibroblasts (HDFs) are used as healthy cells for assessing the compounds' selectivity towards tumor cells. Preliminary screening involved treating cells with concentrations of 10 and 50 μM for 48 h to identify the most responsive cell lines.

Results indicate that the dimers exhibited activity against Jurkat, A375, WM266, and HeLa cells, while showing no interference with the growth of PANC, MCF-7, HDF, or U87 at the tested concentrations (Figure 3.2). This highlights a noteworthy tumor cell selectivity, a critical aspect for therapeutic compound optimization. Jurkat cells, derived from leukemia, displayed significant activity even at the lowest concentration (10 μM), with a proliferation reduction of approximately 20%, escalating to over 40% at 50 μM. Interestingly, dimers exhibited greater activity than monomers on melanoma cell lines (WM266 and A375) (Figure 3.2).

Subsequent dose-response curves and IC_{50} values calculation focused on the leukemia cell line Jurkat, which was more sensitive to compound treatment. Despite the similarity in IC_{50} values for all tested molecules (Table 3.2), SilB emerged as the most active compound with an IC_{50} of 36 μM. Importantly, all molecules demonstrated low activity on HDFs, pointing out their selectivity towards tumor cells. Monomers displayed an IC_{50} of approximately 200 μM, while dimers exhibited even greater selectivity with higher IC_{50} values (Figure 3.3).

These findings are notable considering that in analogous experiments, silibinin compounds are typically employed at concentrations up to 300 μM.[14] Significantly, the identification of a low toxicity molecule in healthy cells is a valuable outcome.

Given that silibinin's cytotoxic effect is known to activate the apoptotic pathway, further investigation was conducted to ascertain whether dimers induce apoptosis to a similar extent as their corresponding monomers. To investigate this further, Jurkat cells were exposed to the molecules at a concentration of 200 μM, and flow cytometric analysis using annexin V/propidium iodide (PI) double staining was conducted. The findings reveal that **7aa** and **7ab** could induce apoptosis comparably to the monomers, albeit with a lower percentage of apoptotic cells.

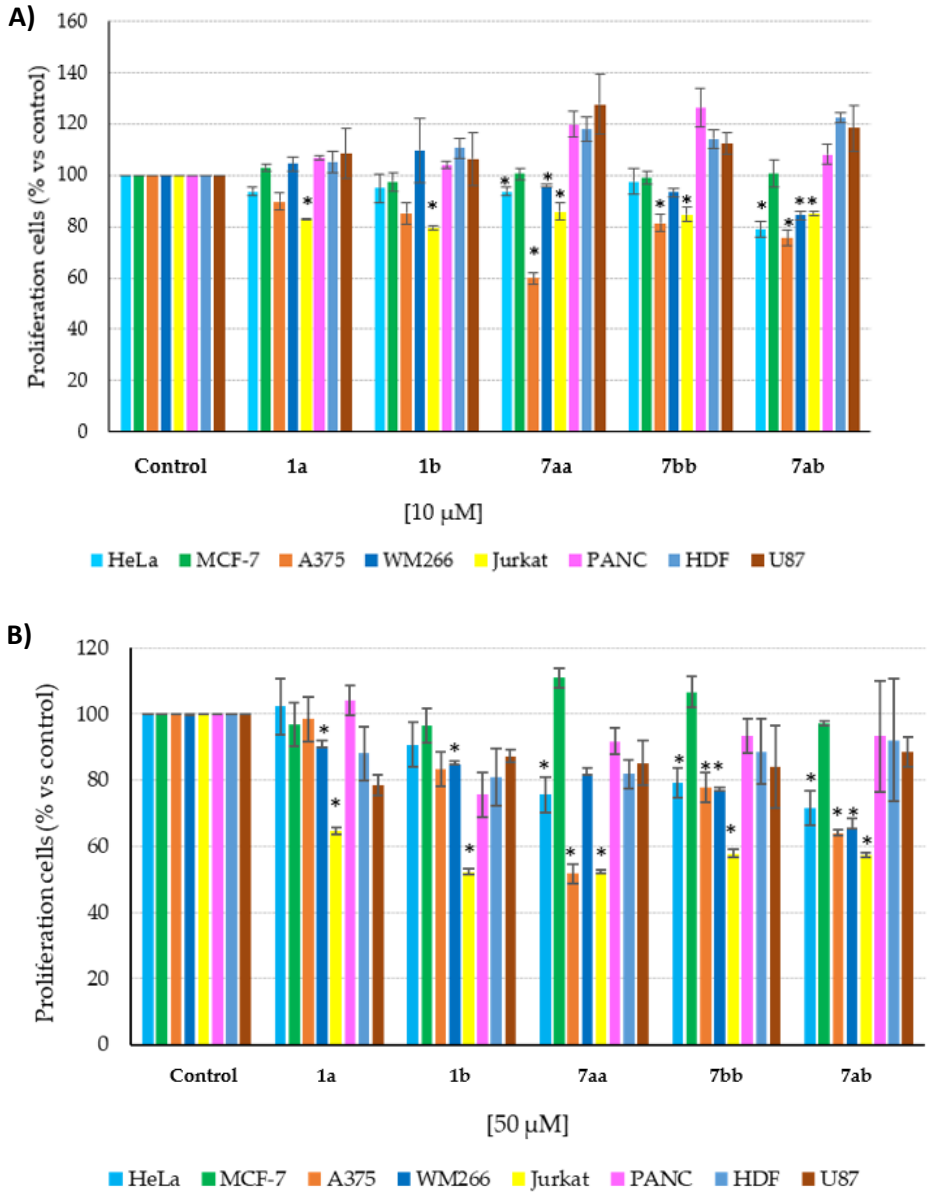

Figure 3.2. Effect of compounds on tumor and healthy cell proliferation. The cells were incubated in the presence of the compounds at 10 μM or 50 μM for 48 h at 37 °C. The results are presented as the percentage of proliferating cells with respect to the control (vehicle-treated cells) and are expressed as means ± SE, * $p < 0.05$.

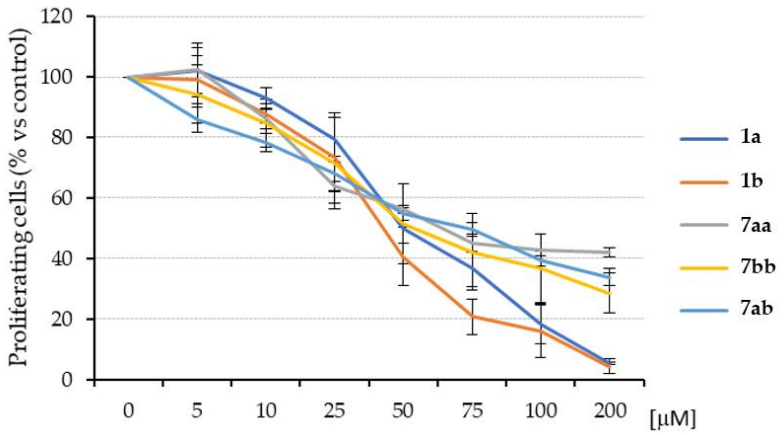

Figure 3.3. Dose–response curves obtained using the indicated concentrations of compounds on responsive cells. The proliferation was determined by CCK8 assay. The results are presented as the percentage of proliferating cells compared to the control (vehicle-treated cells) and are expressed as means ± SE of two independent experiments performed in triplicate.

Table 3.2. IC_{50} values of compounds after 48 h incubation.

	IC_{50} ± DS (μM)				
	1a	**1b**	**7aa**	**7bb**	**7ab**
Jurkat	46.7 ± 14.1	36 ± 14.3	71 ± 15.5	59 ± 19.9	64 ± 10.8
HDF	199 ± 34.5	172 ± 39.0	>200	>200	>200

Specifically, 20% of cells treated with **7aa** exhibited apoptosis (both early and advanced stages) compared to the control, and **7ab** showed approximately 25% apoptotic cells (early and advanced). In contrast, 70% of cells treated with **1a** or **1b** underwent apoptosis (Figure 3.4). Intriguingly, **7bb** did not induce apoptosis, with only 4% of treated cells displaying apoptotic features compared to the control (Figure 3.4). These results suggest not only a probable difference in the mechanism of action between the dimers and monomers but also variability among the dimers themselves. This unerlines the significance of molecules' stereochemistry, implying that it could

influence the activity of silibinin compounds through specific and selective interactions with protein partners.

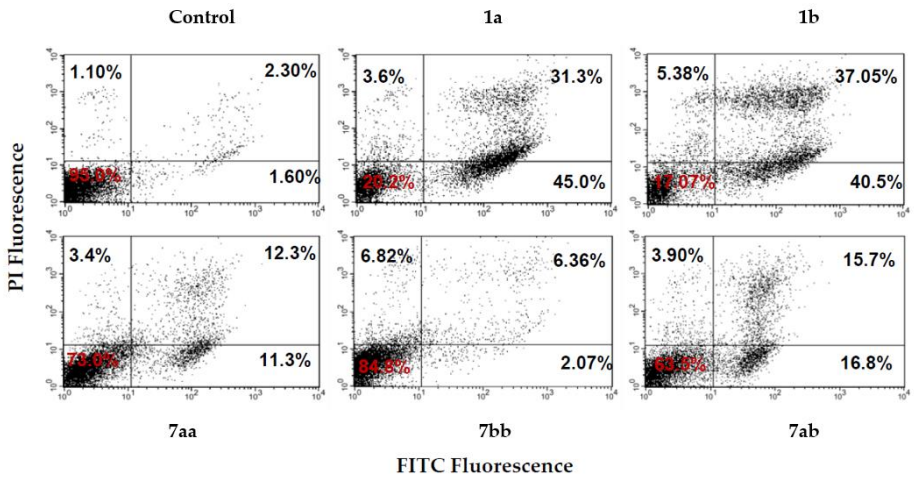

Figure 3.4. Apoptosis analysis with annexin V-FITC/PI double-staining method on Jurkat cells. The cells were treated with the indicated compounds at a concentration of 200 µM at 37 °C for 48 h. The control is the vehicle-treated sample. Lower left quadrant: viable cells; upper left: necrotic cells; upper right: advanced apoptotic cells; lower right: early apoptotic cells. This picture is representative of two independent experiments.

3.3 Conclusions

This study presents the synthesis of optically pure phosphodiester dimers of silybins using a highly efficient synthetic approach, employing orthogonal protection of various hydroxyl groups. Through the use of phosphoramidite chemistry and starting from the two distinct diastereoisomers, the novel 9"-9" dimers of silybin A and silybin B (**7aa**, **7ab**, and **7bb**) were successfully synthesized, demonstrating high purity and good yields. Their notable capability to scavenge reactive oxygen species (ROS), specifically the hydroxyl radical (HO•), highlights the substantial antioxidative activity of all three dimers, comparable to the potency exhibited by the well-known antioxidant quercetin. Despite being diastereomers, **7aa**, **7ab**, and **7bb** exhibit remarkably similar radical scavenger activity.

To elucidate a structure-activity relationship, a preliminary screening involving treatment of cells with concentrations of 10 and 50 μM for 48 h was conducted for both monomers (**1a** and **1b**) and dimers (**7aa**, **7ab**, and **7bb**). The results reveal that both monomers and dimers display selective anti-proliferative activity against leukemia cells at the concentrations employed, with all silybin compounds exhibiting comparable IC_{50} values in the mid-micromolar range. Importantly, these compounds demonstrated low activity on normal cells.

However, the cytotoxic mechanisms employed by the various silybin compounds appear to differ. Cells treated with monomers undergo complete apoptosis, whereas only a portion of cells treated with **7aa** and **7ab** were found to be in the apoptotic stage. In contrast, treatment with the **7bb** dimer did not lead to a significant number of cells in the apoptotic stage. These results underscore the pivotal role of stereochemistry in the activation of the apoptotic mechanism for these flavonolignans, offering a new avenue for in-depth investigations into the interactions of such compounds with proteins involved in cancer metabolic pathways.

3.4 Experimental Session

3.4.1 General Methods

All chemicals were purchased from Sigma–Aldrich (Milano, Italy). HPLC–grade ACN and MeOH were purchased from Carlo Erba Reagents and Sigma-Aldrich, respec- tively. Reactions were monitored by TLC (F254 precoated silica gel plates, Merck) and column chromatography (Merck Kieselgel 60, 70–230 mesh, Milano, Italy). HPLC analysis of dimers 6aa, 6bb and 6ab, was performed with a Shimadzu LC–8A PLC system (Shi- madzu Analytical and Measuring Instruments, Milano, Italy) equipped with a Shimadzu SCL–10A VP System control and a Shimadzu SPD–10A VP UV–Vis detector. Mass spectrometric analyses were performed on AB SCIEX TOF/TOF 5800 in positive or negative mode and Waters Micromass ZQ Instrument (Waters, Milano, Italy) equipped with an electrospray source in positive mode. The NMR spectra were recorded at 25 °C on an NMR spectrometer Bruker DRX, Bruker Advance (Bruker Italia Srl, Milano, Italy).

3.4.2 Synthesis of Silybins Building Blocks

9"-*O*-(4,4'-dimethoxytrityl) silybin (2a or 2b). Silybin A **1a** (or silybin B, **1b**) (1.075 g, 2.228 mmol), previously dried by repeated coevaporation with anhydrous THF, was dissolved in 10 mL of anhydrous pyridine and 4,4'-dimethoxytriphenylmethylchloride (906 mg, 2.674 mmol) was added to the solution. The mixture was kept under stirring at room temperature and the reaction was monitored by TLC using DCM/MeOH 98:2 (v/v) as eluent system. After 3 h, with the disappearance of the initial substrate (**1a** or **1b**), the reaction was stopped by adding 2 mL of MeOH. The crude was extracted three times with water and DCM. The organic phase was dried with anhydrous sodium sulphate, filtered, concentrated by rotavapor evaporation at reduced pressure and dried *in vacuo*. Subsequently the crude was purified by silica gel column chromatography (DCM/MeOH 98:2, v/v, with increasing

methanol gradient, with 0.5% pyridine), obtaining product **2a** or **2b** (1.54g, 88% and 1.64 g, 94%, respectively).

3,5,7,4"-tetra-*O*-isobutyryl-9"-*O*-(4,4'-dimethoxytrityl) silybin (3a or 3b). The 9"-*O*-dimethoxytrityl silybin (**2a** or **2b**) (419 mg, 0.534 mmol) was dried by repeated coevaporation with dry DCM and solubilized in 15 mL of dry DCM. Subsequently, it was added pyridine (0.432 mL, 5.34 mmol) and TEA (0.311 mL, 2.24 mmol) at 0 °C, and after a few min, isobutyryl chloride (0.236 mL, 2.24 mmol). The reaction mixture was kept under stirring for 1 h, at 0 °C. After control by TLC, using hexane/EtOAc 7:3 (v/v) as the eluent system, the reaction was stopped by the addition of 2 mL of MeOH at 0 °C. The mixture was transferred into a separating funnel and extracted for 3 times with water and DCM. The organic phase was dried with anhydrous sodium sulfate, filtered, concentrated by rotavapor evaporation at reduced pressure and dried *in vacuo*, subsequently the crude was purified by silica gel column chromatography (hexane/EtOAc 7:3, v/v, with 0.5% pyridine), obtaining product **3a** or **3b** (524 mg, 92% and 489 mg, 86% respectively).

3,5,7,4"-tetra-*O*-isobutyryl silybin (4a or 4b). 3,5,7,4"-tetra-*O*-isobutyryl-9"-*O*-(4,4'-dimethoxytrityl) silybin (**3a** or **3b**) (481 mg, 0.451 mmol) was treated by repeated coevaporation with toluene and solubilized in 0.750 mL of DCM. Subsequently, I_2 (45 mg, 0.177 mmol) previously dissolved in MeOH (4.5 mL, 0.451 mmol) was added. The reaction mixture was kept under stirring for 1 h. After control by TLC, using hexane/EtOAc 6:4 (v/v) as the eluent system, having verified the disappearance of **3a** or **3b**, the reaction was stopped by adding $Na_2S_2O_3$ until the mixture was discolored. The crude was transferred into a separating funnel and extracted three times with water and DCM. The organic phase was dried with anhydrous sodium sulfate, filtered, concentrated by evaporation in the rotavapor at reduced pressure and dried *in vacuo*. and subsequently purified by silica gel column

chromatography (hexane/EtOAc 7:3, v/v, with increasing gradient of EtOAc), recovering product **4a** or **4b** (268 mg, 78%, and 289 mg, 84%, respectively).

4a ^{1}H-NMR (400 MHz, $CDCl_3$, 25 °C, δ ppm, J Hz): δ = 7.13–6.96 (complex signals, 6H, H-2', H-5', H-6', H-2", H-5", H-6"); 6.74 (d, *J* = 2.2, 1H, H-6); 6.55 (d, *J* = 2.2, 1H, H-8); 5.66 (d, *J* = 12.2, 1H, H-3); 5.35 (d, *J* = 12.2, 1H, H-2); 5.02 (d, *J* = 8.0, 1H, H-7"); 4.02–3.97 (m, 1H, H8"); 3.87–3.82 (overlapped signals, 4H, OCH_3 and H-9"a); 3.57 (dd, *J* = 12.5, 3.6, 1H, H-9"b); 2.97–2.71 (m, 3H, CH of isobutyryl groups in 5, 7 and 4"); 2.59–2.49 (m, 1H, CH of isobutyryl group in 3); 1.37–1.22 (m, 18H, CH_3 of isobutyryl groups in 5, 7 and 4"); 1.12–0.97 (m, 6H, CH_3 of isobutyryl group in 3). ^{13}C NMR (100 MHz, $CDCl_3$, 25 °C, δ ppm): δ = 185.0; 175.3; 175.0 (x2); 174.1; 162.4; 156.5; 151.7; 151.6; 144.1; 143.6; 140.5; 134.5; 128.6; 123.0; 120.8; 119.8; 117.0, 116.5, 111.1 (x2); 110.7; 108.7; 81.1; 78.3; 76.0; 72.9; 61.4; 56.1; 34.2; 34.0; 33.9; 33.6; 19.0; 18.8; 18.7; 18.5. MS (MALDI-TOF, positive ions): m/z calculated for $C_{41}H_{46}O_{14}$ = 762.289; found: 763.996 $[M+H]^+$, 785.229 $[M+Na]^+$, 801.652 $[M+K]^+$.

4b ^{1}H NMR (400 MHz, $CDCl_3$, 25 °C, δ ppm, J Hz): δ = 7.11–6.96 (complex signals, 6H, H-2', H-5', H-6', H-2", H-5", H-6"); 6.75 (d, *J* = 2.2, 1H, H-6); 6.55 (d, *J* = 2.2, 1H, H-8); 5.67 (d, *J* = 12.1, 1H, H-3); 5.36 (d, *J* = 12.2, 1H, H-2); 5.04 (d, *J* = 8.0, 1H, H-7"); 4.02–3.97 (m, 1H, H8"); 3.86–3.80 (overlapped signals, 4H, OCH_3 and H-9"a); 3.56 (dd, *J* = 12.4, 3.6, 1H, H-9"b); 2.96–2.73 (m, 3H, CH of isobutyryl groups in 5, 7 and 4"); 2.60–2.50 (m, 1H, CH of isobutyryl group in 3); 1.35–1.26 (m, 18H, CH_3 of isobutyryl groups in 5, 7 and 4"); 1.02–0.92 (m, 6H, CH_3 of isobutyryl group in 3) ppm. ^{13}C NMR (100 MHz, $CDCl_3$, 25 °C, δ ppm): δ = 185.0; 175.1; 175.0 (2C); 174.1; 162.4; 156.5; 151.7; 151.6; 144.1; 143.6; 140.6; 134.5; 128.5; 123.1; 120.9; 119.7; 117.1, 116.4, 111.3; 111.1; 110.8; 108.7; 81.0; 78.3; 75.9; 72.8; 61.4; 56.0; 34.2; 34.0; 33.9; 33.6; 19.0; 18.8; 18.7; 18.5 ppm. MS (MALDI-TOF, positive

ions): m/z calculated for $C_{41}H_{46}O_{14}$ = 762.289; found: 763.425 $[M+H]^+$, 785.784 $[M+Na]^+$, 801.358 $[M+K]^+$.

3.4.3. Synthesis of Phosphoramidite Silybins

To 3,5,7,4"-tetra-*O*-iBu-silybin (**4a** or **4b**) (0.26 mmol; 200 mg) dissolved in anhydrous DCM (4.5 mL), DIEA (181 µL, 1.05 mmol), and 2-cyanoethyl-N,N-diisopropylamino- chlorophosphoramidite (73 µL, 0.31 mmol) were mixed. After 20 min the solution was concentrated and silica gel chromatography of the residue (eluent n-hexane/EtOAc 6:4, v/v, with 3% v/v of TEA), afforded desired compound **5a** or **5b** in yields of 86% and 80% respectively.

5a ^{1}H NMR (400 MHz, $CDCl_3$, 25 °C, δ ppm, *J* Hz): δ = 7.11–6.94 (complex signals, 6H, H-2', H-5', H-6', H-2", H-5", H-6"); 6.74 (d, *J* = 2.2, 1H, H-6); 6.55 (d, *J* = 2.2, 1H, H-8); 5.66 (d, *J* = 12.2, 1H, H-3); 5.65 (d, *J* = 12.2, 1H, H-3); 5.35 (d, *J* = 12.2, 1H, H-2); 5.34 (d, *J* = 12.2, 1H, H-2); 5.02 (d, *J* = 7.8, 1H, H-7"); 4.14–4.06 (m, 1H, H-8"); 3.97–3.49 (m, 9H, OCH_3, 2H-9", $O\underline{CH_2}CH_2CN$, $N[\underline{CH}(CH_3)_2]_2$; 2.97–2.48 (m, 6H, CH of isobutyryl groups, $OCH_2\underline{CH_2}CN$); 1.36–1.26 (m, 18H, CH_3 of isobutyryl groups in 5, 7 and 4"); 1.20–1.07 (m, 15H, CH_3 of isobutyryl groups in 3, $N[CH(\underline{CH_3})_2]_2$) ppm. ^{13}C NMR (100 MHz, $CDCl_3$, 25 °C, δ ppm): δ = 185.0 (x2); 175.2 (x2); 175.0 (x2); 174.1; 162.5; 156.5; 151.7; 151.5 (x2); 144.2; 143.5; 143.4; 140.5(x2); 134.6; 128.3; 128.2; 123.0; 122.9; 120.9; 120.8; 119.9; 119.8; 117.6; 117.5; 117.1; 116.9; 116.5; 116.4; 111.4; 111.2; 111.1; 110.7, 108.7; 81.2; 81.1; 76.2; 75.8; 72.9 (x2); 62.5; 62.2; 62.0; 58.7; 58.6; 58.5; 58.3; 56.0 (x2); 43.3; 43.2; 34.2; 34.0; 33.9; 33.6; 24.6; 24.5; 20.4; 20.3 (x3); 19.0; 18.8; 18.7; 18.5 ppm. ^{31}P NMR ($CDCl_3$, 161.98 MHz, 25 °C, δ ppm): δ = 150.3; 149.9 ppm. MS (MALDI-TOF, positive ions): m/z calculated for $C_{50}H_{63}N_2O_{15}P$ = 962.397; found: 964.229 $[M+H]^+$, 986.033 $[M+Na]^+$, 1002.553 $[M+K]^+$.

5b ^{1}H NMR (400 MHz, $CDCl_3$, 25 °C, δ ppm, *J* Hz): δ = 7.11-6.94 (complex signals, 6H, H-2', H-5', H-6', H-2", H-5", H-6"); 6.75 (d, *J* = 2.2, 1H, H-6); 6.55 (d, *J* = 2.2, 1H, H-8); 5.67 (d, *J* = 12.1, 1H, H-3); 5.35 (d, *J* = 12.1, 1H, H-2); 5.34 (d, *J* = 12.1, 1H, H-2); 5.02 (d, *J* = 7.8, 1H, H-7"); 4.14–4.05 (m, 1H, H-8"); 3.97–3.50 (m, 9H, OCH_3, 2H-9", $O\underline{CH_2}CH_2CN$, $N[\underline{CH}(CH_3)_2]_2$; 2.96–2.49 (m, 6H, CH of isobutyryl groups, $OCH_2\underline{CH_2}CN$); 1.36–1.26 (m, 18H, CH_3 of isobutyryl groups in 5, 7 and 4"); 1.20–1.07 (m, 15H, CH_3 of isobutyryl groups in 3, $N[CH(\underline{CH_3})_2]_2$) ppm. ^{13}C NMR (100 MHz, $CDCl_3$, 25 °C, δ ppm): δ = 185.0; 175.1 (x2); 175.0; 174.9; 174.1; 162.4; 156.5; 151.7; 144.3; 144.2; 143.5 (x2); 140.5 (x2); 134.7; 128.2; 128.1; 123.0; 122.9; 121.0; 119.9; 119.8; 117.6; 117.5; 117.1; 116.5; 116.3; 111.1; 110.8, 108.7; 81.1; 81.0; 76.1; 75.8; 72.8; 62.7; 62.5; 62.2; 62.1; 58.7; 58.5 (x2); 58.3; 56.0 (x2); 43.3; 43.2; 34.2; 34.0; 33.9; 33.6; 24.6 (x2); 24.5 (x2); 20.3 (x3); 19.0; 18.8; 18.7 (x3); 18.5 ppm. ^{31}P NMR ($CDCl_3$, 161.98 MHz, 25 °C, δ ppm): δ = 150.2; 149.8 ppm. MS (MALDI-TOF, positive ions): m/z calculated for $C_{50}H_{63}N_2O_{15}P$ = 962.397; found: 964.215 $[M+H]^+$, 986,212 $[M+Na]^+$, 1002.322 $[M+K]^+$.

3.4.4 General Procedure for the Synthesis of Phosphotriester Dimers 6aa, 6bb and 6ab

For the synthesis of **6aa**, 219 mg (0.22 mmol) of phosphoramidites **5a** and the building block **4a** 155 mg (0.20 mmol) previously dried and kept under reduced pressure, were reacted with a 0.25 M DCI solution in anhydrous ACN (1.5 mL, 0.37 mmol). To obtain the **6bb** dimer, the phosphoramidite **5b** and the derivative **4b** were coupled under the same conditions as previously reported. For the **6ab** dimer, the best yields were obtained by coupling the phosphoramidite **5a** and the derivative **4b**. The reaction was left under stirring at RT and monitored by TLC with an eluent system hexane/EtOAc (6:4, v/v). After 30 min, the reaction was over, and then a 5.5 M tert-Butyl hydroperoxide (tButOOH) solution in decane (150 µL) was added and left stirring at RT. After 30 min the reaction mixture was concentrated under reduced

pressure, and purified by flash chromatography, eluting with hexane/EtOAc (7:3, v/v), to afford pure **6** (**6aa**, **6bb** and **6ab**) yellow-brown amorphous powder in 83%, 80% and 77% yields, respectively.

6aa ^{1}H-NMR (400 MHz, $CDCl_3$, 25 °C, δ ppm, *J* Hz): δ = 7.11–6.91 (complex signals, 12H, H-2', H-5', H-6', H-2", H-5", H-6"); 6.76 (s, 2H, H-6); 6.55 (s, 2H, H-8); 5.66 (d, *J* = 12.1, 2H, H-3); 5.36 (d, *J* = 12.1, 2H, H-2); 4.93 (t, *J* = 8.0, 2H, H-7"); 4.32–3.95 (m, 8H, H8", 2H9", O$\underline{CH_2}CH_2CN$); 3.86–3.80 (overlapped signals, 6H, OCH_3); 2.95–2.49 (m, 10H, CH of isobutyryl groups, $OCH_2\underline{CH_2}CN$); 1.39–1.25 (m, 18H, CH_3 of isobutyryl groups in 5, 7 and 4"); 1.14–1.08 (m, 6H, CH_3 of isobutyryl groups in 3); 1.01–0.96 (m, 6H, CH_3 of isobutyryl groups in 3) ppm. ^{13}C NMR (100 MHz, $CDCl_3$, 25 °C, δ ppm): δ = 184.9; 175.1; 175.0; 174.1; 162.4; 156.5; 151.7; 143.6; 143.4; 143.3; 140.8; 133.7; 128.9; 123.3; 123.2; 121.3; 121.1; 119.8 (x2); 117.2; 117.1; 116.6; 116.5; 116.4; 111.5, 111.4; 111.1; 110.7, 108.7; 80.9; 76.0; 75.9; 75.7; 72.8; 72.7; 66.5; 62.3; 56.0; 34.2; 34.0; 33.9; 33.6; 19.0; 18.8; 18.7 (x2); 18.5. ^{31}P NMR (161 MHz, $CDCl_3$, 25 °C, δ ppm): δ = -2.4 ppm. MS (MALDI-TOF, positive ions): m/z calculated for $C_{85}H_{94}NO_{30}P$ = 1639.560; found: 1641.838 $[M+H]^+$, 1663.652 $[M+Na]^+$, 1679.154 $[M+K]^+$.

6bb ^{1}H NMR (400 MHz, $CDCl_3$, 25 °C, δ ppm, *J* Hz): δ = 7.11–6.91 (complex signals, 12H, H-2', H-5', H-6', H-2", H-5", H-6"); 6.76 (s, 2H, H-6); 6.55 (s, 2H, H-8); 5.66 (d, *J* = 12.1, 2H, H-3); 5.36 (d, *J* = 12.1, 2H, H-2); 4.93 (t, *J* = 8.0, 2H, H-7"); 4.32–3.95 (m, 8H, H8", 2H9", O$\underline{CH_2}CH_2CN$); 3.86–3.80 (overlapped signals, 6H, OCH_3); 2.95–2.49 (m, 10H, CH of isobutyryl groups, $OCH_2\underline{CH_2}CN$); 1.36–1.24 (m, 18H, CH_3 of isobutyryl groups in 5, 7 and 4"); 1.13–1.09 (m, 6H, CH_3 of isobutyryl groups in 3); 1.02–0.98 (m, 6H, CH_3 of isobutyryl groups in 3) ppm. ^{13}C NMR (125 MHz, $CDCl_3$, 25 °C, δ ppm, *J* Hz): δ = 184.9; 175.1; 175.0 (x2); 174.1; 162.4; 156.5; 151.7 (x2); 143.6; 143.4; 143.3; 140.8; 133.7; 128.9; 123.3 (x2); 121.2; 121.1; 119.8 (x2); 117.2; 117.1; 116.6 (x2); 116.4; 111.5, 111.4; 111.1; 110.7, 108.7; 80.9; 75.9;

75.7; 72.8; 66.5 (x2); 62.3; 62.2; 56.0; 34.2; 34.0; 33.9; 33.6; 19.0; 18.8; 18.7; 18.5 ppm. ^{31}P NMR (161 MHz, $CDCl_3$, 25 °C, δ ppm): δ = -2.4 ppm. MS (MALDI-TOF, positive ions): m/z calculated for $C_{85}H_{94}NO_{30}P$ = 1639.560; found: 1641.554 $[M+H]^+$, 1663,159 $[M+Na]^+$, 1679.555 $[M+K]^+$.

6ab ^{1}H NMR (400 MHz, $CDCl_3$, 25 °C, δ ppm, *J* Hz): δ = 7.12–6.88 (complex signals, 12H, H-2', H-5', H-6', H-2", H-5", H-6"); 6.76–6.73 (m, 2H, H-6); 6.56–6.54 (m, 2H, H-8); 5.69–5.61 (m, 2H, H-3); 5.38–5.32 (m, 2H, H-2); 4.99–5.90 (m, 2H, H-7"); 4.35–3.97 (m, 8H, H8", 2H9", O$\underline{CH_2}CH_2CN$); 3.88–3.79 (overlapped signals, 6H, OCH_3); 2.96–2.48 (m, 10H, CH of isobutyryl groups, $OCH_2\underline{CH_2}CN$); 1.36–1.24 (m, 18H, CH_3 of isobutyryl groups in 5, 7 and 4"); 1.13–1.08 (m, 6H, CH_3 of isobutyryl groups in 3); 1.02–0.96 (m, 6H, CH_3 of isobutyryl groups in 3) ppm. ^{13}C NMR (100 MHz, $CDCl_3$, 25 °C, δ ppm): δ = 184.9; 175.1; 175.0 (x2); 174.1; 162.4; 156.5; 151.7 (x2); 143.6; 143.4; 143.3; 140.8; 133.7; 128.9; 123.3 (x2); 121.2; 121.1; 119.8 (x2); 117.2; 117.1; 116.6 (x2); 116.4; 111.5, 111.4; 111.1; 110.7, 108.7; 80.9; 76.1; 76.0; 75.9; 75.7; 72.8; 66.5 (x2); 62.3; 62.2; 56.0; 34.2; 34.0; 33.9; 33.6; 19.0; 18.8; 18.7 (x2); 18.5 ppm. ^{31}P NMR (161 MHz, $CDCl_3$, 25 °C, δ ppm): δ = -2.3; -2.6 ppm. MS (MALDI-TOF, positive ions): m/z calculated for $C_{85}H_{94}NO_{30}P$ = 1639.560; found: 1641.497 $[M+H]^+$, 1663.132 $[M+Na]^+$, 1679.115 $[M+K]^+$.

3.4.5 General Procedure for the Synthesis of Dimers 7aa, 7bb and 7ab

200 mg (0.12 mmol) of dimer **6aa** (or **6ab** or **6bb**) were treated with 7 mL of a mixture conc. aq NH_3/MeOH (1:1, v/v) for 5 h at 50 °C, leading to full removal of the *i*bu and 2-cyanoethyl (CE) groups. The mixture was dried under reduced pressure, suspended in a buffer solution and then purified on RP-HPLC carried out on Phenomenex Kromasil® C18 column (10 µm particle size, 10.0 mm × 250 mm i.d.) using a linear gradient of ACN in 0.1 M NH_4OAc in H_2O (pH 7.0) from 5% to 95%

over 20 min at a flow rate of 6 mL/min with detection at 288, 260 nm. Compounds thus obtained were converted into the corresponding sodium salts by cation exchange on a DOWEX (Na^+ form) resin to obtain homogeneous samples. RP-HPLC analysis was carried out on Luna C18 (2) (5 µm particle size, 150 mm × 4.6 mm i.d.) using a linear gradient of ACN in in 0.1 M NH_4OAc in H_2O (pH 7.0) from 5% to 95% over 20 min at a flow rate of 0.8 mL/min with detection at 288 nm. The three dimers presented a purity ≥ 99%.

7aa ^{1}H NMR (400 MHz, DMSO-d6 + 5% D_2O, 25 °C, δ ppm, *J* Hz): δ = 7.11–6.74 (complex signals, 12H, H-2', H-5', H-6', H-2", H-5", H-6") 5.85 (s, 4H, H-6 and H-8); 5.05 (d, *J* = 11.0, 2H, H-2); 4.82 (d, *J* = 7.6, 2H, H-7"); 4.57 (d, *J* = 11.0, 1H, H-3); 4.35–4.27 (m, 2H, H8"); 3.80–3.65 (overlapped signals, 8H, OCH_3, H-9"a); 3.58– 3.47 (m, 2H, H-9"b) ppm. ^{13}C NMR (100 MHz, DMSO-d6 + 5% D_2O, 25 °C, δ ppm): δ = 197.8; 168.2; 163.7; 162.8; 148.0; 147.5; 143.8; 143.6; 130.5; 127.6; 121.8; 120.8; 116.8; 116.7; 115.7; 112.1, 100.6; 96.7; 95.7; 82.9; 77.1; 76.2; 71.8; 63.6; 56.0 ppm. ^{31}P NMR (161 MHz, DMSO-d6 + 5% D_2O, 25 °C, δ ppm): δ = -1.6 ppm. MS (MALDI-TOF, negative ions): m/z calculated for $C_{50}H_{43}O_{22}P$ = 1026.198; found: 1025.355 $[M-H]^-$.

7bb ^{1}H NMR (400 MHz, DMSO-d6, 25 °C, δ ppm, *J* Hz): δ = 11.90 (s, 2H, OH-5); 11.08 (s, 2H, OH-7); 9.19 (s, 2H, OH-4"); 7.10–6.73 (complex signals, 12H, H-2', H-5', H-6', H-2", H-5", H-6") 5.91 (s, 4H, H-6 and H-8); 5.85–5.79 (m, 2H, OH-3); 5.05 (d, *J* = 11.1, 2H, H-2); 4.83 (d, *J* = 7.8, 2H, H-7"); 4.60 (d, *J* = 11.1, 1H, H-3); 4.58 (d, *J* = 11.1, 1H, H-3); 4.34–4.26 (m, 2H, H8"); 3.79–3.65 (overlapped signals, 8H, OCH_3, H-9"a); 3.58– 3.48 (m, 2H, H-9"b) ppm. ^{13}C NMR (100 MHz, DMSO-d6, 25 °C, δ ppm, *J* Hz): δ = 198.2; 167.4; 163.7; 162.9; 148.0; 147.5; 143.8; 143.5; 130.5; 127.6; 121.6; 120.8; 117.0; 116.8; 115.7; 112.1, 100.8; 96.5; 95.5; 83.0; 77.1; 76.2; 71.9; 63.6; 56.0 ppm. ^{31}P NMR (161 MHz, DMSO-d6, 25 °C, δ ppm): δ = -1.7 ppm.

MS (MALDI-TOF, negative ions): m/z calculated for $C_{50}H_{43}O_{22}P$ = 1026.198; found: 1025.196 $[M-H]^-$.

7ab ^{1}H NMR (400 MHz, MeOD-d4, 25 °C, δ ppm, *J* Hz): 7.15–6.79 (complex signals, 12H, H-2', H-5', H-6', H-2", H-5", H-6") 5.92 (s, 4H, H-6 and H-8); 5.02–4.94 (m, 4H, H-2 and H7"); 4.53 (d, 11.5, 1H, H-3); 4.26–4.20 (m, 2H, H8"); 3.91–3.80 (overlapped signals, 8H, OCH_3, H-9"a); 3.79– 3.75 (m, 2H, H-9"b) ppm. ^{13}C NMR (100 MHz, MeOD-d4, 25 °C, δ ppm): 196.9; 167.3; 163.9; 162.9; 147.7; 146.9; 143.9; 143.8; 143.6; 130.0; 127.8; 120.6; 120.3; 116.5; 116.3; 116.1; 114.9; 110.9, 100.4; 96.9; 94.9; 83.3 (2C); 77.0; 76.1; 76.0; 72.2; 64.0; 55.1. ^{31}P NMR (161 MHz, MeOD-d4, 25 °C, δ ppm, *J* Hz): -0.2. MS (MALDI-TOF, negative ions): m/z calculated for $C_{50}H_{43}O_{22}P$ = 1026.198; found: 1025.144 $[M-H]^-$.

3.4.6 Hydroxyl Radical (HO·) Generation and Reactivity Estimation

The reactivity constants between the newly synthesized silybin dimers and hydroxyl radicals were assessed using a Laser Flash Photolysis system. The methodology involves the generation of di-thiocyanate radical anion ($SCN_2^{\bullet -}$) through the reactivity of photo-generated hydroxyl radicals (HO•) with thiocyanate (SCN^-) in the presence of hydrogen peroxide. The second-order rate constants between HO• and the silybin dimers were achieved using the following equation:

$$\frac{Abs_0}{Abs} = 1 + \frac{k^{II}_{HO^\bullet,Dimer}[Dimer]}{k^{II}_{HO^\bullet,SCN^-}[SCN^-]}$$

where Abs_0 and Abs represent the absorption of $SCN_2^{\bullet -}$ at 475 nm in the absence and presence of dimers. $k^{II}_{HO^\bullet,SCN^-}$ and $k^{II}_{HO^\bullet,Dimer}$ are the second-order rate constants of hydroxyl radicals (HO•) with thiocyanate and dimers at varying concentrations.

A linear correlation plot of $\frac{Abs_0}{Abs}$ against the concentration of dimers (**7aa**, **7bb**, or **7ab**) is generated. The slope of this plot is used to determine the value of $k^{II}_{HO^{\bullet},Dimer}$. The reported results represent the mean values obtained from three replicates. Statistical analysis was performed using one-way analysis of variance (ANOVA), and post hoc tests of least significance were applied to assess significant differences. Differences with a p-value < 0.05 were considered statistically significant.

3.4.7 Culture Conditions

The cell culture conditions for various human cell lines were as follows:

- Jurkat (Human T lymphoblastoid) and WM266 (Human Metastatic Melanoma):
  - Medium: RPMI medium
  - Supplements: 10% heat-inactivated fetal bovine serum (FBS), 2.5 mM glutamine, 100 U/mL penicillin, and 100 µg/mL streptomycin (Euroclone).
- HeLa (Human Cervix Adenocarcinoma), A549 (Human Lung Carcinoma), PANC (Human Pancreatic Cancer), U87 (Human Glioblastoma), and HDF (Normal Human Fibroblasts):
  - Medium: DMEM
  - Supplements: 10% fetal bovine serum (FBS), 1% glutamine, 100 U/mL penicillin, and 100 µg/mL streptomycin (Euroclone, Milano, Italy).

All cell lines were cultured in a humidified environment with 5% CO_2 at a temperature of 37°C.

3.4.8 Antiproliferative Activity

The experimental setup for cell proliferation assays involved the following steps:

- Cell Plating:

- Jurkat cells were plated at a density of 10,000 cells/well.
- WM266 and HDF cells were plated at 2,000 cells/well.

- HeLa cells were plated at 1,200 cells/well.

- PANC, U87, and A375 cells were plated at 1,000 cells/well.

- 96-well microplates (Thermofisher, Waltham, MA, USA) were used for cell plating.

- Incubation:

- After 24 h of incubation, cells were treated with increasing concentrations of synthetized compounds. These compounds were previously solubilized in DMSO at a concentration of 50 mM.

- Cell Proliferation Assay:

- For Jurkat cells, cell proliferation was determined using the CCK-8 assay (2-(2-methoxy-4-nitrophenyl)-3-(4-nitrophenyl)-5-(2,4-disulfophenyl)-2H-tetrazolium, monosodium salt).

- For HeLa, WM266, PANC, U87, and HDF cells, the MTT assay (3-(4,5-dimethylthiazol-2-yl)-2,5-diphenyltetrazolium bromide) was used.

- The assays were performed after a 48 h treatment period.

- Analysis:

- Plates were analyzed using a microplate reader (Enspire, Perkin Elmer Italia Spa, Milano, Italy) at 450 nm (CCK-8) or 570 nm (MTT).

- Results were presented as the percentage of proliferating cells relative to the control (vehicle-treated cells).

- Data are expressed as means ± SE of at least three independent experiments conducted in triplicate.

- Statistical Analysis:

- Statistical analysis was performed using Student's t-test (unpaired, two-sided), and significance was considered at $p < 0.05$.

- IC_{50} Calculation:

- IC_{50} values were calculated using GraphPad Prism software.

3.4.9. Apoptosis assay

The apoptosis analysis was conducted on Jurkat cells, initially seeded at a density of 2.5×10^5 cells/mL in a 6-well plate. Following the seeding, cells were incubated at 37 °C in the absence or presence of a 200 μM concentration of the tested compounds. After 48 h of incubation, apoptosis induction was assessed through double staining with annexin V/FITC and propidium iodide (PI), utilizing the eBioscience kit from Affimetrix (Santa Clara, CA, USA).

The quantification of cells undergoing apoptosis was performed using a flow cytometer equipped with a 488 nm argon laser (Becton Dickinson, Franklin Lakes, NJ, USA). Analysis was carried out using Cell Quest software. The entire apoptosis analysis was replicated at least two times to ensure consistency and reliability of the results.

4 Silybins 7-*O*-Alkyl Derivatives

Polyphenols are a family of compounds attractive due to their ability to scavenge radical species, crucial for normal cell function. Imbalances in pro- and antioxidant species leading to oxidative stress are implicated in different diseases.[7]

Even if the antioxidant activity is not the crucial role for drug design, it often serves as a starting point. Many natural products with potent radical scavenging properties provide diverse structures useful as lead compounds for drug development. However, challenges like low bioavailability and rapid metabolism limit their pharmacological use. To overcome these limitations, hybrid molecules, combining features of different compounds, have shown promise in drug development.[15]

One focus of recent research is on silibinin, a metabolite with diverse pharmacological properties but low bioavailability.[16] Although silibinin itself does not exhibit significant antioxidant activity, studies on its hydroxyl groups have revealed both pro-oxidant and antioxidant characteristics.[17] Furthermore, silibinin has demonstrated inhibitory effects on various cancer cells, making it a lead compound for prostate cancer treatment.[18]

2,3-dehydro-silybin (DHS), an oxidation product of silibinin, has shown better antitumor activity on certain cells compared to silibinin. Chemical modification studies indicate that the *in vitro* antiproliferative activity of silibinin and DHS against different prostate cancer cell lines can be further improved.[19,20] However, many studies overlook the structure-activity relationship of isomers, using silibinin as a natural mixture. Understanding the influence of the flavonolignan structural core and functional properties on pharmacological activity is crucial for more effective drug development.

4.1 Aim of Research Work

In this context, a regioselective synthesis of new 7-*O*-alkyl derivatives of Sil and DHS has been presented (Scheme 4.1). The aim is to combine the pharmacological properties of silybins with those of tyrosol-based metabolites, potentially leading to new molecules with improved antioxidant and anticancer activities.

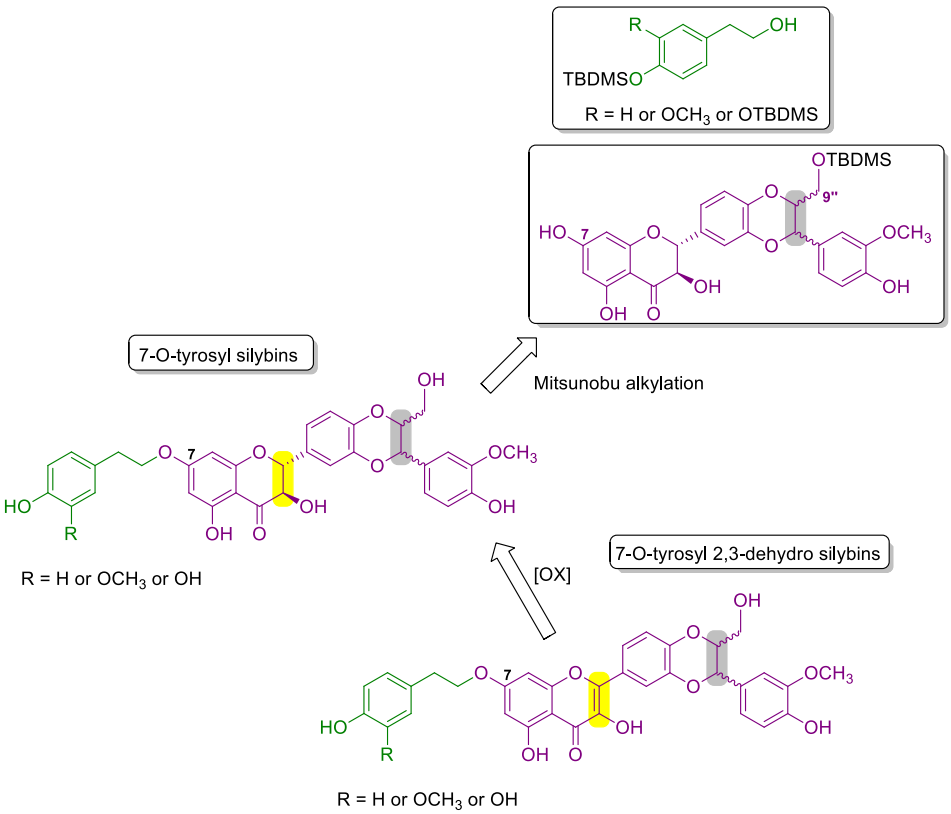

Scheme 4.1. Retrosynthetic route for new 7-*O*-tyrosyl silybins and 2,3-dehydro-silybins derivatives starting from 9''-protected silybins

The synthesis involved alkylation of the 7-OH of silybins with tyrosol-based moieties, specifically 3-methoxytyrosol (MTYR) and 3-hydroxytyrosol (HTYR), known for their antioxidant and pharmacological properties.[21,22]

The introduction of a weak antioxidant, tyrosol (TYR), was also considered to contribute to the structure-activity relationship. The synthesized derivatives, obtained with satisfactory yields, were fully characterized using various analytical techniques. The radical scavenger activity of these derivatives was evaluated through DPPH and ORAC assays. Subsequently, it was investigated the anticancer activity of the new derivatives in prostate cancer cell line (PC-3).

4.2 Results and Discussion

The synthesis of selectively alkylated silibinin derivatives has been a subject of extensive investigation, involving variations in different parameters such as bases, solvents, and reagent equivalents.[23,24,25] However, when these methods were applied to generate alkylated derivatives of silibinin, they often resulted in low or no yields, primarily due to the complete oxidation of silibinin into 2,3-dehydro silybin derivatives.[26,27]

The synthetic strategy proposed aim to develop a mild and regioselective alkylation method that prevents the oxidation of silybin into 2,3-dehydro-silybin derivatives. To achieve this goal, it was opted for alkylation via the Mitsunobu reaction[28], that exploit the higher acidity of the OH in position 7 of silybins and the increased nucleophilicity of the primary OH of tyrosol-based derivatives. Considering the presence of different OH groups (one primary, one secondary, and three phenolic OH) on silybins, it was chosen to conduct a Mitsunobu alkylation starting from suitably protected building blocks. To optimize selectivity and avoid self-alkylation by-products of silybins, the process started with 9"-O-protected silybins and protected tyrosols at the phenolic OHs. The *tert*-butyldimethylsilyl (TBDMS) group was selected as the protecting group due to its selective insertion and removability under mild conditions for both starting metabolites. Starting from the tyrosol-based metabolites **3** – **5** (Scheme 4.2), a refined protection method was applied to

exclusively protect the phenolic functions. In summary, all hydroxyl (OH) groups were protected with an excess of *tert*-butyldimethylsilyl chloride (TBDMSCl) in ACN/DMF (3/1 v/v) in the presence of triethylamine (TEA). Following regioselective deprotection of the aliphatic OH group using 1% weight iodine (I_2) in methanol (MeOH), building blocks **6** – **8** were obtained in good yields (83 – 86%).

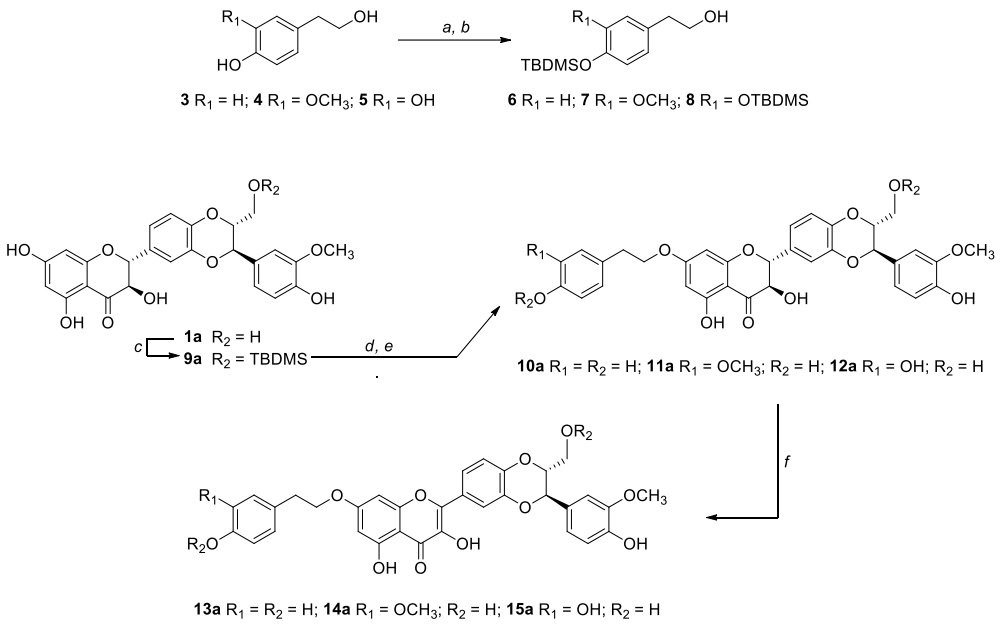

Scheme 4.2. Reagents and conditions: a) TBDMSCl, TEA, ACN/DMF (3:1, v/v), rt, 3h; b) 1% wt I_2/MeOH, rt, 3h; c) TBDMSCl, Pyridine, ACN/DMF (3:1, v/v), 0 °C, 2h; d) tyrosol-based alcohol (**6** or **7** or **8**), TPP/DIAD, THF 0 °C, 2h; e) TEA·3HF, THF, rt; f) KOAc, DMF, 50 °C, 45 min.

For the synthesis of the 9"-OTBDMS silybins building blocks, silibinin (**1ab**), silybin A or B (**1a** or **1b**) were treated with TBDMSCl in ACN/DMF (3/1 v/v) in the presence of pyridine (Scheme 4.2). This resulted in the formation of **9ab**, **9a**, and **9b** in 75%, 74%, and 79% yields, respectively. To proceed with the 7-*O*-alkylation, using tyrosol-based building blocks **6** – **8** and 9"-O-protected silybins **9a**, **9b**, and silibinin **9ab**, a Mitsunobu reaction was established. In a typical Mitsunobu reaction, the

protected tyrosols (**6** – **8**) were reacted with 9"-OTBDMS silybins (**9a**, **9b**, and **9ab**) in the presence of triphenylphosphine (TPP) and diisopropyl azodicarboxylate (DIAD) in anhydrous tetrahydrofuran (THF) at 0 °C. The crude reaction mixtures were challenging to purify, and after a simple chromatographic purification, they were treated with triethylamine trihydrofluoride (TEA·3HF) in THF at room temperature. Following RP-HPLC purification, the identity and complete signal assignment of compounds **10** – **12** were confirmed by 1D and 2D-NMR analysis in combination with mass spectrometry (MS) data. All the obtained compounds exhibited good yields (Table 4.1). Subsequent treatment of derivatives **10** – **12** with KOAc in DMF at 50 °C (Scheme 4.2) leads to DHS derivatives **13** – **15** obtained in good yields (Table 4.1). Following HPLC purifications, the identity of structures **13** – **15** was confirmed by 1D and 2D-NMR analysis.

4.2.1 *In medium* and Chemical Stability

The stability of 7-*O*-tyrosylsilybin derivatives (**10a**, **11a**, and **12a**), as representative compounds, was investigated to ensure that the observed effects are attributed to the compounds themselves rather than to other byproducts formed. HPLC experiments were conducted at different time points. Derivatives **10a** – **12a** were dissolved in assay medium and incubated for 48 h. Samples were collected at various intervals (0, 1, 3, 7, 24 and 48 h), and the areas under curves were determined.

The results indicate a relatively slow alteration of **10a** and **11a**, with 87% and 93% of the products still present after 48 h, respectively (Figure 4.1). However, for the conjugate with hydroxytyrosol (HTYR), **12a**, a less pronounced stability was observed, with 33% of the product remaining after 48 h. This lower stability is likely attributed to the presence of the catechol function in HTYR, which is known to be more sensitive to auto-oxidation compared to phenolic functions. The ability of the catechol function to auto-oxidize is a known aspect of its reactivity toward protein

targets, and it is considered crucial in the design of neuroprotective drugs. It's important to note that this specific aspect was not investigated in the current study.

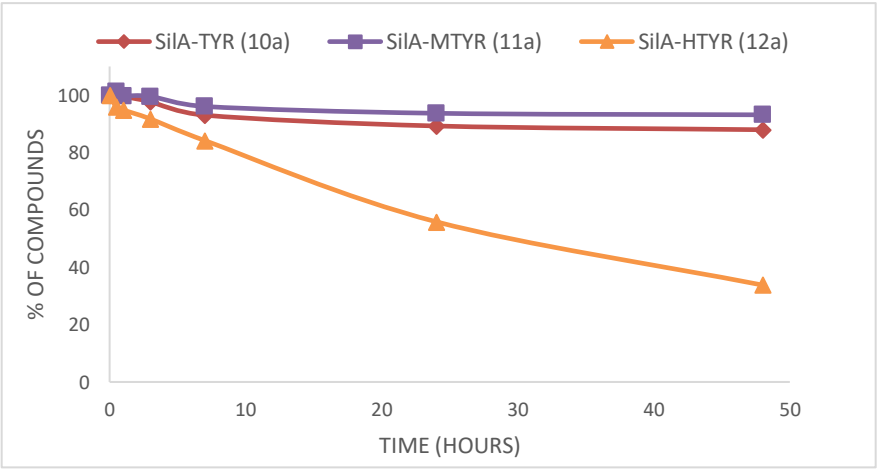

Figure 4.1 Percentage of SilA−TYR (**10a**), SilA−MTYR (**11a**) and SilA−HTYR (**12a**) remaining over time *in medium*, calculated by the change in the integration of the corresponding HPLC peak.

The stability over time in phosphate buffer at pH 7.4 appears to be relatively consistent with that observed in the medium. We noted a sustained presence (≥ 88%) of products **10a** and **11a** even after a 48 h duration. As seen before, product **12a**, which contains the HTYR moiety, demonstrates a higher susceptibility to alteration but still maintains a persistence of over 50% at 48 h. It's noteworthy that, for derivative **10a**, appreciable percentages (approximately 50%) of silybin oxidation product in 2,3-dehydrosilybin were observed only after a 5-day interval.

4.2.2 Antioxidant Activity

Recent investigations into the redox properties and chelating capabilities of silibinin have shed light on the distinct roles of its various hydroxyl functions, particularly highlighting the pro-oxidant nature of the 7-OH function.[13] Notably,

derivatizing this function with an antioxidant moiety has been proposed as a strategy to generate silybin derivatives with enhanced antioxidant activity.

To preliminarily assess the antioxidant properties of the novel compounds, we conducted ORAC (Oxygen Radical Absorption Capacity) and DPPH (2,2-diphenyl-1-picrylhydrazyl) assays. The antioxidant activities are presented in Table 4.1 together with three well-known phenols based on tyrosol, TYR, MTYR, and HTYR (**3**, **4**, and **5**), as well as silybins (**1ab**, **1a**, and **1b**), the reference flavonolignans.

According to ORAC results, comparable antioxidant capacity was observed for compounds **10** – **12** and their counterparts (**1a**, **1b**, and **1ab**), with compounds **12** remaining the most active. Conversely, derivatives **13** – **15** exhibited a decrease in activity compared to their progenitors (**2ab**, **2a**, and **2b**). In the DPPH assay, a significant contribution of the tyrosol moieties in position 7 was evident. All derivatives (**10** – **15**) displayed greater activity than their progenitors, with a notably enhanced free radical scavenging ability of 2,3-dehydro derivatives (**13** – **15**) compared to silybin derivatives (**10** – **12**). These results should be interpreted considering the role of position 7-OH in the antioxidant activity of the starting compounds, silybins, and 2,3-dehydrosilybins. As reported in the literature[29], the 7-OH function in silibinin is a pro-oxidant position; therefore, its masking led to an increase in the antioxidant activity in the new derivatives, even when linked to a non-antioxidant compound (TYR). A further increase is observed for derivatives **11** – **12** where MTYR and HTYR are known antioxidants by themselves. In DHS, position 7-OH was found to be an important prerequisite for decreasing the 3-OH bond dissociation enthalpy.[13] Consequently, for the DPPH assay, with an electron transfer mechanism, a synergic contribution of the activity of DHS and the tyrosol moiety is observed. Conversely, for the ORAC assay, where the bond dissociation enthalpy plays a crucial role, the new derivatives exhibit an impairment of resonance stabilization of 3-OH, leading to a decrease in antioxidant activity.

Table 4.1. Yields and antioxidant activity (ORAC and DPPH) for derivatives **10** – **15**

Compound	Yield (%)[a]	ORAC (TE)[b]	DPPH (EC_{50}, µM)
Sil (**1ab**)	–	4.76 ± 0.20	620 ± 0.2
SilA (**1a**)	–	4.21 ± 0.16	360 ± 0.2
SilB (**1b**)	–	4.36 ± 0.15	580 ± 0.5
DHS (**2ab**)	–	3.57 ± 0.23	29.6±0.18
DHSA (**2a**)	–	3.88 ± 0.20	15.5 ± 0.3
DHSB (**2b**)	–	3.86 ± 0.13	11.6 ± 0.4
TYR	–	2.18 ± 0.12	>1000
MTYR	–	2.90 ± 0.21	31.0 ± 2.6
HTYR	–	7.40 ± 0.17	12.3 ± 1.0
10a	35	4.81 ± 0.45	290 ± 0.2
11a	28	2.50 ± 0.29	13.5 ± 0.6
12a	26	5.57 ± 0.17	6.53 ± 0.6
13a	95	1.16 ± 0.05	17.1 ± 0.1
14a	78	1.25 ± 0.02	9.01 ± 0.5
15a	95	1.28 ± 0.02	4.98 ± 0.4
10b	83	4.89 ± 0.22	220.0 ± 0.1
11b	21	3.22 ± 0.52	17.8 ± 0.6
12b	65	5.38 ± 0.17	5.65 ± 0.5
13b	72	1.15 ± 0.02	19.3 ± 0.1
14b	82	1.32 ± 0.04	9.10 ± 0.6
15b	81	1.25 ± 0.04	4.76 ± 0.4
10ab	51	4.88 ± 0.09	200 ± 0.2
11ab	33	4.91 ± 0.17	9.4 ± 0.5
12ab	40	5.45 ± 0.54	4.9 ± 0.6
13ab	90	1.47 ± 0.05	26.9 ± 0.2
14ab	76	1.01 ± 0.12	9.27 ± 0.6
15ab	74	1.44 ± 0.14	6.19 ± 0.7

a For the silybin derivatives (**10** – **12**) yields refer to intermediates (**9**), while for DHS derivatives (**13** – **15**) yields refer only to the oxidation step of 10 – 12; b Trolox equivalent

4.2.3 Anti-proliferative effects towards Prostate Cancer cell lines

The Trypan blue assay demonstrated that various silybin derivatives, when administered at concentrations of 5 and 10 μM for 48 and 72 h, led to a decrease in live cell numbers and induced cell death in PC-3 prostate cancer cells. Of all silybin derivatives tested, compounds **15ab**, **15a**, and **15b** exhibited the highest potency in restricting cell growth and inducing cell death in PC-3 cells at both 48 and 72 h of treatment. Specifically, these compounds resulted in a significant reduction in the percentage of live PC-3 cells by approximately 5% to 41% (at 5 μM) and around 72% to 78% (at 10 μM) after 48 h ($P < 0.001$ for all, Figure 4.2A). Similarly, at 72 h, the reduction was 33% to 62% (at 5 μM) and approximately 79% to 86% (at 10 μM) compared to the control ($P < 0.001$ for all, Figure 4.3A).

Furthermore, treatment with compounds **15ab**, **15a**, and **15b** significantly increased the percentage of dead cells by 1.6 to 2.5-fold (at 5 μM) and 3.2 to 4.4-fold (at 10 μM) after 48 h ($P < 0.01 – 0.001$, Figure 4.2B) and by 1.6 to 2.6-fold (at 5 μM) and 1.8 to 2.8-fold (at 10 μM) after 72 h ($P < 0.05 – 0.001$, Figure 4.3B) compared to the control. Results also showed that compounds **14ab**, **14a**, and **14b** exhibited somewhat similar effects as compounds **15ab**, **15a**, and **15b**, but the effects were more prominent at a higher concentration of 10 μM and at 72 h (Figure 4.2A and B and Figure 4.3A and B). Therefore, for further studies, only compounds **15ab**, **15a**, and **15b** were chosen. Compound **1ab** was used as parent control in subsequent experiments.

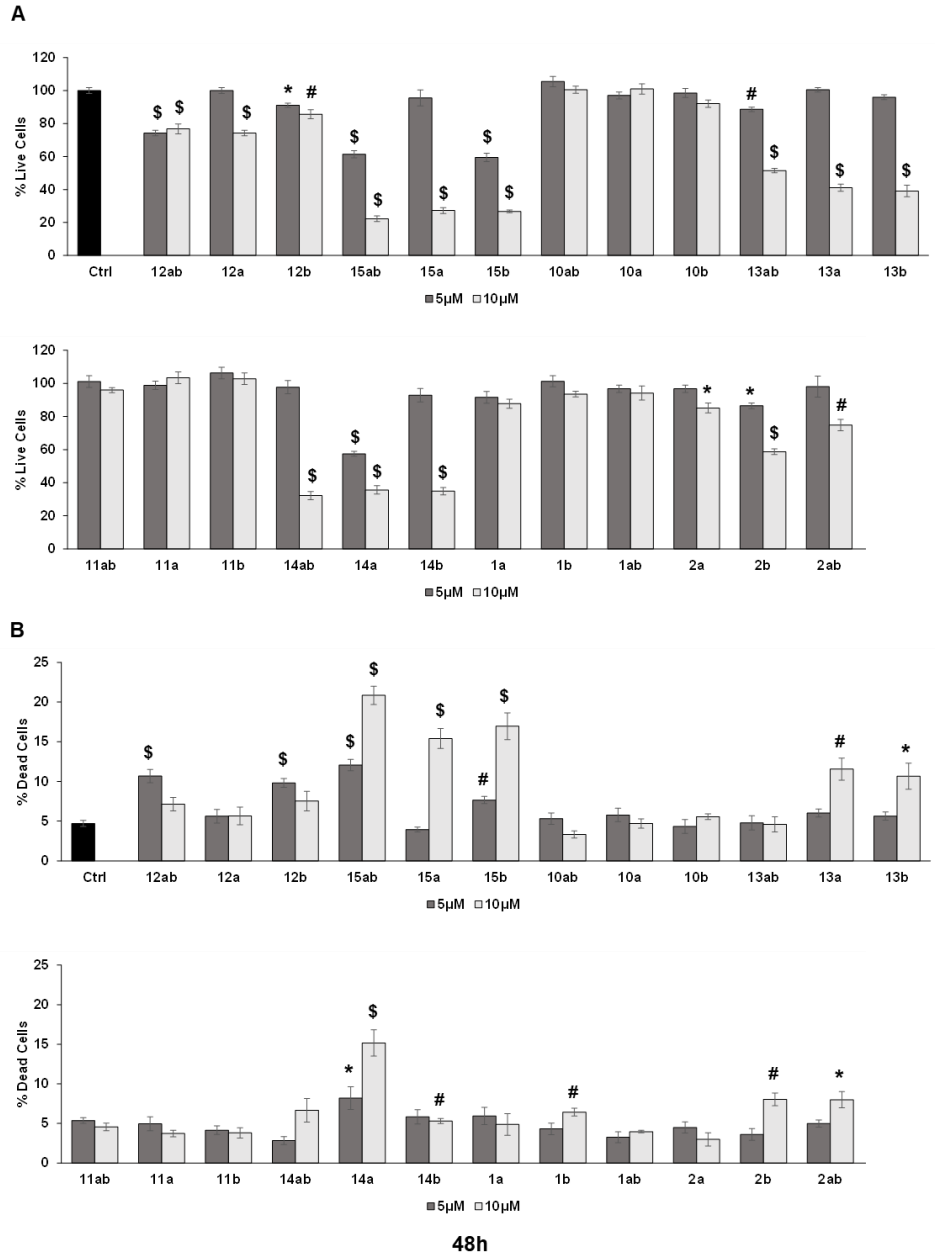

Figure 4.2 PC-3 prostate cancer cells were treated with different silybin derivatives for 48 h and a trypan blue assay was performed. Bar graphs depict (A) percent live cells and (B) percent dead cells. Each bar represents the mean ± SEM. of three experiments. $P < 0.001$ ($), $P < 0.01$ (#), $P < 0.05$ (*) compared to control scores.

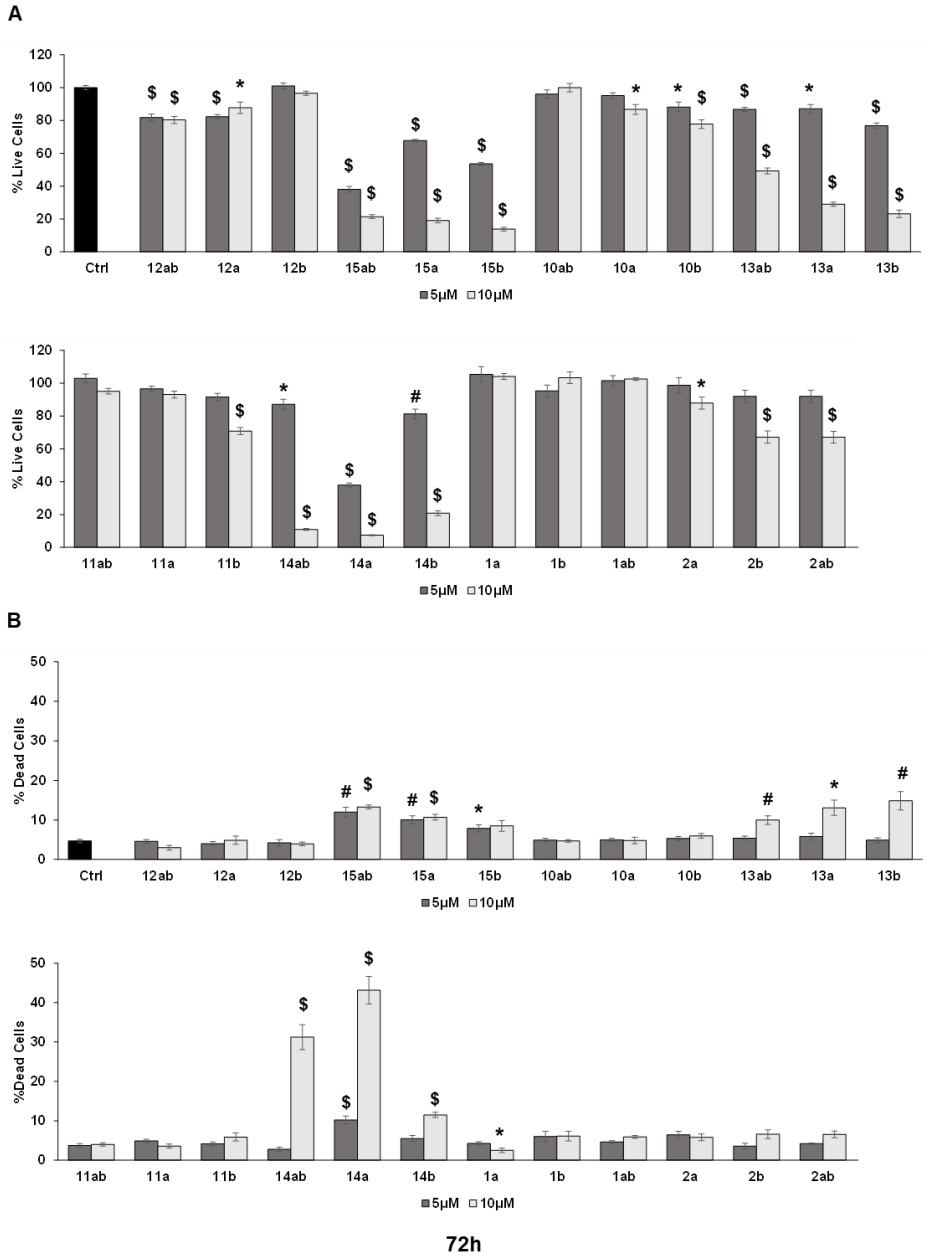

Figure 4.3 PC-3 prostate cancer cells were treated with different silybin derivatives for 72 h and a trypan blue assay was performed. Bar graphs depict (A) percent live cells and (B) percent dead cells. Each bar represents the mean ± SEM of three experiments. $P < 0.001$ ($), $P < 0.01$ (#), $P < 0.05$ (*) compared to control scores.

4.2.4 Effects of Silybin Derivatives on PC-3 Apoptosis and Cell Cycle Progression

Prostate cancer PC-3 cells were seeded in 35-mm culture plates at a density of 5×10^4 cells/plate. Following a 24 h incubation period, the cells underwent treatment with various concentrations (5 or 10 μM) of compound **15ab**, **15a**, **15b** and **1ab** for 24 and 48h. Subsequently, the cells were harvested with trypsinization and then subjected to centrifugation (at 2500 rpm for 5 min), followed by staining with Annexin V and PI as per manufacturer's instructions. Results revealed that compounds **15ab** and **15b** were able to induce a significant increase in the late apoptotic cell population in PC-3 cells, which is positive for both annexin V and PI staining. Specifically, a 10 μM concentration of compound **15ab** increased the late apoptotic cell population by 4 fold ($P < 0.05$, Figure 4.4B) and compound **15b** increased the late apoptotic cell population by 4.7 fold ($P < 0.001$, Figure 4.4B) at 24 h. Similarly, at 48 h, 10 μM of compound **15ab** increased the late apoptotic cell population by 3 fold ($P < 0.001$, Figure 4.4C), and 10 μM concentration of compound **15b** increased the late apoptotic cell population by 3.5 fold ($P < 0.001$, Figure 4.4C) when compared to control. Results from western blotting for cleaved caspase-3 also confirmed that compounds **15ab** and **15b** induce apoptosis in PC-3 cells. The expression for cleaved caspase 3 was significantly upregulated in 10 μM dose groups of compounds **15ab** and **15b** (Figure 4.5), thus confirming apoptosis induction by these specific silybin derivatives.

Flow cytometric analysis for cell cycle progression revealed that compounds **15ab**, **15a**, and **15b** induced G1 phase arrest in PC-3 prostate cancer cells. Specifically, a 10 μM concentration of compounds **15ab**, **15a**, and **15b** increased the cells in G1 phase by 1.4 fold, 1.2 fold, and 1.4 fold at 24 h respectively ($P < 0.01$-0.001, Figure 4.6B). Similarly, a 10 μM concentration of compounds **15ab**, **15a**, and **15b** increased the cells in G1 phase by 1.12 fold, 1.13 fold, and 1.14 fold at 48 h respectively ($P < 0.01$-0.001, Figure 4.6C).

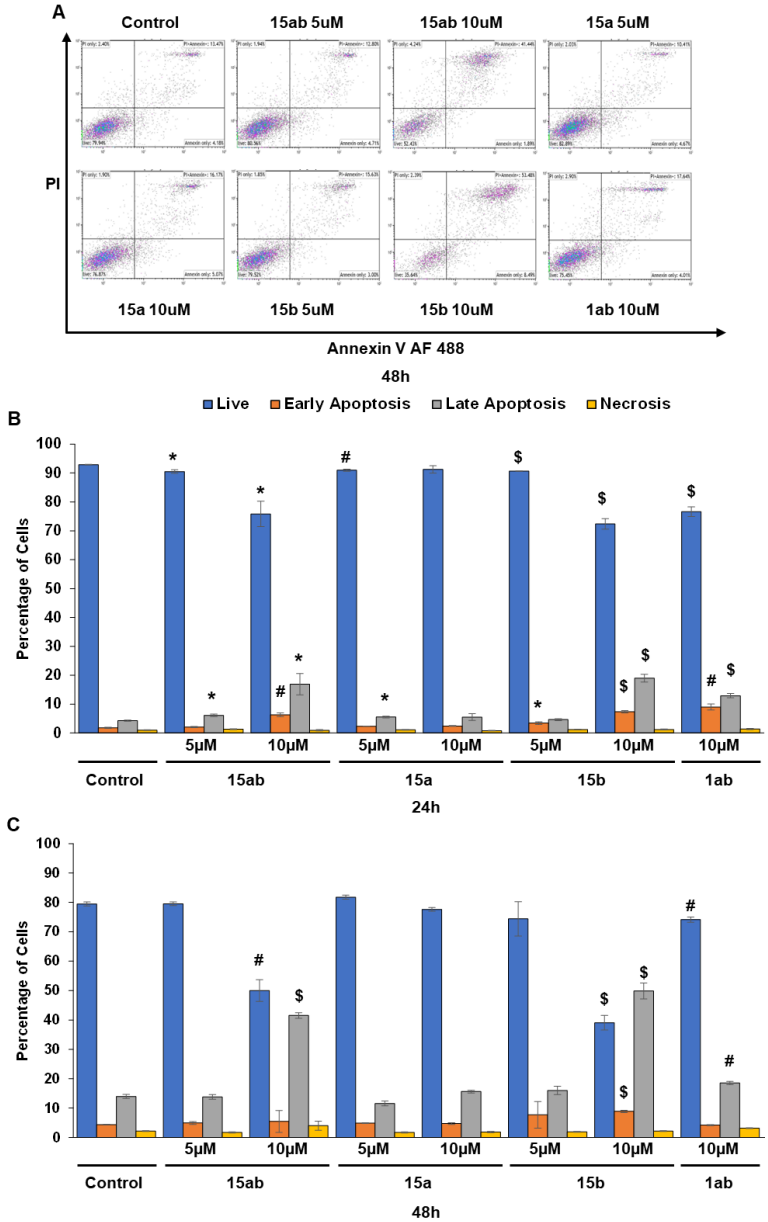

Figure 4.4 (A) Representative flow cytometry images for apoptosis assay in PC-3 cells after treatment with different silybin derivatives after 48 h (B) Bar graph of % apoptotic cells in PC-3 cells after 24 h treatment with different silybin derivatives treatment. (C) Bar graph of % apoptotic cells in PC-3 cells after 48 h treatment with different silybin derivatives. Each bar represents the mean ± SEM. of three experiments. $P < 0.001$ ($), $P < 0.01$ (#), $P < 0.05$ (*) compared to control scores.

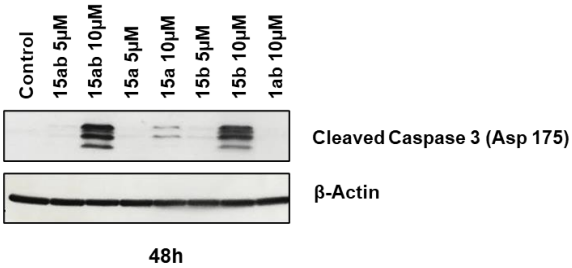

Figure 4.5 Western blotting for apoptotic marker cleaved caspase 3 cells after treatment with different silybin derivatives after 48 h. β-Actin was probed after stripping the membrane as a protein loading control.

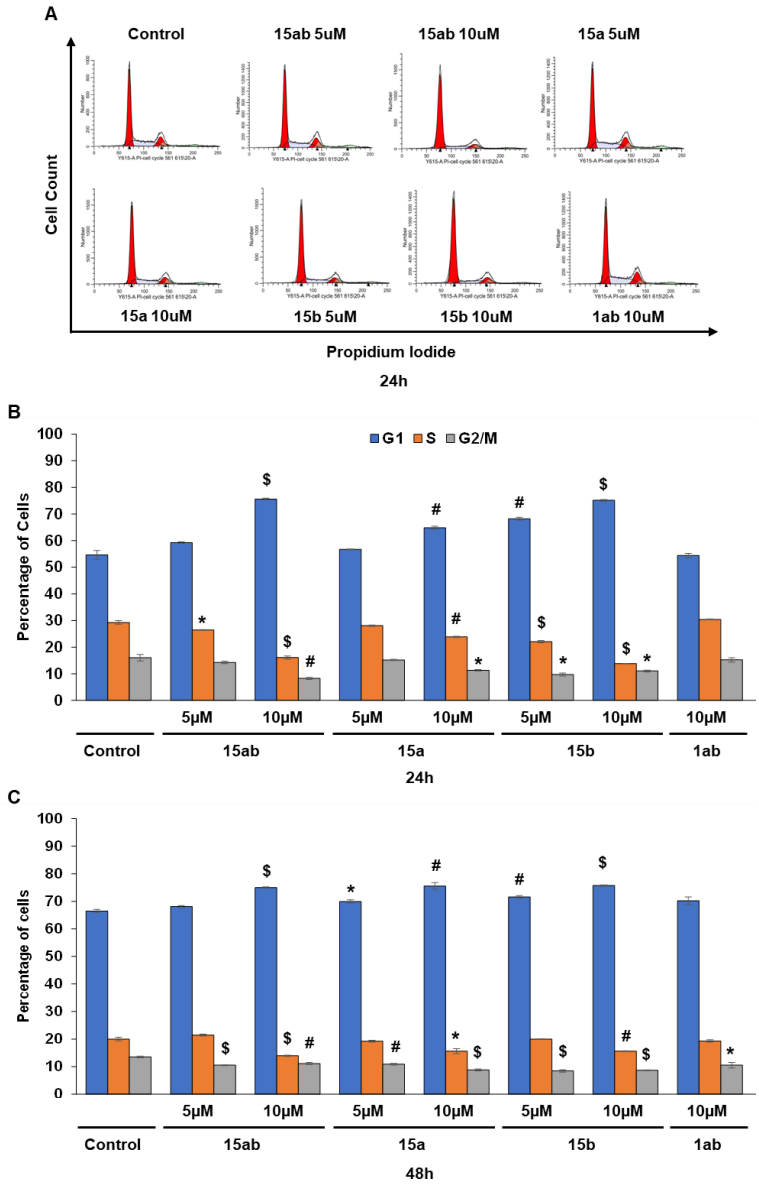

Figure 4.6 (A) Representative flow cytometry images for cell cycle analysis in PC-3 cells after treatment with different silybin derivatives after 48 h (B) Bar graph for cell cycle distribution in PC-3 cells after 24 h treatment with different silybin derivatives. Each bar represents the mean ± SEM. of three experiments. $P < 0.001$ ($), $P < 0.01$ (#), $P < 0.05$ (*) compared to control scores.

4.3 Conclusions

The synthesis of new 7-*O*-alkyl conjugates of the flavonolignan silibinin and tyrosol-based polyphenols (TYR, **3**; MTYR, **4**; HTYR, **5**) was successfully achieved through regioselective alkylation with high yields. The derivatives of silybin A (SilA, **1a**), silybin B (SilB, **1b**), and silibinin (Sil, **1ab**) were prepared starting from silibinin (**9ab**), silybins (**9a** and **9b**), and tyrosol-based phenols (**6**, **7**, and **8**) suitably protected, using a Mitsunobu reaction. Subsequently, all silybin conjugates (**10** – **12** series a, b, and ab) underwent a well-optimized one-step oxidation, leading to the 2,3-dehydrosilybin derivatives (**13** – **15** series **a**, **b**, and **ab**).

The 7-*O*-alkyl derivatives (**10** – **15**, **a**, **b**, and **ab** series) exhibited good stability in both PBS and medium over 24-48 h. The HTYR derivatives (**12** and **15**) showed lower stability due to the high susceptibility to autoxidation of the catechol moiety of HTYR, observed after 48 h. However, this degradation was not attributed to the stability of the new 7-*O* alkyl bond.

In the ORAC assay, there was no significant variation in antioxidant activity, while in the DPPH assay the tyrosolic counterpart plays a crucial role, obtaining new derivatives with pronounced activity (**10** << **11** < **12**, of **a**, **b**, and **ab** series). Notably, the HTYR moiety significantly contributed to the antioxidant activity of **12b** (5.65 ± 0.50 μM), slightly exceeding that of **12a** (6.53 ± 0.60 μM). These values were much higher than those of the corresponding silybins (360 ± 02, 580 ± 0.5, and 620 ± 0.2 μM for **1a**, **1b**, and **1ab**, respectively). The same trend was observed for the 2,3-dehydrosilybin-based derivatives, with a smaller difference (**13** << **14** < **15**, of **a**, **b**, and **ab** series).

The study on silybin derivatives in PC-3 prostate cancer cells aligns with previous research on silybin's anticancer effects, attributing them to the inhibition of proliferation, induction of cell cycle arrest, and apoptosis. The present study, focusing

on silybin derivatives, particularly highlights the potency of compounds **15ab**, **15a**, and **15b** in inhibiting cell proliferation and inducing cell death in PC-3 cells.

The observed effects include G1 cell cycle arrest, a substantial increase in the late apoptotic population, and a marked elevation in the expression of cleaved caspase 3. These results underscore the anticancer efficacy of these silybin derivatives. Importantly, the fact that silibinin has already undergone clinical evaluation for safety and anticancer properties adds significance to these findings. The three identified potent silybin derivatives (**15ab**, **15a**, and **15b**) emerge as promising candidates for further investigation in pre-clinical models and, potentially, clinical trials.

As the research progresses, the focus will be extended to evaluating the *in vivo* anticancer efficacy of these promising silybin derivatives. Additionally, the assessment of their potential toxicity and bioavailability will contribute valuable insights for their potential use in clinical applications.

4.4 Experimental Session

4.4.1 General Methods

Silibinin **1** was purchased from Sigma-Aldrich. HPLC grade ACN, MeOH were purchased from Carlo Erba Reagents and Sigma-Aldrich. Other chemicals were obtained from Sigma Aldrich.

The experimental procedures to the synthesis of compounds **10** – **12** and **13** – **15** are described in detail only for the stereoisomer of silybin A (SilA): the same reaction conditions (temperature, stoichiometric ratios, time of reaction) were used for silybin B (SilB) and silibinin (Sil) as natural mixture.

Reactions were monitored by TLC (precoated silica gel plate F254, Merck) and Column chromatography: Merck Kieselgel 60 (70-230 mesh). The analysis was performed with a Shimadzu LC-8A PLC system equipped with a Shimadzu SCL-10A

VP System control and Shimadzu SPD-10A VP UV-VIS Detector. HPLC purifications were carried out on Phenomenex Gemini RP18 column (10-µm particle size, 21.20 mm × 250 mm i.d.) using a linear gradient of ACN in 0.1 M NH_4Ac in H_2O, pH 7.0 from 20% to 100% over 30 min at a flow rate of 8 mL/min with detection at 288 and 260 nm.

MALDI spectral data was acquired on a MALDI TOF AB Sciex 5800 mass spectrometer. For ESI-MS analysis, a Waters Micromass ZQ Instrument equipped with an electrospray source was used. The NMR spectra were recorded at 25 °C on an NMR spectrometer Bruker DRX, Bruker Advance (Bruker Italia Srl, Milano, Italy) and INOVA-500 NMR instrument (Varian, Milan, Italy).

4.4.2 Synthesis of Tyrosol-based Building Blocks

To a solution of the compound **3** (**4** or **5**; 7.2 mmol) in 15 mL of ACN/DMF 3/1 (v/v), 4.0 mL TEA (32.0 mmol; 2.2 equiv. for each OH group) and 3.57 g of TBDMSCl (23.7 mmol; 1.1 equiv. for each OH group) were added and stirred at RT for 3 h. The reaction was quenched adding MeOH and extracted with H_2O/EtOAc. The combined organic phases were washed with sat. $NaHCO_3$ and brine, dried over anhydrous Na_2SO_4, and evaporated under reduced pressure. The residue was purified by flash column chromatography on silica gel (hexane/EtOAc 80:20, v/v) to give the total protected compounds (**3.1-5.1**) in quantitative yield as a colorless oil.

3.1 ^{1}H NMR (400 MHz, $CDCl_3$, 25 °C, δ ppm, *J* Hz): δ = 7.08 (2H, d, *J* = 8.5, H-2 and H-6), 6.78 (2H, d, *J* = 8.5, H-3 and H-5), 3.80 (2H, t, *J* = 6.8, H-8), 2.78 (2H, t, *J* = 6.8, H-7), 1.01 (9H, s, $(CH_3)_3$ CSiOAr), 0.90 (9H, s, $(CH_3)_3$ $CSiOCH_2$), 0.21 (6H, s, $(CH_3)_2$ SiOAr), 0.005 (6H, s, (CH_3 $SiOCH_2$) ppm. ^{13}C NMR (100 MHz, $CDCl_3$, 25 °C, δ ppm): δ = 153.9, 131.9, 130.0, 119.8, 64.8, 38.8, 25.9, 25.7, 18.4, 18.2, -4.4, -5.4. MS (ESI+): calcd. for $C_{20}H_{39}O_2Si_2$ 367.25, found 367.48 $[M+H]^+$.

4.1 ^{1}H NMR (400 MHz, $CDCl_3$, 25 °C, δ ppm, *J* Hz): δ = 6.77 (1H, d, *J* = 8.4, H-5), 6.73 (1H, d, *J* = 2.2, H-2), 6.65 (1H, dd, *J* = 8.4, 2.2 Hz, H-6), 3.81 (3H, s, OCH_3) 3.80 (2H, t, *J* = 6.7 Hz, H-8), 2.76 (2H, t, *J*=6.9 Hz, H-7), 1.01 (9H, s, $(CH_3)_3CSiOAr$), 0.89 (9H, s, $(CH_3)_3CSiOCH_2$), 0.16 (6H, s, $(CH_3$ SiOAr), 0.005 (6H, s, $(CH_3SiOCH_2$) ppm. ^{13}C NMR (100 MHz, $CDCl_3$, 25 °C, δ ppm): δ = 150.9, 143.6, 131.8, 121.1, 120.9, 113.0, 63.7, 55.5, 38.9, 25.7, 18.4, 18.2, -4.6, -5.5 ppm. MS (ESI+): calcd. for $C_{21}H_{41}O_3Si_2$ 397.26, found 397.55 $[M+H]^+$.

5.1 ^{1}H NMR (400 MHz, $CDCl_3$, 25 °C, δ ppm, *J* Hz): δ = 6.75 (1H, d, *J* = 8.3, H-5), 6.70 (1H, d, *J* = 2.1, H-2), 6.65 (1H, dd, *J* = 8.3, 2.2, H-6), 3.78 (2H, t, *J* = 7.1, H-8), 2.72 (2H, t, *J*=7.1 Hz, H-7), 1.01 (9H, s, $(CH_3)_3CSiOAr$), 1.00 (9H, s, $(CH_3)_3CSiOAr$), 0.90 (9H, s, $(CH_3)_3$ $CSiOCH_2$), 0.21 (6H, s, $(CH_3)_2SiOAr$), 0.20 (6H, s, $(CH_3)_2SiOAr$), 0.02 (6H, s,$(CH_3SiOCH_2$) ppm. ^{13}C NMR (100 MHz, $CDCl_3$, 25 °C, δ ppm): δ = 146.4, 145.1, 132.3, 122.1, 122.0, 120.8, 64.8, 39.0, 26.0, 18.4, 18.4, 18.3, -4.0, -4.1, -5.3 ppm. MS (ESI+): calcd. for $C_{26}H_{53}O_3Si_3$ 497.33, found 497.39 $[M+H]^+$.

Subsequently, 2.20 mmol TBDMS ether **3.1** (**4.1** or **5.1**) were added to a round bottomed flask and diluted to 0.1 M concentration in MeOH. Once the substrate dissolved, 1 wt% (10 mg/mL) of I_2 was added. Reaction progress was monitored by TLC (DCM/MeOH 90:10, v/v). Upon consumption of the alcoholic silyl ether, solid $Na_2S_2O_3$ was added, and the heterogeneous mixture stirred until the I_2 color had dissipated. The methanolic solution was then diluted with DCM and washed with saturated aqueous $NaHCO_3$. Drying over anhydrous Na_2SO_4, filtering, and evaporation to dryness give material that was then purified by flash column chromatography on silica gel (DCM /MeOH 90:10, v/v) to give compound **6** (**7** or **8**) in good yield (82 - 86%).

6 ^{1}H NMR (400 MHz, $CDCl_3$, 25 °C, δ ppm, *J* Hz): δ = 7.10 (2H, d, *J* = 8.6, H-2 and H-6), 6.81 (2H, d, *J* = 8.5, H-3 and H-5), 3.84 (2H, t, *J* = 6.7, H-8), 2.82 (2H, t, *J* = 6.6, H-7), 1.00 (9H, s, $(CH_3)_3$ $CSiOAr$), 0.21 (6H, s, $(CH_3)_2SiOAr$) ppm.^{13}C NMR

(100 MHz, $CDCl_3$, 25 °C, δ ppm): δ = 154.3, 130.9, 130.0, 120.2, 63.8, 38.4, 25.7, 18.2 -4.4 ppm. MS (ESI+): calcd. for $C_{14}H_{25}O_2Si$ 253.16, found 253.86 $[M+H]^+$.

7 ^1H NMR (400 MHz, $CDCl_3$, 25 °C, δ ppm, *J* Hz): δ = 6.81 (1H, d, *J* = 8.0, H-5), 6.74 (1H, d, *J* = 1.9, H-2), 6.69 (1H, dd, *J* = 8.0, 2.1, H-6), 3.84 (2H, t, *J* = 6.5, H-8), 3.82 (3H, s, OCH_3), 2.81 (2H, t, *J* = 6.6, H-7), 1.02 (9H, s, $(CH_3)_3CSiOAr$), 0.17 (6H, s, $(CH_3)_2SiOAr$) ppm. ^{13}C NMR (100 MHz, $CDCl_3$, 25 °C, δ ppm): δ = 150.9, 143.7, 131.8, 121.1, 120.9, 113.0, 63.7, 55.5, 38.9, 25.7, 18.4, -4.6 ppm. MS (ESI+): calcd. for $C_{15}H_{27}O_3Si$ 283.17, found 283.11 $[M+H]^+$.

8 ^1H NMR (400 MHz, $CDCl_3$, 25 °C, δ ppm, *J* Hz): δ = 6.79 (1H, d, *J* = 8.1, H-5), 6.73 (1H, d, *J* = 2.1, H-2), 6.68 (1H, dd, *J* = 8.0, 2.1, H-6), 3.80 (2H, t, *J* = 6.8, H-8), 2.76 (2H, t, *J* = 6.7, H-7), 1.02 and 1.01 (18H, s, $(CH_3)_3CSiOAr$), 0.23 and 0.22 (12H, s, $(CH_3)_2SiOAr$) ppm. ^{13}C NMR (100 MHz, $CDCl_3$, 25 °C, δ ppm): δ = 146.8, 145.5, 131.3, 121.9, 121.8, 121.0, 63.8, 38.5, 25.9, 18.4, -4.0, -4.1 ppm. MS (ESI+): calcd. for $C_{20}H_{39}O_3Si_2$ 383.24, found 383.55 $[M+H]^+$.

4.4.3 Synthesis of Silybins Building Blocks

SilA **1** (1.0 g, 2.0 mmol) previously co-evaporated with anhydrous THF (3 times), was dissolved in 12 mL of anhydrous ACN/DMF 3:1 (v/v) and 760 µL (7.0 mmol) of dry pyridine were added. The mixture was cooled to 0 °C and then TBDMSCl (630 mg, 4.2 mmol) was added and stirred. After 1 h (always at 0 °C) the disappearance of SilA by TLC control was observed, and about 1 mL MeOH was added and kept under stirring for a further 30 min. The mixture was diluted with DCM (100 mL) and was washed three times with saturated $NaHCO_3$ solution. The organic phase was dried over anhydrous Na_2SO_4 and concentrated under reduced pressure. The crude material was purified by column chromatography eluted with DCM/MeOH 97:3 (v/v) and the derivative 9"-OTBDMS (**9a**) was obtained in good yield (1.1 g, 18.8 mmol, 74%).

9a ^{1}H NMR (400 MHz, $CDCl_3$, 25 °C, δ ppm, *J* Hz): δ = 7.20 (*d*, *J* = 1.45 Hz, 1H, H-2'); 7.07 (*dd*, *J* = 8.44, 1.71 Hz, 1H, H-6'); 7.02 (*d*, *J* = 8.26 Hz, 1H, H-5'); 6.96 (*s*, 3H, H-2", H-5" and H-6"); 6.09 (*s*, 1H, H-8); 6.02 (*s*, 1H, H-6); 5.01-4.97 (overlapped signals, 2H, H-2 and H-7"); 4.55 (*d*, *J* = 11.8 Hz, 1H, H-3); 3.97 (*m*, 1H, H-8"); 3.91 (*s*, 3H, $OC\underline{H}_3$); 3.87 (*dd*, *J* = 11.9, 1.87 Hz, 1H, H-9"a); 3.57 (*dd*, *J* = 11.9, 2.84 Hz, 1H, H-9"b); 0.92 (*s*, 9H, $(CH_3)_3CSiOCH_2$); 0.08 (*d*, *J* = 4.79 Hz, 6H, $(CH_3)_2$ $SiOCH_2$) ppm. ^{13}C NMR ($CDCl_3$, 125 MHz, 25 °C, δ ppm): δ = 195.5; 167.5; 163.7; 163.1; 146.7; 146.1; 144.7; 143.9; 129.0; 128.4; 121.2; 120.8; 117.1; 116.3; 114.5; 109.8; 100.2; 97.2; 96.1; 83.0; 78.6; 76.2; 72.2; 62.3; 56.0; 25.8; 18.3; -5.12; -5.42 ppm. MALDI-HRMS (positive ions): *m/z* calculated for ($[C_{31}H_{36}O_{10}Si + Na]^+$) 619.1970; found 619.1977.

9b ^{1}H NMR (400 MHz, $CDCl_3$, 25 °C, δ ppm, *J* Hz): δ = 7.17 (*d*, *J* = 1.84 Hz, 1H, H-2'); 7.08 (*dd*, *J* = 8.43, 1.90 Hz, 1H, H-6'); 7.01 (*d*, *J* = 8.23 Hz, 1H, H-5'); 6.96-6.94 (overlapped signals, 3H, H-2", H-5" and H-6"); 6.08 (*d*, *J* = 2.0 Hz, 1H, H-8); 6.03 (*d*, *J* = 2.0 Hz, 1H, H-6); 5.01-4.98 (overlapped signals, 2H, H-2 and H-7"); 4.55 (*d*, *J* = 11.8 Hz, 1H, H-3); 3.96 (*m*, 1H, H-8"); 3.88-3.85 (overlapped signals, 4H, $OC\underline{H}_3$ and H-9"a); 3.56 (*dd*, *J* = 11.8, 2.84 Hz, 1H, H-9"b); 0.91 (*s*, 9H, $(CH_3)_3CSiOCH_2$); 0.07 (*d*, *J* = 4.98 Hz, 6H, $(CH_3)_2$ $SiOCH_2$) ppm. ^{13}C NMR ($CDCl_3$, 125 MHz, 25 °C, δ ppm): δ = 195.7; 168.3; 163.8; 163.0; 147.2; 146.6; 144.5; 143.9; 129.2; 128.1; 120.8; 120.7; 117.2; 116.5; 114.9; 110.1; 100.2; 97.2; 96.1; 83.1; 78.6; 76.2; 72.3; 62.3; 55.9; 25.8; 18.3; -5.14; -5.44 ppm. MALDI-HRMS (positive ions): *m/z* calculated for ($[C_{31}H_{36}O_{10}Si + Na]^+$) 619.1970; found 619.1977.

4.4.4 Alkylation by Mitsunobu reaction: General procedure for the synthesis of 10a – 12a

To a solution of TPP and DIAD (0.50 mmol of each) dissolved in 2 mL of anhydrous THF and kept at 0 °C for 20 min, a mixture of 9"-O-protect silybin A **9a**

(200 mg, 0.33 mmol) and tyrosyl building block (**5** or **6** or **7**, 0.33 mmol), were sequentially added and the resulting mixture was left stirring at 0 °C for 2 h. The reaction was monitored by TLC (hexane/EtOAc 85:15, v/v) and the crude reaction mixtures were found to be complex to purify and after several attempts at simplification by crystallization, it was decided to carry out a coarse chromatography on silica gel column eluted with hexane/EtOAc (80:20, v/v) and then to treat the crude fractions, previously dried under reduced pressure, with TEA·3HF (65 µL, 0.40 mmol) in 500 µL THF at rt. After silica gel chromatography eluted with DCM/MeOH (95:5, v/v), all compounds **10a** – **12a**, obtained in good yields (26 – 35%, see Table 1), were purified by RP-HPLC using a Phenomenex Gemini RP18 column (10-µm particle size, 21.20 mm × 250 mm i.d.) with a linear gradient of ACN in 0.1 M NH_4OAc in H_2O, pH 7.0 from 20% to 100% over 30 min at a flow rate of 8 mL/min with detection at 288 and 260 nm. The identity of compounds **10a** – **12a**, with a final purity > 95%, were confirmed by 1D and 2D NMR and MALDI-TOF analyses.

10a ^{1}H NMR (500 MHz, CD_3OD, 25 °C, δ ppm, *J* Hz); 7.13 (s, 1H, H2'); 7.10 (d, *J* = 8.1, 2H, H2''', H6'''); 7.06 (dd, *J* = 8.3, 1.8, 1H, H6');7.04 -7.00 (overlapped signals, 2H, H5', H2''), 6.92 (dd, *J* = 8.2, 1.4, 1H, H6''); 6.86 (d, *J* = 8.2, 1H, H5''); 6.73 (d, *J* = 8.1, 2H, H5''', H3'''); 6.08 (d, *J* = 1.8, 1H, H6); 6.04 (d, *J* = 1.8, 1H, H8); 5.02 (d, *J* = 11.4, 1H, H2); 4.94 (d, *J* = 8.0, 1H, H7''); 4.56 (d, *J* = 11.4, 1H, H3); 4.16 (t, *J* = 6.7, 2H, H8'''); 4.12-4.06 (m, 1H, H8''); 3.89 (s, 1H, OCH_3); 3.74 (dd, *J* = 12.4, 2.2, 1H, H9''a); 3.51 (dd, *J* = 12.3, *J* = 4.4, 1H, H9''b); 2.96 (t, *J* = 6.7, 2H, H7''') ppm. ^{13}C NMR (125 MHz, CD_3OD, 25 °C, δ ppm): 197.4; 167.6; 163.6; 162.8; 155.7; 148.0; 147.8; 146.9; 143.7; 130.0; 129.5 (x3); 128.6; 128.0; 120.8; 120.3; 116.4; 116.1; 114.8 (x2); 110.6; 101.1; 95.2; 94.1; 83.4; 78.6; 78.3; 72.3; 69.3; 60.6; 55.0; 34.1 ppm. MS (MALDI-TOF) (+): m/z calculated for $C_{33}H_{30}O_{11}$ = 602.18; found 603.26 $[M + H]^+$

10b ^{1}H-NMR (CD_3OD, 500 MHz, 25 °C, δ ppm, *J* Hz); 7.13 (s, 1H, H2'); 7.10 (d, *J* = 8.1, 2H, H2''', H6'''); 7.06 (dd, *J* = 8.3, *J* = 1.8, 1H, H6');7.04 -7.00 (overlapped

signals, 2H, H5', H2", 6.92 (dd, *J* = 8.2, *J* = 1.4, 1H, H6"; 6.86 (d, *J* = 8.2, 1H, H5"; 6.73 (d, *J* = 8.1, 2H, H5"', H2"'); 6.08 (d, *J* = 1.8, 1H, H6); 6.04 (d, *J* = 1.8, 1H, H8); 5.02 (d, *J* = 11.4, 1H, H2); 4.94 (d, *J* = 8.0, 1H, H7"; 4.56 (d, *J* = 11.4, 1H, H3); 4.16 (t, *J* = 6.7, 2H, H8"'); 4.12-4.06 (m, 1H, H8"; 3.89 (s, 1H, OCH_3); 3.74 (dd, *J* = 12.4, *J* = 2.2, 1H, H9"a); 3.51 (dd, *J* = 12.3, *J* = 4.4, 1H, H9"b); 2.96 (t, *J* = 6.7, 2H, H7"') ppm. ^{13}C-NMR (CD_3OD, 125 MHz, 25 °C, δ ppm): 197.4; 167.6; 163.6; 162.8; 155.7; 148.0; 147.8; 146.9; 143.7; 130.0; 129.5 (x3); 128.6; 128.0; 120.8; 120.3; 116.4; 116.1; 114.8 (x2); 110.6; 101.1; 95.2; 94.1; 83.4; 78.6; 78.3; 72.3; 69.3; 60.6; 55.0; 34.1 ppm. MS (MALDI-TOF) (+): calculated for [M] ($C_{33}H_{30}O_{11}$) 602.18; found 603.25 $[M + H]^+$, 625.84 $[M + Na]^+$.

10ab ^{1}H-NMR (400 MHz, CD_3OD, 25 °C, δ ppm, *J* Hz); 7.15-7.07 (overlapped signals, 3H, H2', H2"', H6"'); 7.07-6.99 (overlapped signals, 3H, H6', H5', H2"; 6.92 (dd, *J* = 8.1, *J* = 1.7, 1H, H6"; 6.85 (d, *J* = 8.0, 1H, H5"; 6.73 (d, *J* = 8.1, 2H, H5"', H2"'); 6.07 (d, *J* = 2.0, 1H, H6); 6.03 (d, *J* = 2.0, 1H, H8); 5.01 (d, *J* = 11.5, 1H, H2); 4.93 (d, *J* = 8.1, 1H, H7"; 4.55 (d, *J* = 11.5, 1H, H3); 4.15 (t, *J* = 6.4, 2H, H8"'); 4.11-4.05 (m, 1H, H8"; 3.88 (s, 1H, OCH_3); 3.72 (dd, *J* = 12.4, *J* = 2.4, 1H, H9"a); 3.50 (dd, *J* = 12.4, *J* = 4.5, 1H, H9"b); 2.95 (t, *J* = 6.4, 2H, H7"') ppm. ^{13}C NMR (100 MHz, DMSO-*d6*, 25 °C, δ ppm): 197.3; 167.6; 163.6; 162.8; 155.7; 148.0); 147.8; 144.1; 143.7; 130.1; 129.6 (x2); 129.0; 127.9; 121.6; 120.8; 120.3; 116.2; 116.3; 114.8 (x2); 110.6; 101.1; 95.1; 94.0; 83.3; 78.2; 76.2; 72.3; 69.3; 60.6; 54.9; 34.1 ppm. MS (MALDI-TOF) (+): calculated for [M] ($C_{33}H_{30}O_{11}$) 602.18; found 603.66 $[M + H]^+$, 625.48 $[M + Na]^+$.

11a ^{1}H-NMR (400 MHz, CD_3OD, 25 °C, δ ppm, *J* Hz); 7.11 (d, *J* = 1.5, 1H, H2'); 7.03 (dd, *J* = 8.2, *J* = 1.8, 1H, H6'); 7.02-6.96 (overlapped signals, 2H, H5', H2"), 6.91 (dd, *J* = 8.0, *J* = 1.7, 1H, H6"); 6.87-6.83 (overlapped signals, 2H, H5", H2"'); 6.72 (d, *J* = 8.0, 1H, H5"'); 6.69 (dd, *J* = 8.0, *J* = 1.6, 1H, H6"'); 6.06 (d, *J* = 2.1, 1H, H6); 6.01 (d, *J* = 2.1, 1H, H8); 4.99 (d, *J* = 11.3, 1H, H2); 4.95-4.89 (overlapped signals with

H_2O, 1H, H7"); 4.52 (d, *J* = 11.3, 1H, H3); 4.15-4.03 (overlapped signals, 3H, H8", H8'"); 3.87 (s, 1H, OCH_3); 3.82 (s, 1H, OCH_3); 3.71 (dd, *J* = 12.4, *J* = 2.4, 1H, H9"a); 3.49 (dd, *J* = 12.3, *J* = 4.3, 1H, H9"b); 2.95 (t, *J* = 6.8, 2H, H7'") ppm. ^{13}C-NMR (125 MHz, CD_3OD, 25 °C, δ ppm): 197.3; 167.6; 163.6; 162.8; 147.8; 147.5; 147.0; 144.8; 144.1; 143.7; 130.0; 129.3; 128.0; 121.1; 120.9; 120.3; 116.4 ; 116.2; 114.9, 114.8; 112.3; 110.7; 101.1; 95.2; 94.1; 83.4; 78.6; 76.3; 72.3; 69.3; 60.7; 55.0; 54.9; 34.6 ppm. MS (MALDI-TOF) (+): calculated for [M] ($C_{34}H_{32}O_{12}$) 632.19; found 633.68 $[M + H]^+$, 655.56 $[M + Na]^+$.

11b ^{1}H-NMR (400 MHz, DMSO-*d6*, 25 °C, δ ppm, *J* Hz); 7.07 (s, 1H, H2'); 7.05-6.96 (overlapped signals, 3H, H5', H6', H2"), 6.90-6.83 (overlapped signals, 2H, H6", H2'"); 6.81 (d, *J* = 8.2, 1H, H5") 6.71–6.64 (overlapped signals, 2H, H-6'", H5'"); 6.13-6.063 (overlapped signals, 2H, H6, H8); 5.11 (d, *J* = 11.1, 1H, H2); 4.90 (d, *J*= 7.8, 1H, H7"); 4.62 (d, *J* = 11.1, 1H, H3); 4.24-4.12 (overlapped signals, 3H, H8", H8'"); 3.77 (s, 1H, OCH_3); 3.73 (s, 1H, OCH_3); 3.66-3.43 (overlapped signals with H_2O, 1H, H9"a); 3.34 (dd, *J* = 12.5, *J* = 4.9, 1H, H9"b); 2.89 (t, *J* = 6.4, 2H, H7'") ppm. ^{13}C-NMR (125 MHz, CD_3OD, 25 °C, δ ppm): 197.3; 167.6; 163.5; 162.8; 147.8; 147.5; 146.9; 144.7; 144.1; 143.7; 130.0; 129.3; 128.0; 121.1; 120.8; 120.2; 116.4 ; 116.1; 114.8, 114.7; 112.3; 110.6; 101.1; 95.2; 94.1; 83.4; 78.6; 76.2; 72.3; 69.3; 60.6; 55.0; 54.9; 34.5 ppm. MS (MALDI-TOF) (+): calculated for [M] ($C_{34}H_{32}O_{12}$) 632.19; found 633.68 $[M + H]^+$, 655.56 $[M + Na]^+$.

11ab ^{1}H-NMR (400 MHz, CD_3OD, 25 °C, δ ppm, *J* Hz, mixture of diastereoisomers); 7.10 (m, 1H, H6'); 7.07-6.98 (complex signals, 3H, H2', H5'", H2"), 6.90 (dd, *J* = 8.2, *J* = 1.6, 1H, H6"); 6.87–6.74 (complex signals, 2H, H-6T, H5'); 6.76–6.65 (complex signals, 2H, H5", H2'"); 6.06 (dd, *J* = 1.8, 1H, H6); 6.01 (dd, *J* = 1.8, 1H, H8); 4.98 (d, *J* = 11.6, 1H, H2); 4.90 (overlapped signal with H_2O, 1H, H7"); 4.51 (d, *J* = 11.5, 1H, H3); 4.14 (t, *J* = 6.9, 2H, H8'"); 4.06 (m, 1H, H8"); 3.87 (s, 1H, OCH_3); 3.82 (s, 1H, OCH_3); 3.71 (dd, *J* = 12.3, *J* = 2.3, 1H, -9"a); 3.49 (dd, *J* = 12.3,

J = 4.6, 1H, H9"b); 2.95 (t, *J* = 6.2, 2H, H7"') ppm. ^{13}C-NMR (125 MHz, CD_3OD, 25 °C, δ ppm): 197.3; 167.6; 163.5; 162.7; 147.8; 147.5; 146.9; 144.7; 144.1; 143.7; 130.0; 129.3; 128.0; 121.1; 120.8; 120.7; 120.2; 116.4 (x2); 116.2; 116.1; 114.8 (x2), 112.3; 110.6 (x2); 101.1; 95.2; 94.1; 83.3 (x2); 78.6; 76.2; 72.3; 69.3; 60.6; 55.0 (x2); 34.5 ppm. MS (MALDI-TOF) (+): calculated for [M] ($C_{34}H_{32}O_{12}$) 632.19; found 633.25 $[M + H]^+$, 655.56 $[M + Na]^+$, 671.56 $[M + K]^+$.

12a ^{1}H NMR (500 MHz, CD_3OD, 25 °C, δ ppm, *J* Hz); 7.11 (s, 1H, H2'); 7.06-6.95 (overlapped signals, 3H, H6', H5', H2"), 6.90 (complex signal, 1H, H6"); 6.85 (d, *J* = 8.2, 1H, H5"); 6.73-6.67 (overlapped signals, 2H, H5"', H2"'); 6.57 (d, *J* = 8.0, 1H, H6"'); 6.05 (s, 1H, H6); 6.00 (s, 1H, H8); 4.98 (complex signal, 1H, H2); 4.90 (overlapped signal with H_2O, 1H, H7"); 4.50 (complex signal, 1H, H3); 4.16-4.00 (overlapped signals, 3H, H8"', H8"); 3.87 (s, 1H, OCH_3); 3.71 (d, *J* = 11.8, 1H, H9"a); 3.49 (dd, *J* = 12.3, *J* = 4.2, 1H, H9"b); 2.87 (s, 2H, H7"') ppm. ^{13}C NMR (125 MHz, CD_3OD, 25 °C, δ ppm): 197.3; 167.6; 163.5; 162.7; 147.8; 146.9; 144.8; 144.1; 143.7; 143.5; 130.0; 129.3; 128.0; 120.8; 120.3; 119.9; 116.4; 116.2 (x2); 115.7; 115.0; 114.9; 110.6; 101.1; 95.2; 94.1; 83.3; 78.6; 76.2; 72.3; 69.3; 60.6; 55.0; 34.3 ppm. (MALDI-TOF) (+): m/z calculated for $C_{33}H_{30}O_{12}$ = 618.17; found 618.69 $[M + H]^+$, 641.77 $[M + Na]^+$

12b ^{1}H-NMR (500 MHz, CD_3OD, 25 °C, δ ppm, *J* Hz); 7.11 (s, 1H, H2'); 7.06-6.95 (overlapped signals, 3H, H6', H5', H2"), 6.90 (complex signal, 1H, H6"); 6.85 (d, *J* = 8.2, 1H, H5"); 6.73-6.67 (overlapped signals, 2H, H5"', H2"'); 6.57 (d, *J* = 8.0, 1H, H6"'); 6.05 (s, 1H, H6); 6.00 (s, 1H, H8); 4.98 (complex signal, 1H, H2); 4.90 (overlapped signal with H_2O, 1H, H7"); 4.50 (complex signal, 1H, H3); 4.16-4.00 (overlapped signals, 3H, H8"', H8"); 3.87 (s, 1H, OCH_3); 3.71 (d, *J* = 11.8, 1H, H9"a); 3.49 (dd, *J* = 12.3, *J* = 4.2, 1H, H9"b); 2.87 (s, 2H, H7"') ppm. ^{13}C-NMR (125 MHz, CD_3OD, 25 °C, δ ppm): 197.3; 167.6; 163.5; 162.7; 147.8; 146.9; 144.8; 144.1; 143.7; 143.5; 130.0; 129.3; 128.0; 120.8; 120.3; 119.9; 116.4; 116.2 (x2); 115.7; 115.0;

114.9; 110.6; 101.1; 95.2; 94.1; 83.3; 78.6; 76.2; 72.3; 69.3; 60.6; 55.0; 34.3 ppm. MS (MALDI-TOF) (+): calculated for [M] ($C_{33}H_{30}O_{12}$) 618.17; found 618.69 $[M + H]^+$, 641.77 $[M + Na]^+$, 657.87 $[M + K]^+$.

12ab ^{1}H-NMR (500 MHz, CD_3OD, 25 °C, δ ppm, *J* Hz); 7.10 (d, 1H, H2'); 7.05-6.96 (overlapped signals, 3H, H6', H5', H2"), 6.89 (d, *J* = 7.7, 1H, H6"); 6.84 (d, *J* = 7.7, 1H, H5"); 6.75-6.67 (overlapped signals, 2H, H5"', H2"'); 6.57 (d, *J* = 7.7, 1H, H6"'); 6.05 (s, 1H, H6); 6.00 (s, 1H, H8); 4.98 (dd, *J* = 11.5, *J* = 2.1, 1H, H2); 4.90 (overlapped signal with H_2O, 1H, H7"); 4.50 (dd, *J* =11.5, *J* = 2.1, 1H, H3); 4.15-4.01 (overlapped signals, 3H, H-8T, H8"); 3.86 (s, 1H, OCH_3); 3.70 (d, *J* = 12.3, 1H, H9"a); 3.49 (dd, *J* = 11.4, *J* = 4.3, 1H, H9"b); 2.87 (t, *J* = 6.0, 2H, H7"') ppm. ^{13}C-NMR (125 MHz, CD_3OD, 25 °C, δ ppm): 197.2; 167.6; 163.5; 162.7; 147.7; 146.9; 144.7; 144.0; 143.7; 143.5; 129.9; 129.3; 128.0; 120.8 (x2); 120.3; 119.9; 116.4 (x2); 116.2 (x2); 115.7; 115.0; 114.9; 110.6 (x2); 101.1; 95.2; 94.1; 83.3; 78.6; 76.3; 72.3; 69.3; 60.6; 55.0; 34.3 ppm. MS (MALDI-TOF) (+): calculated for [M] ($C_{33}H_{30}O_{12}$) 618.17; found 618.55 $[M + H]^+$, 641.67 $[M + Na]^+$, 657.88 $[M + K]^+$.

4.4.5 Synthesis of 7-*O*-tyrosyl-2,3-dehydro silybin derivatives (13a - 15a): General procedure

7-*O*-tyrosyl SilA derivatives **10a** – **12a** (0.08 mmol), was dissolved in 500 µL of DMF and 24 mg of KOAc (0.24 mmol) were added. The mixture was kept at 50 °C and after 45 min the disappearance of SilA derivative followed by TLC (DCM/MeOH/AcOH, 90:10:0.01, v/v/v) control, was observed. The crude material was purified by column chromatography eluted with DCM/MeOH 90:10 (v/v) and the derivative 7-*O*-tyrosyl-2,3-dehydro silybin (**13a** – **15a**) were obtained in good yield (78 – 85%, see Table 1). RP-HPLC purification was carried out on Phenomenex Gemini RP18 column (10-µm particle size, 21.20 mm × 250 mm i.d.) using a linear gradient of ACN in 0.1 M NH_4OAc in H_2O, pH 7.0 from 20% to 100% over 30 min

at a flow rate of 8 mL/min with detection at 288 and 260 nm. The purity of final products (**13a** – **15a**) was on average 99.0%.

13a ^{1}H-NMR (500 MHz, DMSO-*d6*, 25 °C, δ ppm, *J* Hz); 7.82-7.81 (overlapped signals, 2H, H2', H6'); 7.12-7.09 (overlapped signals, 3H, H5', H3''', H5'''), 7.04 (s, 1H, H2''); 6.88 (d, *J* = 7.7, 1H, H6''); 6.82–6.80 (overlapped signals, 2H, H8, H5''); 6.69 (d, *J* = 7.9, 2H, H2''', H6'''); 6.31 (s, 1H, H6); 4.96 (d, *J* = 8.3, 1H, H7''); 4.27 (m, 1H, H8''); 4.22 (t, *J* = 6.6, 2H, H8'''); 3.78 (s, 3H, OMe); 3.56 (d, *J* = 11.7, 1H, H9''a); 3.36 (overlapped signal with H_2O , 1H, H9''b) 2.93 (t, *J* = 6.6, 2H, H-7''') ppm. ^{13}C-NMR (125 MHz, DMSO-d6, 25 °C, δ ppm): 176.6; 164.7; 160.8; 156.6; 156.4; 148.1; 147.5; 146.5; 145.6; 143.9; 137.2; 130.4; 128.3 (x2); 127.7; 124.2; 121.9; 121.0; 117.3; 116.7; 115.8; 115.6 (x2); 112.1; 104.5; 98.3; 93.1; 79.0; 76.3; 69.8; 60.6; 56.2; 34.3 ppm. MS (MALDI-TOF) (+): calculated for [M] ($C_{33}H_{28}O_{11}$) 600.16; found 600.38 $[M + H]^+$, 623.44 $[M + Na]^+$, 639.49 $[M + K]^+$.

13ab ^{1}H-(500 MHz, CD_3OD, 25 °C, δ ppm, *J* Hz); 7.79-7.73 (overlapped signals, 2H, H2', H6'); 7.12 (d, *J* = 8.35, 2H, H3''', H5'''), 7.05-7.02 (overlapped signals, 2H, H5', H2''); 6.93 (d, *J* = 7.71, 1H, H6''); 6.87 (d, *J* = 8.35, 1H, H5''); 6.74 (d, *J* = 7.71, 2H, H2''', H6'''); 6.45 (s, 1H, H8); 6.21 (s, 1H, H6); 4.92 (overlapped signal with H_2O, 1H, H7''); 4.15-4.11 (complex signal, 3H, H8'', H8'''); 3.90 (s, 3H, OMe); 3.73 (d, *J* = 11.3, 1H, H9''a); 3.50 (dd, *J* = 12.4, *J* = 4.19, 1H, H9''b) 2.96 (t, *J* = 6.6, 2H, H-7''') ppm. ^{13}C-NMR (125 MHz, CD_3OD, 25 °C, δ ppm): 176.0; 164.8; 160.7; 156.6; 155.7; 147.9; 147.0; 145.8; 145.2; 143.6; 137.2; 129.6 (x2); 128.7; 127.8; 124.2; 121.2; 120.4; 116.5; 116.3; 114.9; 114.8 (x2); 110.7; 104.0; 97.5; 91.9; 79.0; 76.3; 69.4; 60.6; 55.1; 34.2 ppm. MS (MALDI-TOF) (+): calculated for [M] ($C_{33}H_{28}O_{11}$) 600.16; found 600.56 $[M + H]^+$, 623.63 $[M + Na]^+$, 639.89 $[M + K]^+$.

14a ^{1}H-NMR (500 MHz, DMSO-d6, 25 °C, δ ppm, *J* Hz); 7.82-7.81 (overlapped signals, 2H, H2', H6'); 7.12 (d, *J* = 9.8, 1H, H5'), 7.04 (s, 1H, H2''); 6.89-6.87 (overlapped signals, 2H, H6'', H2'''); 6.83–6.80 (overlapped signals, 2H, H8, H5'''');

6.69 (overlapped signals, 2H, H5", H6'"); 6.33 (s, 1H, H6); 4.96 (d, *J* = 7.91, 1H, H7"); 4.28 (complex signal, 1H, H8"); 4.25 (t, *J* = 6.8, 2H, H8'"); 3.78 (s, 3H, OMe); 3.75 (s, 3H, OMe); 3.56 (d, *J* = 12.2, 1H, H9"a); 3.36 (overlapped signal with H_2O , 1H, H9"b) 2.94 (t, *J* = 6.8, 2H, H7'") ppm. ^{13}C-NMR (125 MHz, DMSO-*d6*, 25 °C, δ ppm): 176.6; 164.7; 160.7; 156.6; 148.1; 147.9; 147.5; 146.5; 145.6; 145.5; 143.9; 137.1; 129.0; 127.7; 124.2; 121.9; 121.6; 121.0; 117.3; 116.7; 115.8 (x2); 113.6; 112.1; 104.5; 98.3; 93.1; 79.0; 76.3; 69.8; 60.5; 56.1; 56.0; 34.7 ppm. MS (MALDI-TOF) (+): calculated for [M] ($C_{34}H_{30}O_{12}$) 630.17; found 631.66 $[M + H]^+$, 653.56 $[M + Na]^+$, 669.47 $[M + K]^+$.

14ab ^{1}H-NMR (500 MHz, CD_3OD, 25 °C, δ ppm, *J* Hz); 7.70-7.66 (overlapped signals, 2H, H2', H6'); 7.02-7.95 (overlapped signals, 2H, H5', H2"), 6.90-6.84 (overlapped signals, 3H, H5", H6", H2'"); 6.74-6.68 (overlapped signals, 2H, H5'", H6'"); 6.32 (s, 1H, H8); 6.13 (s, 1H, H6); 4.87 (overlapped signal with H2O, 1H, H7"); 4.06 (overlapped signal, 3H, H8", H8'"); 3.78 (s, 3H, OMe); 3.82 (s, 3H, OMe); 3.70 (d, *J* = 11.7, 1H, H9"a); 3.48 (dd, *J* = 12.5, *J* = 3.9, 1H, H9"b) 2.92 (s, 2H, H7'") ppm. ^{13}C-NMR (125 MHz, CD_3OD, 25 °C, δ ppm): 175.7; 164.6; 160.5; 156.4; 147.8; 147.5; 147.0; 145.5; 145.2; 144.7; 143.6; 136.5; 129.4; 127.8; 124.0; 121.1 (x2); 120.4; 116.5; 116.2; 114.9; 114.8; 112.3; 110.7; 103.9; 97.4; 91.8; 79.0; 76.2; 69.2; 60.6; 55.1; 56.0; 34.6 ppm. MS (MALDI-TOF) (+): calculated for [M] ($C_{34}H_{30}O_{12}$) 630.17; found 631.28 $[M + H]^+$, 653.24 $[M + Na]^+$, 669.49 $[M + K]^+$.

15a ^{1}H-NMR (500 MHz, Acetone-*d6*, 25 °C, δ ppm, *J* Hz); 7.90 (overlapped signals, 2H, H2', H6'); 7.12 (s, 1H, H2"), 7.08 (d, *J* = 8.07, 1H, H5'); 6.97 (d, *J* = 7.26, 1H, H6"); 6.88 (d, *J* = 7.66, 1H, H5"); 6.78 (s, 2H, H8, H2'"); 6.72 (d, *J* = 7.26, 1H, H5'"); 6.61 (d, *J* = 7.66, 1H, H6'") 6.30 (s, 1H, H6); 5.03 (d, *J* = 7.92, 1H, H7"); 4.29-4.20 (overlapped signals, 3H, H8", H8'"); 3.86 (s, 3H, OMe); 3.73 (d, *J* = 11.6, 1H, H9"a); 3.49 (dd, *J* = 12.3, *J* = 3.6, 1H, H9"b); 2.94 (t, *J* = 6.3, 2H, H7'") ppm. ^{13}C-NMR (125 MHz, DMSO-*d6*, 25 °C, δ ppm): 176.6; 164.9; 161.1; 156.7; 148.0; 147.7;

146.1; 145.6; 145.5; 144.2; 143.9; 137.4; 129.0; 127.8; 124.3; 121.5; 120.8; 119.9; 116.9; 116.5; 116.4; 115.5; 115.4; 111.16; 104.3; 97.9; 92.4; 79.3; 76.4; 69.7; 60.7; 55.6; 34.5 ppm. MS (MALDI-TOF) (+): calculated for [M] ($C_{33}H_{28}O_{12}$) 616.16; found 617.88 $[M + H]^+$, 639.63 $[M + Na]^+$, 655.46 $[M + K]^+$.

15ab ^{1}H-NMR (400 MHz, DMSO-*d6* +H_2O, 25 °C, δ ppm, *J* Hz); 7.75-7.73 (overlapped signals, 2H, H2', H6'); 7.06 (d, *J* = 8.55, 1H, H5'); 6.97 (d, *J* = 0.94, 1H, H2"); 6.83 (dd, *J* = 8.20, *J* = 1.41, 1H, H6"); 6.78-6.72 (overlapped signals, 2H, H5", H8); 6.64 (d, *J* = 1.41, 1H, H2'"); 6.60 (d, *J* = 7.97, 1H, H5'"); 6.49 (dd, *J* = 8.03, *J* = 1.72, 1H, H6'"); 6.24 (s, 1H, H6); 4.89 (d, *J* = 7.98, 1H, H7"); 4.21 (complex signal, 1H, H8") 4.14 (t, *J* = 6.27, 2H, H8'"); 3.72 (s, 3H, OMe); 3.50 (d, *J* = 11.4, 1H, H9"a); 3.30 (dd, *J* = 12.6, *J* = 4.6, 1H, H9"b); 2.80 (t, *J* = 6.48, 2H, H7'") ppm. ^{13}C-NMR (100 MHz, CD_3OD, 25 °C, δ ppm): 176.1; 164.8; 160.7; 156.6; 147.9; 147.0; 145.8; 145.2; 144.8; 143.6; 143.5; 136.8; 129.5; 127.8; 124.2; 121.2; 120.3; 119.9; 116.5; 116.3; 115.8; 115.0; 114.9; 110.6; 104.0; 97.5; 91.9; 79.0; 76.3; 69.4; 60.6; 55.1; 34.4 ppm. MS (MALDI-TOF) (+): calculated for [M] ($C_{33}H_{28}O_{12}$) 616.16; found 617.35 $[M + H]^+$, 639.66 $[M + Na]^+$, 655.87 $[M + K]^+$.

4.4.6 *In medium* and Chemical Stability (10a, 11a and 12a)

The sample solutions were prepared by dissolving the accurately weighed compounds (**10a**, **11a** and **12a**) in DMSO and diluted with either RPMI1640 media supplemented with 100 U/mL penicillin, 100mg/mL streptomycin and 10% FBS or PBS at pH 7.4 to reach a final concentration of 100 µM (1% DMSO). The solutions were placed at 37 °C in a heater. Samples of 0.2 mL were taken after t = 0, 0.5, 1h, 3h, 7h, 24h and 48h. The samples were treated with 0.2 mL of ice-cold ACN. Precipitated proteins were removed by centrifugation (SIGMA 1-14, SIGMA Laborzentrifugen GmbH, An der Unteren Sose 50, Germany) with 10000 g for 15 min

and filtered. 80 µL of the solutions were directly analysed by HPLC system (Shimadzu LC-9A, equipped with a Shimadzu SPD-6A Detector λ=288nm) using a RP18 column Phenomenex LUNA (5-µm particle size, 4.6 mm × 150 mm i.d.) eluted with NH_4OAc 0.1 M with a linear gradient 5-100% ACN in 20 min (flow = 0.8 mL/min).

4.4.7 DPPH assay

The free radical scavenging activity of different concentrations of the test compounds were evaluated by their abilities to quench the stable 1,1-diphenyl-2-picrylhydrazyl radical (DPPH) *in vitro*. The DPPH solution (200 µM) was prepared in methanol and placed in the dark for 30 min before the analyses. The compounds were dissolved in methanol to prepare the stock solutions (1 mM – 100 µM). DPPH solution was placed in test tubes (final concentration 50 µM), and the solutions of each compound (final concentration range 1 – 1000 µM) were rapidly added and mixed into every test tube to reach a final volume of 2 mL. The reaction was followed by a spectrophotometric analysis continuously measuring the absorbance at λ = 517 nm for 30 min.

The percentage of inhibition (% inhibition) was calculated following the equation:

$$\%\ inhibition = \frac{A_{control} - A_{sample}}{A_{control}}\ x\ 100$$

The EC_{50} value (the inhibition concentration of a sample at 50% fall in absorbance of DPPH) was used to compare the DPPH scavenging activities.

4.4.8 ORAC assay

The ORAC assay relies on free radical damage to a fluorescent probe, most commonly fluorescein, caused by an oxidizing reagent resulting in a loss of fluorescent intensity over time. Antioxidant protection can then be quantified by subtraction of AUC (Area Under the kinetic Curve) of the blank reaction from those reactions containing antioxidant. The resultant difference is considered to be the antioxidant protection conferred by the sample compound. ORAC results are commonly referred to as Trolox equivalents (TE) as calculated from comparison to a Trolox calibration curve. Briefly 150 µL of the fluorescein solution (11.12×10^{-2} µM in phosphate buffer 0.75 mM, pH 7.4) was added into each well of a 96-well plate. Subsequently, 23 µL of buffer and 2 µL of stock solutions in DMSO of tested compounds were added to the wells to reach the final concentration range 1.25–20 µM. The plate was incubated for 30 min at 37 °C and then 25 µL of AAPH (2,2′-Azobis(2-methylpropionamidine) dihydrochloride) (152.6 mM) was added to each well. Immediately, the fluorescence was recorded by a microplate reader for 2 h in 1 min steps at 37 °C (λ_{ecc} = 485 nm, λ_{em} = 528 nm).

4.4.9 Cell culture, Reagents, and treatments

Prostate carcinoma PC-3 cells were purchased from the American Type Culture Collection (Manassas, VA, USA). PC-3 cells were maintained in RPMI-1640 medium, supplemented with 10% heat-inactivated fetal bovine serum, 100 U/ml penicillin G, and 100 µg/ml streptomycin sulfate from Thermo Fisher Scientific (Waltham, MA, USA). Cells were cultured at 37 °C in a humidified incubator with 5% CO_2. Cells were initially plated and treated when they reached a confluency level of 70% to 80%. Cells exposed to varying doses of silybin or its derivatives (5 or 10 µM) dissolved initially in DMSO. These treatments were administered for specific time intervals as described for each experiment. The concentration of DMSO in all treatments did not exceed 0.1% (v/v) in the medium.

The antibodies for cleaved caspase 3 (Asp175) (#9661) and β-Actin (#3700) were from Cell Signaling Technology (Beverly, MA, USA). Dimethyl sulfoxide (DMSO) was purchased from Sigma-Aldrich (St. Louis, MO, USA). Amersham™ ECL™ western blotting detection reagents were from Fisher Scientific (Hampton, NH, USA).

4.4.10 Cell growth and death assay

PC-3 cells were seeded in 35 mm plates at a density of 5×10^4 cells per plate following the culture conditions described earlier. After a 24 h incubation period, cells were exposed to different treatments, including DMSO alone as a control or different silybin derivatives at (5 or 10 μM concentration) dissolved initially in DMSO for 48 and 72 h. Three separate plates were used for each treatment and time point. At 48 and 72 h post-treatment, adherent and suspended cells were harvested through trypsinization, centrifuged at 1200 rpm, washed with 1X phosphate-buffered saline (PBS), and placed into separate tubes. Each sample was counted in duplicate using a hemocytometer and an inverted microscope to ascertain the total cell count. The distinction between live and deceased cells was established by applying the previously described trypan blue dye exclusion method.

4.4.11 Flow cytometry for apoptosis and cell cycle determination

It was used an Alexa Fluor 488 Annexin V/PI kit from Invitrogen, ThermoScientific Scientific (Waltham, MA, USA) to assess cell death. Cells were seeded at a density of 5×10^4 cells per well in a 35 mm plate and treated with different derivatives of silybin, following the same protocol as in the cell growth assay, after a 24 and 48 h incubation period. The cell processing method described earlier was used to determine apoptotic cell death through flow cytometry.[30] Flow cytometric analysis was conducted using a flow cytometer (NovoCyte Penteon Flow Cytometer, Agilent

Technologies, Santa Clara, CA, USA) within 30 min to quantify cells exhibiting annexin V and/or PI positivity.

4.4.12 Lysate preparation and immunoblot analysis

Cell lysates were prepared using a non-denaturing lysis buffer. To ensure uniform protein loading in each well, we employed the BCA method Bio-Rad (Hercules, CA, USA) to measure protein concentrations in the lysates. Samples containing 30 – 50 μg of protein per sample were then subjected to electrophoresis and transferred onto a nitrocellulose membrane. After blocking with a suitable blocking buffer, the membranes were exposed to a specific primary antibody for overnight incubation at 4 °C, followed by incubation with the appropriate peroxidase-linked secondary antibody and using ECL detection for visualization as described previously.[30] Membranes were re-probed with an anti-β-actin antibody as a loading control.

Bibliography

(1) Zawilska, J. B.; Wojcieszak, J.; Olejniczak, A. B. Prodrugs: A Challenge for the Drug Development. *Pharmacological Reports* **2013**, *65* (1), 1–14. https://doi.org/10.1016/S1734-1140(13)70959-9.

(2) Ellis, G. A.; McGrath, N. A.; Palte, M. J.; Raines, R. T. Ribonuclease-Activated Cancer Prodrug. *ACS Medicinal Chemistry Letters* **2012**, *3* (4), 268–272. https://doi.org/10.1021/ml2002554.

(3) Palte, M. J.; Davis, A. K. F.; McGrath, N. A.; Spiegel, C. A.; Raines, R. T. Ribonucleoside 3′-Phosphates as Pro-Moieties for an Orally Administered Drug. *ChemMedChem* **2012**, *7* (8), 1361–1364. https://doi.org/10.1002/cmdc.201200243.

(4) Cuchillo, C. M.; Nogués, M. V.; Raines, R. T. Bovine Pancreatic Ribonuclease: Fifty Years of the First Enzymatic Reaction Mechanism. *Biochemistry* **2011**, *50* (37), 7835–7841. https://doi.org/10.1021/bi201075b.

(5) Sorrentino, S.; Libonati, M. Human Pancreatic-Type and Nonpancreatic-Type Ribonucleases: A Direct Side-by-Side Comparison of Their Catalytic Properties. *Archives of Biochemistry and Biophysics* **1994**, *312* (2), 340–348. https://doi.org/10.1006/ABBI.1994.1318.

(6) Sosa, V.; Moliné, T.; Somoza, R.; Paciucci, R.; Kondoh, H.; Lleonart, M. E. Oxidative Stress and Cancer: An Overview. *Ageing Research Reviews* **2013**, *12*, 376–390. https://doi.org/10.1016/j.arr.2012.10.004.

(7) Quideau, S.; Deffieux, D.; Douat-Casassus, C.; Pouységu, L. Plant Polyphenols: Chemical Properties, Biological Activities, and Synthesis. *Angewandte Chemie International Edition* **2011**, *50* (3), 586–621. https://doi.org/10.1002/anie.201000044.

(8) Rahman, M.; Riaz, M.; Desai, U. R. Synthesis of Biologically Relevant Biflavanoids - A Review. *Chemistry and Biodiversity* **2007**, *4* (11), 2495–2527. https://doi.org/10.1002/cbdv.200790205.

(9) Kim, H. P.; Park, H.; Son, K. H.; Chang, H. W.; Kang, S. S. Biochemical Pharmacology of Biflavonoids: Implications for Anti-Inflammatory Action. *Archives of Pharmacal Research* **2008**, *31* (3), 265–273. https://doi.org/10.1007/s12272-001-1151-3.

(10) Romanucci, V.; Di Fabio, G.; Zarrelli, A. A New Class of Synthetic Flavonolignan-Like Dimers: Still Few Molecules, but with Attractive Properties. *Molecules* **2018**, *24* (1), 108. https://doi.org/10.3390/molecules24010108.

(11) Rafat Husain, S.; Cillard, J.; Cillard, P. Hydroxyl Radical Scavenging Activity of Flavonoids. *Phytochemistry* **1987**, *26* (9), 2489–2491. https://doi.org/10.1016/S0031-9422(00)83860-1.

(12) Trouillas, P.; Marsal, P.; Svobodová, A.; Vostálová, J.; Gažák, R.; Hrbáč, J.; Sedmera, P.; Křen, V.; Lazzaroni, R.; Duroux, J. L.; Walterová, D. Mechanism of the Antioxidant Action of SiIybin and 2,3-Dehydrosilybin Flavonolignans: A Joint Experimental and Theoretical Study. *Journal of Physical Chemistry A* **2008**, *112* (5), 1054–1063. https://doi.org/10.1021/jp075814h.

(13) Gažák, R.; Sedmera, P.; Vrbacký, M.; Vostálová, J.; Drahota, Z.; Marhol, P.; Walterová, D.; Křen, V. Molecular Mechanisms of Silybin and 2,3-Dehydrosilybin Antiradical Activity-Role of Individual Hydroxyl Groups.

Free Radical Biology and Medicine **2009**. https://doi.org/10.1016/j.freeradbiomed.2008.11.016.

(14) Guo, S.; Bai, X.; Liu, Y.; Shi, S.; Wang, X.; Zhan, Y.; Kang, X.; Chen, Y.; An, H. Inhibition of TMEM16A by Natural Product Silibinin: Potential Lead Compounds for Treatment of Lung Adenocarcinoma. *Frontiers in Pharmacology* **2021**, *12* (April), 1–10. https://doi.org/10.3389/fphar.2021.643489.

(15) Decker, M. Hybrid Molecules Incorporating Natural Products: Applications in Cancer Therapy, Neurodegenerative Disorders and Beyond. *Current Medicinal Chemistry* **2011**, *18* (10), 1464–1475. https://doi.org/10.2174/092986711795328355.

(16) Gazak, R.; Walterova, D.; Kren, V. Silybin and Silymarin - New and Emerging Applications in Medicine. *Current Medicinal Chemistry* **2007**, *14* (3), 315–338. https://doi.org/10.2174/092986707779941159.

(17) Gažák, R.; Sedmera, P.; Vrbacký, M.; Vostálová, J.; Drahota, Z.; Marhol, P.; Walterová, D.; Křen, V. Molecular Mechanisms of Silybin and 2,3-Dehydrosilybin Antiradical Activity—Role of Individual Hydroxyl Groups. *Free Radical Biology and Medicine* **2009**, *46* (6), 745–758. https://doi.org/10.1016/j.freeradbiomed.2008.11.016.

(18) Polachi, N.; Bai, G.; Li, T.; Chu, Y.; Wang, X.; Li, S.; Gu, N.; Wu, J.; Li, W.; Zhang, Y.; Zhou, S.; Sun, H.; Liu, C. Modulatory Effects of Silibinin in Various Cell Signaling Pathways against Liver Disorders and Cancer – A Comprehensive Review. *Eur J Med Chem* **2016**, *123*, 577–595. https://doi.org/10.1016/j.ejmech.2016.07.070.

(19) Gažák, R.; Svobodová, A.; Psotová, J.; Sedmera, P.; Přikrylová, V.; Walterová, D.; Křen, V. Oxidised Derivatives of Silybin and Their Antiradical and Antioxidant Activity. *Bioorganic & Medicinal Chemistry* **2004**, *12* (21), 5677–5687. https://doi.org/10.1016/j.bmc.2004.07.064.

(20) Agarwal, C.; Wadhwa, R.; Deep, G.; Biedermann, D.; Gažák, R.; Křen, V.; Agarwal, R. Anti-Cancer Efficacy of Silybin Derivatives - A Structure-Activity Relationship. *PLoS ONE* **2013**, *8* (3), e60074. https://doi.org/10.1371/journal.pone.0060074.

(21) Maruca, A.; Catalano, R.; Bagetta, D.; Mesiti, F.; Ambrosio, F. A.; Romeo, I.; Moraca, F.; Rocca, R.; Ortuso, F.; Artese, A.; Costa, G.; Alcaro, S.; Lupia, A.

The Mediterranean Diet as Source of Bioactive Compounds with Multi-Targeting Anti-Cancer Profile. *Eur J Med Chem* **2019**, *181*, 111579. https://doi.org/10.1016/j.ejmech.2019.111579.

(22) Hu, T.; He, X.-W.; Jiang, J.-G.; Xu, X.-L. Hydroxytyrosol and Its Potential Therapeutic Effects. *Journal of Agricultural and Food Chemistry* **2014**, *62* (7), 1449–1455. https://doi.org/10.1021/jf405820v.

(23) Biedermann, D.; Vavříková, E.; Cvak, L.; Křen, V. Chemistry of Silybin. *Nat. Prod. Rep.* **2014**, *31* (9), 1138–1157. https://doi.org/10.1039/C3NP70122K.

(24) Vue, B.; Zhang, S.; Zhang, X.; Parisis, K.; Zhang, Q.; Zheng, S.; Wang, G.; Chen, Q. H. Silibinin Derivatives as Anti-Prostate Cancer Agents: Synthesis and Cell-Based Evaluations. *European Journal of Medicinal Chemistry* **2016**, *109*, 36–46. https://doi.org/10.1016/j.ejmech.2015.12.041.

(25) Althagafy, H. S.; Graf, T. N.; Sy-Cordero, A. A.; Gufford, B. T.; Paine, M. F.; Wagoner, J.; Polyak, S. J.; Croatt, M. P.; Oberlies, N. H. Semisynthesis, Cytotoxicity, Antiviral Activity, and Drug Interaction Liability of 7-O-Methylated Analogues of Flavonolignans from Milk Thistle. *Bioorganic & Medicinal Chemistry* **2013**, *21* (13), 3919–3926. https://doi.org/10.1016/j.bmc.2013.04.017.

(26) Vue, B.; Zhang, X.; Lee, T.; Nair, N.; Zhang, S.; Chen, G.; Zhang, Q.; Zheng, S.; Wang, G.; Chen, Q.-H. 5- or/and 20-O-Alkyl-2,3-Dehydrosilybins: Synthesis and Biological Profiles on Prostate Cancer Cell Models. *Bioorganic & Medicinal Chemistry* **2017**, *25* (17), 4845–4854. https://doi.org/10.1016/j.bmc.2017.07.035.

(27) Yang, L. X.; Huang, K. X.; Li, H. B.; Gong, J. X.; Wang, F.; Feng, Y. B.; Tao, Q. F.; Wu, Y. H.; Li, X. K.; Wu, X. M.; Zeng, S.; Spencer, S.; Zhao, Y.; Qu, J. Design, Synthesis, and Examination of Neuron Protective Properties of Alkenylated and Amidated Dehydro-Silybin Derivatives. *Journal of Medicinal Chemistry* **2009**, *52* (23), 7732–7752. https://doi.org/10.1021/jm900735p.

(28) Fletcher, S. The Mitsunobu Reaction in the 21 St Century. *Organic Chemistry Frontiers* **2015**, *2* (6), 739–752. https://doi.org/10.1039/C5QO00016E.

(29) Trouillas, P.; Marsal, P.; Svobodová, A.; Vostálová, J.; Gažák, R.; Hrbáč, J.; Sedmera, P.; Křen, V.; Lazzaroni, R.; Duroux, J. L.; Walterová, D.

Mechanism of the Antioxidant Action of SiIybin and 2,3-Dehydrosilybin Flavonolignans: A Joint Experimental and Theoretical Study. *Journal of Physical Chemistry A* **2008**, *112* (5), 1054–1063. https://doi.org/10.1021/jp075814h.

(30) Kandhari, K.; Mishra, J. P. N.; Agarwal, R.; Singh, R. P. Acacetin Induces Sustained ERK1/2 Activation and RIP1-Dependent Necroptotic Death in Breast Cancer Cells. *Toxicology and Applied Pharmacology* **2023**, *462* (July 2022), 116409. https://doi.org/10.1016/j.taap.2023.116409.

5 Phosphodiester Curcumin Mimics

Cardiovascular disorders and cancer collectively account for a significant number of deaths in Western countries, with pancreatic, prostate, and colorectal cancers ranking among the top five most lethal malignancies when considering data from both men and women. Consequently, researchers are actively looking for improved methods for controlling, preventing, managing, and treating these cancers.

Curcumin has demonstrated efficacy not only in preventing carcinogenesis but also in providing direct therapeutic benefits in various types of cancer.[1,2] Unfortunately, curcumin's potential utility is limited by its poor bioavailability and stability in physiological media. It has been demonstrated that the active methylene group and β-diketone moiety contribute to its instability, poor absorption and rapid metabolism.[3] So the research is active to the design of synthetic analogues aimed to replace the central diketone structure with a moiety that enhances the chemical stability, water solubility and improves bioavailability while preserving the methoxy–tyrosol portion.[4] Recent approaches have been explored combining two polyphenolic fragments to create libraries of polyphenol dimers.[5] Dimerization or linking of these moieties has the potential to enhance or change their biological activity, and the incorporation of lipophilic or hydrophilic moieties into each scaffold can significantly modulate their behavior in lipidic or aqueous cell compartments, resulting in novel hybrid compounds with enhanced efficacies.[6]

5.1 Aim of Research Work

With the aim of synthesizing curcumin mimics with broad molecular diversity, a rapid solid-phase synthetic strategy has been carried out to obtain tyrosol-based phosphodiester dimers which retain the two aromatic rings with distinct hydroxyl substituents and a distance between them comparable to that of curcumin. The phosphodiester linker was chosen with the aim of increasing the water solubility and the stability of the new mimics For the new compounds it was evaluated the stability in biological media and the anticancer activity against human pancreatic (PANC1), prostate (PC-3), and colorectal (SW480) cancer cell lines by cell growth assay.

Figure 5.1 Tyrosol-based phosphodiester dimers as curcumin mimics

5.2 Results and Discussion

The NovaSyn® support was pre-derivatized with 4-hydroxy-3-nitrophenyl-acetic acid and functionalized with a series of suitable tyrosol-based phosphoramidite derivatives (**2**–**4**, Scheme 5.1) using standard phosphoramidite protocols (phosphoramidite chemistry). Following phosphate deprotection from the CE group, the supports were coupled with TYR, HVA, and HDT using MSNT as the activator reagent in pyridine (phosphotriester chemistry) and left overnight. Monitoring the esterification reaction through diagnostic ^{31}P NMR peaks, centred at approximately −7.0 ppm, facilitated the evaluation of phosphodiester–triester conversion yields. Post-treatment with TEA·3HF in THF, detachment from the supports was achieved by treatment with NaOH/MeOH, and the crude released material underwent analysis through RP–HPLC. The HPLC profiles of the detached materials exhibited a major peak, typically constituting over 95% of the total integrated area. High purity was

attained since only the phosphotriester linkage was readily hydrolyzed, and the phosphodiester tyrosols, i.e., the unreacted material, remained attached to the resin after alkaline treatment. The identities of dimers **8**–**13** were confirmed through a comparison of ^{1}H and ^{13}C NMR spectra conducted directly on the crude material with recently reported data. Following HPLC purification, dimers **8**–**13** were recovered in yields ranging from 48 to 55% (Scheme 5.1).

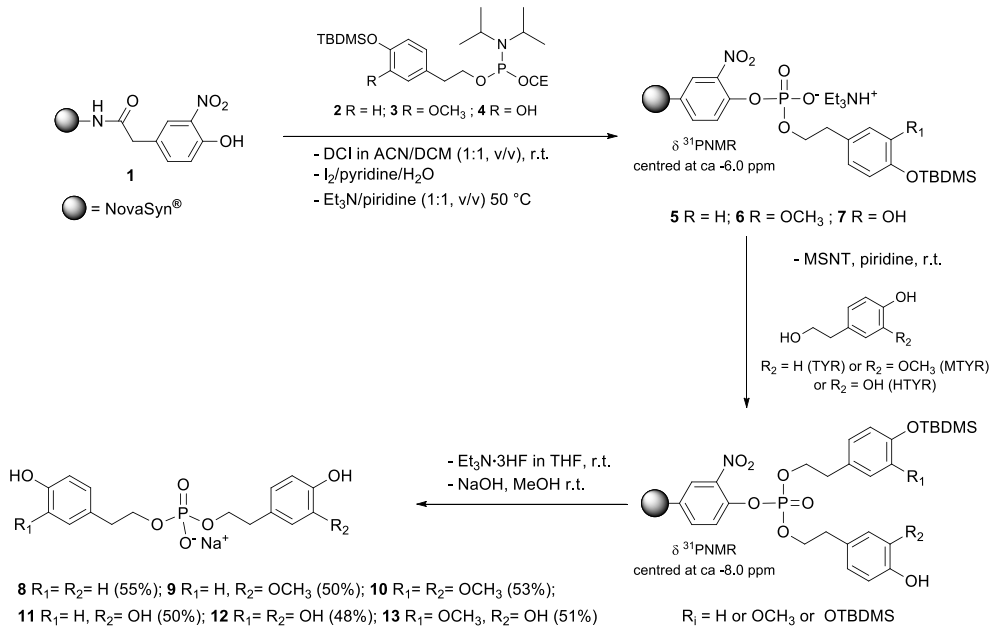

Scheme 5.1 Solid phase synthesis of curcumin mimics (**8**–**13**).

5.2.1 Stability in Biological Media

Any therapeutic small molecule or formulation intended for oral administration should undergo early-stage *in vitro* testing to assess its stability in the gastric and intestinal media. The phosphodiester dimers (**8** – **13**) demonstrated high chemical stability under various pH conditions in simulated gastric and intestinal fluids, as well as resistance to degradation by alkaline phosphatase (ALP) and in human serum (Figure 5.2 and Figure 5.3). Notably, at pH 1.2, all phosphodiesters (**8** – **13**) remained

stable, with less than 5% degradation observed even after 48 h. Dimers **8**–**13** exhibited exceptional stability at pH 6.8, in human serum, and in the presence of ALP, where no noticeable alteration was observed even after an extended duration.

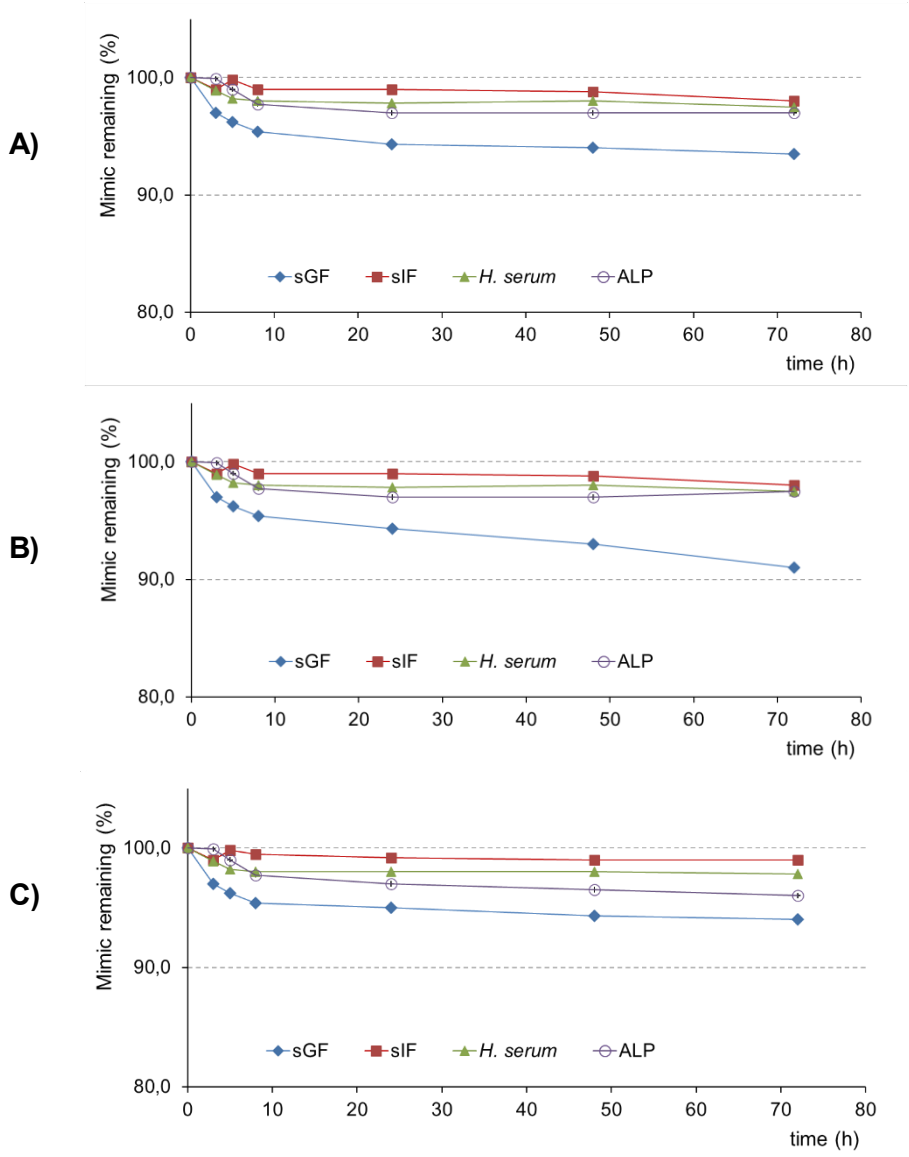

Figure 5.2 Percentage of compound **8** (**A**), **9** (**B**), and **10** (**C**) remaining over time in sGF, sIF, human serum and in ALP calculated by the change in the integration of the corresponding HPLC peaks.

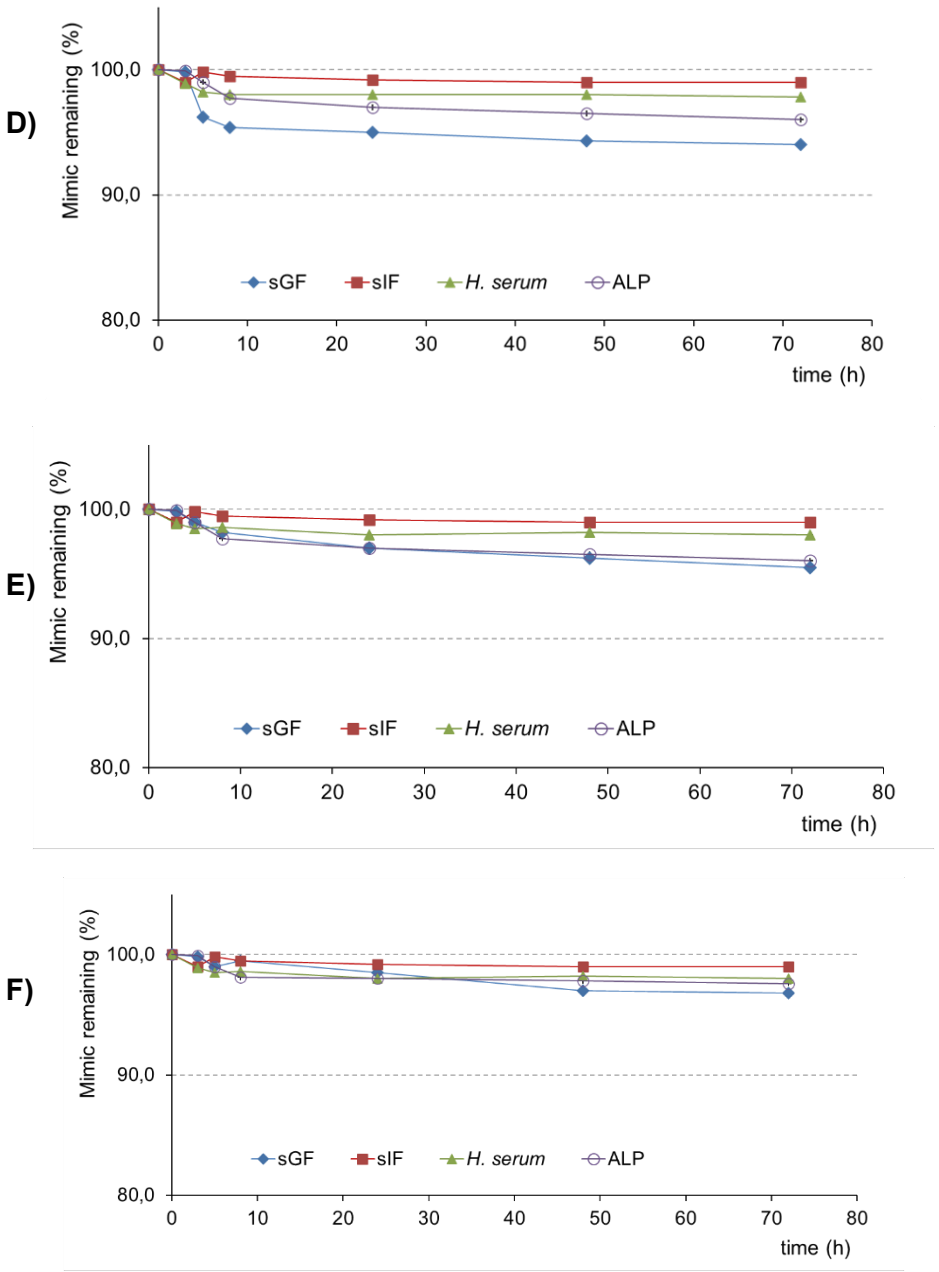

Figure 5.3 Percentage of compound **11** (**D**), **12** (**E**) and **13** (**E**) remaining over time in sGF, sIF, human serum and in ALP calculated by the change in the integration of the corresponding HPLC peaks.

5.2.2 Anticancer Activity

For the human pancreatic cancer cell line PANC1 (Figure 5.4A), the parent compound HDT caused a statistically significant decrease (15%, $p \leq 0.05$) in live cells compared to the DMSO vehicle controls. Substitution of the parent HDT with derivatives **8** – **13** did not enhance this activity, and compounds HVA and TYR, along with their derivatives, did not exhibit better activity than HDT. An increase of % cell death was observed for all parent compounds and their derivatives, although not statistically significant. Total cell number results were consistent with the live cell data, suggesting marginal growth inhibitory and cell death activities in PANC1 cells for HDT, HVA, TYR, and their derivatives.

In the human prostate cancer cell line PC-3 (Figure 5.4B), HDT demonstrated a strong and statistically significant decrease (33%, $p \leq 0.001$) in live cells compared to DMSO controls. HVA and TYR were less effective, and a para-HVA substitution to TYR (compound **9**) resulted in a 28% ($p \leq 0.001$) decrease in live PC-3 cell numbers. Interestingly, para substitutions of HDT with HVA or TYR decreased cell growth inhibitory activity. % cell death data showed a strong increase, statistically significant in most cases, indicating promising results for PC-3 cells. The most significant finding was a 23% ($p \leq 0.001$) cell death by compound **9** compared to its parent structure TYR with 7% ($p \leq 0.05$) cell death. Total cell number results were in line with live cell data.

In the human colorectal carcinoma cell line SW480 (Figure 5.4C), HDT significantly reduced cell growth by 38% ($p \leq 0.001$) compared to DMSO controls. HVA and TYR were marginally effective, and para-HDT or HVA substitutions to HDT reduced the cell growth inhibitory activity of the parent HDT. Derivatization of HVA and TYR resulted in the loss of marginal cell growth inhibitory effects. Cell death effects were remarkable, similar to those observed in PANC1 cells. Total cell number results were consistent with live cell data. Overall, HDT showed promising activity in

PC-3 and SW480 cells, suggesting potential as an effective agent in pancreatic and colorectal cancers.

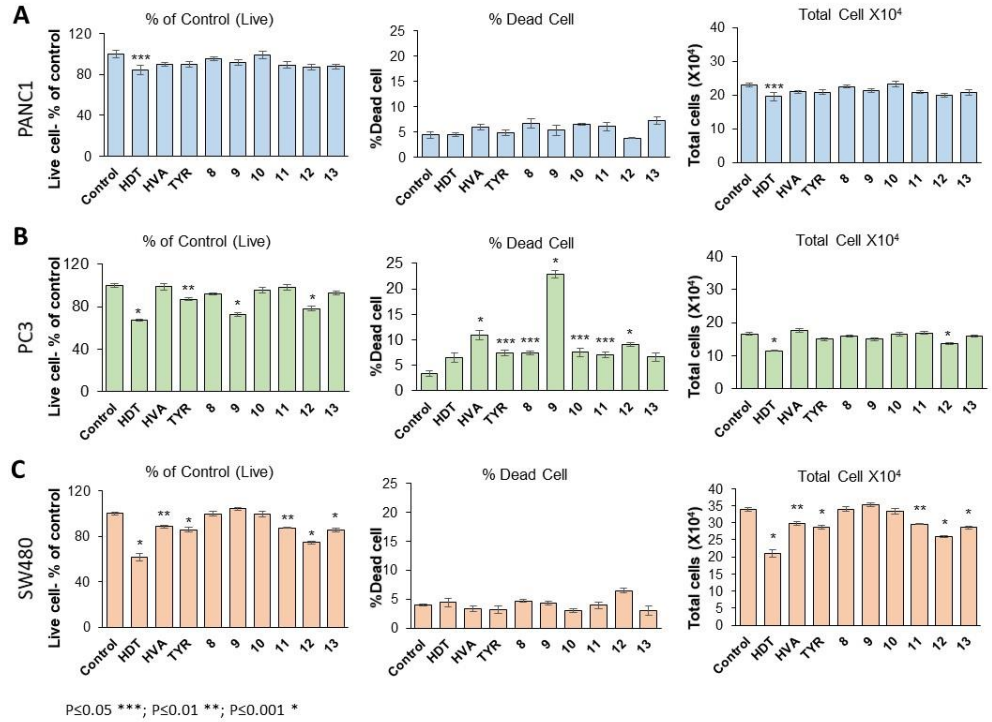

Figure 5.4 Cell growth inhibition by curcumin mimics **8**–**13** on pancreatic (**A**), prostate (**B**), and colorectal (**C**) cancer cell lines

5.3 Conclusions

In conclusion, a series of curcumin mimics (**8** – **13**), maintaining the seven-atoms distance between two phenylethanoid moieties, were efficiently obtained using a combinatorial synthetic approach. The phosphodiester dimers exhibited high stability in simulated intestinal fluid (sIF), simulated gastric fluid (sGF), alkaline phosphatase, and serum buffers, making them ideal curcumin mimics. Subsequent evaluation of these mimics, along with parent tyrosol-based compounds (HDT, HVA, and TYR),

revealed marginal growth inhibitory and cell death activities in PANC1 human pancreatic cancer cells under the examined conditions.

Remarkably, these non-effective findings in pancreatic cancer cells transitioned to potent growth inhibition and cell death efficacy in PC-3 prostate cancer cells. Compound TYR with a para-HVA substitution (**9**) demonstrated substantial effectiveness not only in cell growth inhibition but also in inducing significant cell death, contrasting with its limited effectiveness in PANC1 cells (Figure 5.4A, B, and C).

Furthermore, the findings in SW480 human colorectal carcinoma cells mirrored those in PC-3 cells concerning growth inhibitory effects, but the lack of cell death effect was more consistent with PANC1 cells. These results suggest that genetic differences and the cells' origin may contribute to the observed variations in biological activities. Additional studies with parent compound HDT and HVA-substituted TYR (**9**) across various concentrations and time points, particularly in a panel of prostate and colorectal cancer cell lines, are warranted to further explore their efficacy against these malignancies.

5.4 Experimental Session

5.4.1 General Methods

NovaSyn®-NH_2 (0.77 meq/g) resin was purchased from Novabiochem. The functionalization of the solid support was carried out in a short glass column (5 cm length, 1 cm i.d.) equipped with a sintered glass filter, a stopcock, and a cap. The activator solution (0.45 M tetrazole in ACN) and oxidizer solution (tButOOH 5.5M in decane) were purchased from Sigma–Aldrich (Italy). HPLC-grade ACN and MeOH were purchased from Carlo Erba Reagents. Reactions were monitored by thin-layer chromatography (TLC) (precoated silica gel plates F254, Merck) and column

chromatography (Merck Kieselgel 60, 70–230 mesh). HPLC analysis was performed using a Shimadzu LC–8A HPLC system equipped with a Shimadzu SCL–10A VP System control and a Shimadzu SPD–10A VP UV–Vis detector. HPLC analysis was carried out on a Phenomenex Luna RP18 column (5 μm particle size, 4.6 mm × 150 mm i.d.) using a gradient that started at 5% ACN in 0.1 M NH_4OAc in H_2O (pH 7.0) for 5 min and increased to 100% ACN over 30 min at a flow rate of 0.8 mL/min with detection at 260 nm. For ESI–MS analysis, a Waters Micromass ZQ instrument equipped with an electrospray source was used. ^{31}P NMR spectra were recorded at 161.98 MHz on a Bruker AWM-400 spectrometer using 85% H_3PO_4 as an external standard.

5.4.2 General procedure for the preparation of the support 1

500 mg of NovaSyn®-NH_2 (0.77 meq/g, 0.38 mmol), swelled in anhydrous pyridine, was reacted overnight at room temperature with a mixture of 380 mg (1.9 mmol) of 4-hydrox-3-nitroyphenylacetic acid, 450 μL (2.9 mmol) of DIC, 490 μL (2.9 mmol) of DIEA dissolved in 8 mL of anhydrous pyridine. After exhaustive washing with pyridine, DCM, and Et_2O, the support was dried under reduced pressure. After capping the unreacted amino functions with 10 mL of Ac_2O/Py (1:1, v/v) for 1 h at room temperature, the support was treated with concentrated aqueous ammonia (28%) at 50 °C for 1 h. Using the Kaiser test, the incorporation of the linker was almost quantitative. After exhaustive washing with MeOH, DCM, and Et_2O, support **1** was dried under reduced pressure.

5.4.3 Synthesis of tyrosol phosphoramidites 2–4

0.93 mmol of TBDMS ether of TYR (or HVA, or HDT) (for details see paragraph 4.4.2) were dissolved in anhydrous DCM (7 mL), DIEA (516 µL, 3.70 mmol) and then 2–cyanoethyl–N,N–diisopropylamino–chlorophosphoramidite (250 µL, 0.39 mmol) were added. Reaction progress was monitored by TLC (Hexane/EtOAc 80:20 v/v). After 1 h, the solution was diluted with EtOAc, and the organic phase was washed twice with brine and then concentrated. Column chromatography of the residue (hexane/EtOAc 80:20, v/v with 1% TEA) afforded desired compound **2** (**3** or **4**) in good yields.

2 ^{1}H NMR (400 MHz, $CDCl_3$, 25 °C, δ ppm, *J* Hz): δ = 7.09 (2H, d, *J* = 8.5, H–2 and H–6), 6.78 (2H, d, *J* = 8.5, H–3 and H–5), 3.91–3.76 (4H, m, $CNCH_2CH_2OP$ and H–8), 3.65–3.56 (2H, m, $[(CH_3)_2CH]_2N$), 2.87 (2H, t, *J* = 7.0, H–7), 2.60 (2H, *t*, *J* = 6.6, $CNCH_2CH_2OP$), 1.20 (6H, d, *J* = 6.7, $[(CH_3)_2CH]_2N$), 1.17 (6H, d, *J* = 6.7, $[(CH_3)_2CH]_2N$), 1.00 (9H, s, $(CH_3)_3CSiOAr$), 0.20 (6H, s, $(CH_3)_2SiOAr$) ppm. ^{13}C NMR (100 MHz, $CDCl_3$, 25 °C, δ ppm): δ = 154.1, 131.3, 129.9, 119.9, 117.6, 64.6, 64.5, 58.4, 58.2, 43.1, 43.0, 37.1, 37.0, 25.7, 24.8, 24.7, 24.6, 24.5, 20.4, 20.3, 18.2, –4.4 ppm. ^{31}P NMR (161.98 MHz, $CDCl_3$, 25 °C, δ ppm): δ = 147.3 ppm. MS (ESI^+): calcd. for $C_{23}H_{42}N_2O_3PSi$ 453.27, found 453.39 $[M+H]^+$.

3 ^{1}H NMR (400 MHz, $CDCl_3$, 25 °C, δ ppm, *J* Hz): δ = 6.78 (1H, d, *J* = 8.1, H–5), 6.74 (1H, d, *J* = 1.8, H–2), 6.68 (1H, dd, *J* = 8.0, 1.9, H–6), 3.92–3.72 (4H, m, $CNCH_2CH_2OP$ and H–8), 3.81 (3H, s, OCH_3), 3.65–3.56 (2H, m, $[(CH_3)_2CH]_2N$), 2.87 (2H, t, *J* = 7.0, H–7), 2.60 (2H, t, *J* = 6.6, $CNCH_2CH_2OP$), 1.19 (6H, d, *J* = 6.7, $[(CH_3)_2CH]_2N$), 1.16 (6H, d, *J* = 6.7, $[(CH_3)_2CH]_2N$), 1.01 (9H, s, $(CH_3)_3CSiOAr$), 0.16 (6H, s, $(CH_3)_2SiOAr$) ppm. ^{13}C NMR (100 MHz, $CDCl_3$, 25 °C, δ ppm): δ = 150.7, 143.4, 132.0, 121.2, 120.7, 117.7, 113.1, 64.7, 64.5, 58.4, 58.2, 55.5, 43.1, 43.0, 37.5, 37.4, 25.7, 24.7, 24.6, 24.5, 20.4, 20.3, 18.4, –4.6 ppm. ^{31}P NMR (161.98 MHz,

$CDCl_3$, 25 °C, δ ppm): δ = 147.3 ppm. MS (ESI^+): calcd. for MS (ESI^+): calcd. for $C_{24}H_{44}N_2O_4PSi$ 483.28, found 483.37 $[M+H]^+$.

4 ^1H NMR (400 MHz, $CDCl_3$, 25 °C, δ ppm, *J* Hz): δ = 6.76 (1H, d, *J* = 8.1, H–5), 6.70 (1H, d, *J* = 1.9, H–2), 6.67 (1H, dd, *J* = 8.0, 2.1, H–6), 3.88–3.70 (4H, m, $CNCH_2CH_2OP$ and H–8), 3.66–3.56 (2H, m, $[(CH_3)_2CH]_2N$), 2.82 (2H, t, *J* = 7.3, H–7), 2.62 and 2.61 (2H, *t*, *J* 6.6 and 6.4 Hz, $CNCH_2CH_2OP$), 1.20 (6H, d, *J* 6.8 Hz, $[(CH_3)_2CH]_2N$), 1.17 (6H, d, *J* = 6.8 Hz, $[(CH_3)_2CH]_2N$), 1.01 (9H, s, $(CH_3)_3CSiOAr$), 1.00 (9H, s, $(CH_3)_3CSiOAr$), 0.21 (6H, s, $(CH_3)_2SiOAr$), 0.20 (6H, s, $(CH_3)_2SiOAr$) ppm. ^{13}C NMR (100 MHz, $CDCl_3$, 25 °C, δ ppm): δ = 146.5, 145.3, 131.5, 121.9, 121.8, 120.8, 117.6, 64.6, 64.4, 58.5, 58.3, 43.1, 43.0, 37.2, 37.1, 26.0, 24.7, 24.6, 24.5, 24.4, 20.4, 20.3, 18.5, 18.4, –4.1 ppm. ^{31}P NMR (161.98 MHz, $CDCl_3$, 25 °C, δ ppm): δ = 147.2 ppm. MS (ESI^+): calcd. for $C_{29}H_{56}N_2O_4PSi_2$ 583.35, found 583.43 $[M+H]^+$.

5.4.4 General procedure for the synthesis of dimers 8–13

30 mg of dried support **5** (**6** or **7**) (loading 0.77 mmol/g, 0.023 mmol) was swelled in anhydrous pyridine and then reacted with 70 mg (0.23 mmol) of MSNT in 500 µL of anhydrous pyridine. After 30 min at room temperature, 0.23 mmol of TYR (HVA or HDT) was added to the mixture and maintained for 12 h at room temperature. After exhaustive washing with pyridine, DMF, DCM, and Et_2O, the resulting supports were dried under reduced pressure and then treated using 180 µL of TEA·3HF (1.5 mmol) complex in 1 mL of THF, and the mixture was stirred at room temperature for 2 h. After exhaustive washing with THF, DCM, and Et_2O, the target compounds were detached from the support using $NaOH_{aq}$/MeOH (1:1, v/v) treatment at room temperature for 1 h. The final crude detachment was neutralized with a diluted AcOH

solution and then analyzed by HPLC on an analytical RP18 column, showing, in all cases, one main peak with a purity of over 95%.

8 ^{1}H NMR (400 MHz, $CDCl_3$, 25 °C, δ ppm, *J* Hz): δ = 7.03 (4H, d, *J* = 8.4, H–2, H–2', H–6 and H–6'), 6.72 (4H, d, *J* = 8.4, H–3, H–3', H–5 and H–5'), 3.90 (4H, q, *J* = 6.9, H–8 and H–8'), 2.77 (4H, t, *J* = 7.1, H–7 and H–7') ppm. ^{13}C NMR (100 MHz, $CDCl_3$, 25 °C, δ ppm, *J* Hz): δ = 155.4, 129.6, 129.2, 114.7, 66.2, 66.1, 36.1, 36.0 ppm. ^{31}P NMR (161.98 MHz, $CDCl_3$, 25 °C, δ ppm): δ = 0.56 ppm. MS (ESI^+): calcd. for $C_{16}H_{20}O_6P$ 339.10, found 339.22 $[M+H]^+$, 361.22 $[M+Na]^+$, 377.59 $[M+K]^+$.

9 ^{1}H NMR (400 MHz, $CDCl_3$, 25 °C, δ ppm, *J* Hz): δ = 7.01 (2H, d, *J* = 8.5, H–2' and H–6'), 6.82 (1H, d, *J* = 1.8, H–2), 6.73 (1H, d, *J* = 8.5, H–5), 6.71 (2H, d, *J* = 8.5, H–3'and H–5'), 6.66 (1H, dd, *J* = 8.1, 1.8, H–6), 3.93 (4H, m, H–8 and H–8'), 3.83 (3H, s, OCH_3), 2.76 (4H, q, *J* = 7.1 Hz, H–7 and H–7') ppm. ^{13}C NMR (100 MHz, $CDCl_3$, 25 °C, δ ppm): δ = 155.5, 147.3, 144.5, 130.1, 129.6, 129.1, 121.2, 114.8, 114.7, 112.4, 66.3, 66.2, 55.0, 36.4, 36.0 ppm. ^{31}P NMR (161.98 MHz, $CDCl_3$): δ = 0.30 ppm. MS (ESI^+): calcd. for $C_{17}H_{22}O_7P$ 369.11, found 369.55 $[M+H]^+$, 391.88 $[M+Na]^+$, 407.65 $[M+K]^+$.

10 ^{1}H NMR (400 MHz, $CDCl_3$, 25 °C, δ ppm, *J* Hz): δ = 6.83 (2H, d, *J* = 1.9, H–2 and H–2'), 6.72 (2H, d, *J* = 8.0, H–5 and H–5'), 6.64 (2H, dd, J = 8.0, 1.9, H–6 and H–6') 3.95 (4H, q, *J* = 6.9, H–8 and H–8'), 3.80 (6H, s, OCH_3), 2.78 (4H, t, *J* = 7.0, H–7 and H–7') ppm. ^{13}C NMR (100 MHz, $CDCl_3$, 25 °C, δ ppm): δ = 147.3, 144.5, 130.0, 121.2, 114.7, 112.4, 66.3, 66.2, 55.0, 36.4, 36.3 ppm. ^{31}P NMR (161.98 MHz, $CDCl_3$, 25 °C, δ ppm): δ = 0.36 ppm. MS (ESI^+): calcd. for $C_{18}H_{24}O_8P$ 399.12, found 399.23 $[M+H]^+$, 421.68 $[M+Na]^+$, 438.21 $[M+K]^+$.

11 ^{1}H NMR (400 MHz, $CDCl_3$, 25 °C, δ ppm, *J* Hz): δ = 7.03 (2H, d, *J* = 8.3, H–2' and H–6'), 6.71 (2H, d, *J* = 8.3, H–3' and H–5'), 6.69 (2H, d, *J* = 8.2, H–5), 6.67

(1H, m, H–2), 6.53 (1H, dd, *J* = 7.8, 1.8, H–6), 3.93 (4H, q, *J* = 6.3, H–8 and H–8'), 2.78 (2H, t, *J* = 6.8, H–7), 2.73 (2H, t, *J* = 6.7, H–7') ppm. ^{13}C NMR (100 MHz, $CDCl_3$, 25 °C, δ ppm): δ = 155.4, 144.7, 143.3, 129.9, 129.6, 129.1, 119.9, 115.8, 114.8, 114.7, 66.3, 66.2, 36.0, 35.9 ppm. ^{31}P NMR (161.98 MHz, $CDCl_3$, 25 °C, δ ppm): δ = –2.3 ppm. MS (ESI^+): calcd. for $C_{16}H_{20}O_7P$ 355.09, found 355.38 $[M+H]^+$, 377.12 $[M+Na]^+$, 393.08 $[M+K]^+$.

12 ^{1}H NMR (400 MHz, CD_3OD, 25 °C, δ ppm, *J* Hz): δ = 6.69 (2H, d, *J* = 8.3, H–5 and H–5'), 6.68 (2H, d, *J* = 2.2, H–2 and H–2'), 6.54 (2H, dd, *J* = 7.9, 1.8, H–6 and H–6'), 3.96 (4H, q, *J* = 6.6, H–8 and H–8'), 2.74 (4H, t, *J* = 6.8, H–7 and H–7') ppm. ^{13}C NMR (100 MHz, CD_3OD, 25 °C, δ ppm): δ = 144.7, 143.4, 129.7, 120.0, 115.8, 114.9, 66.8, 66,7, 36.0, 35.9 ppm. ^{31}P NMR (161.98 MHz, CD_3OD, 25 °C, δ ppm): δ = –2.1 ppm. MS (ESI^+): calcd. for $C_{16}H_{20}O_8P$ 371.09, found 371.38 $[M+H]^+$, 393.46 $[M+Na]^+$, 409.38 $[M+K]^+$.

13 ^{1}H NMR (400 MHz, CD_3OD, 25 °C, δ ppm, *J* Hz): δ = 6.79 (1H, d, *J* =1.9, H–2'), 6.72 (1H, d, *J* = 7.8, H–5), 6.69 (1H, d, *J* = 7.6, H–5'), 6.68 (1H, br s, H–2), 6.65 (1H, dd, *J* = 7.8, 2.0, H–6), 6.53 (1H, dd, *J* = 7.6, 1.9, H–6'), 3.94 (4H, m, H–8 and H–8'), 3.82 (3H, s, O*CH*$_3$), 2.80 (2H, t, *J* = 6.8, H–7), 2.73 (2H, t, *J* = 6.9, H–7') ppm. ^{13}C NMR (100 MHz, CD_3OD, 25 °C, δ ppm): δ = 147.4, 144.6, 144.5, 143.3, 130.0, 129.9, 121.1, 120.0, 115.8, 114.9, 114.7, 112.3, 66.4, 66.3, 55.0, 36.2, 36.0 ppm. ^{31}P NMR (161.98 MHz, CD_3OD, 25 °C, δ ppm): δ = -3.0 ppm. MS (ESI^+): calcd. for $C_{17}H_{22}O_8P$ 385.10, found 385.38 $[M+H]^+$, 407.36 $[M+Na]^+$, 423.57 $[M+K]^+$.

5.4.5 Simulated Gastric and Intestinal Fluid (sGF and sIF) assays

The procedure for preparing simulated gastric fluid (sGF) involved dissolving sodium chloride in bidistilled water, and the pH was then adjusted to 1.2 by adding 37% aqueous hydrochloric acid (HCl). Simulated intestinal fluid (sIF) was prepared by dissolving monopotassium phosphate in bidistilled water, and the pH was adjusted to 6.8 by adding 0.2 M sodium hydroxide (NaOH). The stability of each compound was assessed at 37 ℃ in both simulated fluids, monitored using high-performance liquid chromatography (HPLC) over time. Each compound was dissolved to a final concentration of 1 mM in sGF and sIF solutions. Stability assessments were conducted at 37°C, with aliquots of the reaction injected into the HPLC system for analysis. HPLC analyses were performed using a Phenomenex Luna RP18 column (5 μm particle size, 4.6 mm × 150 mm i.d.), employing a gradient of solvent B (ACN) in solvent A (0.10 NH_4OAc) from 20% to 100% over 15 minutes at a flow rate of 0.8 mL/min, with detection at 260 nm.

5.4.6 Alkaline Phosphatase assay

All compounds were dissolved to a final concentration of 1 mM in Tris-HCl (20 mM, pH 7.4). The hydrolysis rate in an alkaline phosphatase (ALP) solution was determined at 37°C by adding 40 U of ALP (from bovine intestinal mucosa, 2.745 U/mg protein) to a dimer solution (0.5 μmol) in a 500 μL buffer solution. At each time point, a 30 μL aliquot of the reaction was withdrawn, and 120 μL of methanol was added to halt enzymatic hydrolysis. After centrifugation (13000 rpm, 15 min), the samples (70 μL) were analyzed using a Shimadzu LC-9A HPLC system equipped with a Shimadzu SPD-6A UV/Vis detector. HPLC analyses were performed on a Phenomenex Luna RP18 column (5 μm particle size, 4.6 mm × 150 mm i.d.), eluted

in a gradient of solvent B (ACN) in solvent A (0.10 M NH_4OAc) from 20% to 100% over 15 minutes at a flow rate of 0.8 mL/min, with detection at 260 nm.

5.4.7 Serum Stability assay

A suitable amount of the compound was dissolved in one volume (e.g., 100 µL) of Tris-HCl buffer (50 mM, pH 7.4) at 37°C. Subsequently, high volumes (e.g., 800 µL) of preheated human serum were added, and the solutions were maintained in a water bath at 37°C (initial concentrations were 0.6–0.7 mM). At appropriate intervals (t_i, i = 0, 1, 3, 5, 24, 48, 72, and 96 h), 100 µL samples were withdrawn and "deproteinized" by adding 500 µL of MeOH. After mixing and centrifugation, the supernatants were filtered using a syringe filter with a regenerated cellulose membrane (diameter 4 mm, pore size 0.2 µm). Subsequently, 100 µL of the filtered solution was injected into the HPLC. HPLC analyses were performed on a Phenomenex Luna RP18 column (5 µm particle size, 4.6 mm × 150 mm i.d.), eluted in a gradient of solvent B (ACN /A 95:5) in solvent A (0.10 M NH_4OAc) from 20% to 100% over 15 minutes at a flow rate of 0.8 mL/min, with detection at 260 nm.

5.4.8 Anticancer Activity

The human pancreatic cancer cell line PANC1, prostate cancer cell line PC-3, and colorectal cancer cell line SW480 were procured from the American Type Culture Collection (Manassas, VA) and cultured under standard conditions.[7]

For biological activity assays, each compound was dissolved in DMSO at a 100 mM stock concentration and then diluted 1000 times directly in a culture medium, resulting in a final concentration of 100 µM for the test compound. In the cell growth assay, cells were trypsinized from 100 mm plates, collected, spun down, and counted. After counting, the cells were plated at a density of 5000 cells/cm^2 in 60 mm dishes

to achieve a confluency of approximately 30%–40%, which typically took ~24 h from the initial cell seeding.

After 24 h of cell plating, the cells were treated with different compounds at a final concentration of 100 μM in triplicate, while controls were treated with DMSO, the solvent for the compounds. Unless specified otherwise, the final concentration of DMSO in the culture medium during different treatments did not exceed 0.1% (v/v). After 72 h of treatment, cells were collected by trypsinization, washed with cold phosphate-buffered saline (PBS), and counted using a hemocytometer. The trypan blue dye method was employed to count live and dead cells, as previously described. The statistical significance of differences between the control and treated samples was calculated by one-way analysis of variance (ANOVA) using Sigma Stat version 2.03 software (Jandel Scientific, San Rafael, CA).

6 Ethyl Phosphonates Curcumin Mimics

Several studies demonstrated that many natural compounds could regulate ferroptosis and could be promising drugs for targeting ferroptosis-related pathologies. Among them, curcumin has stimulated cell death by ferroptosis via accumulating iron ions in breast cancer cells and sabotaging GPX4 activity in glioblastoma cells.[8,9] On the contrary, curcumin triggered the antioxidant defense mechanism against induced ferroptosis in renal tubular cells and thus decreased lipid peroxidation.[10] This controversiality requires more studies that underline the biochemical and/or cellular conditions that regulate these compounds' mode of action.

6.1 Aim of Research Work

In order to expand the library of curcumin mimics, new tyrosol-based ethyl phosphonates were synthesized. The new mimics retain the phenolic moieties based on TYR HVA and HDT alcohols discussed before in addition to the 5-methoxy tryptophol (MEL). The linker was replaced with an uncharged ethyl phosphonate with a length of seven atoms.

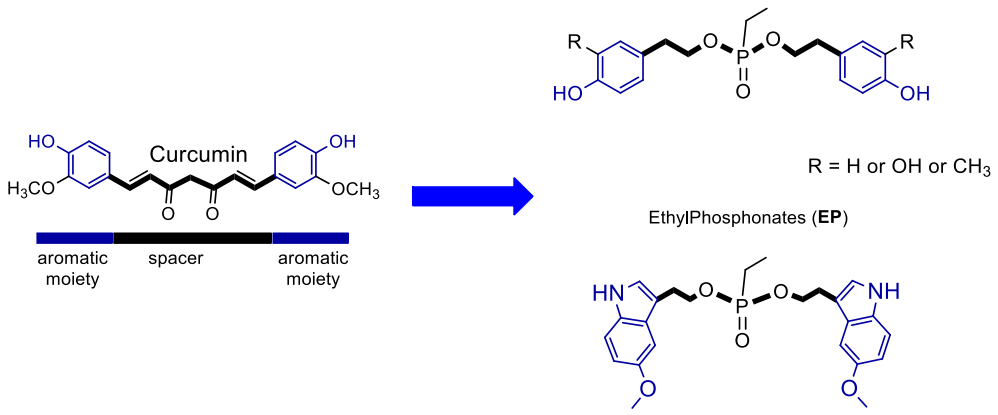

Scheme 6.1 Ethyl Phosphonate: new curcumin mimics

The antioxidant activity of the new mimics was estimated using DPPH and ORAC assays and their ability to inhibit or induce different cell death ferroptosis and apoptosis was evaluated.

6.2 Results and Discussion

The selected tyrosols are identified as TYR (**1**), HDT (**2**), HVA (**3**), which differ for the substituent on the aromatic ring, and MEL (**4**), which possess an indole ring (Scheme 6.2).

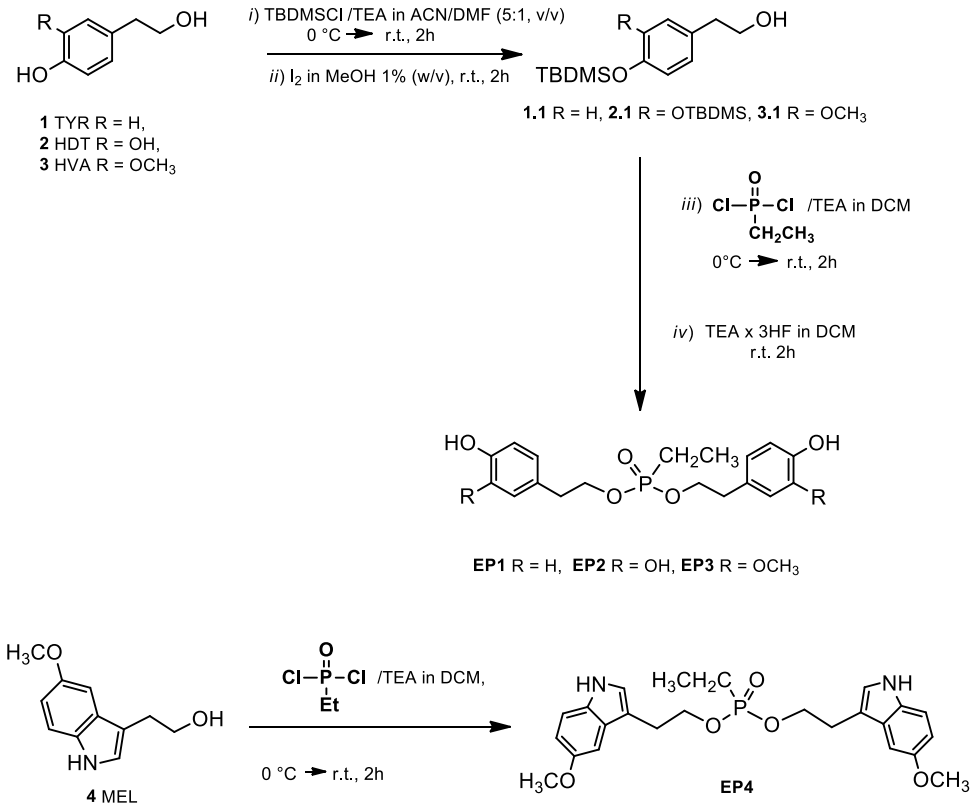

Scheme 6.2 Synthesis of Ethyl Phosphonates (**EP**).

The TBDMS group was chosen to protect the phenolic functionalities due to the easy installation procedure and the mild regioselective removal conditions with I_2 in

MeOH to obtain the building blocks, with free primary hydroxyl function, in excellent yields (82-86%). **4** was used without protections. These scaffolds were reacted with a bidentate phosphorylating agent, and after the treatment with the complex TEA·3HF in THF, to remove TBDMS groups, the new mimics were obtained with about 34-75% overall yields (Scheme 6.2). All new compounds were purified by RP-HPLC and full characterized by ^{1}H, ^{13}C and ^{31}P NMR.

6.2.1 Antioxidant Activity

To evaluate the antioxidant activity of new mimics DPPH and ORAC assays were performed. The antioxidant activities are presented in Table 6.1 together with the four starting compounds, TYR, HVA, HDT and MEL (**1**, **2**, **3** and **4**), and curcumin as reference.

All the new mimics (**EP1**-**EP4**) showed a greater antioxidant activity than the starting products. For both experiments, the compound **EP2** emerges, resulting in a clear increase in antioxidant power compared to curcumin. Once again, the role of the catechol moiety is crucialappearing to be essential for a strong antioxidant activity.

Table 6.1 Yields and antioxidant activity (ORAC and DPPH) for **EP1**-**EP4**

Compound	Yield (%)	ORAC (TE)	DPPH (EC_{50}, μM)
Curcumin	–	5.03 ± 0.14	13.5 ± 0.50
TYR	–	2.18 ± 0.12	>1000
HVA	–	2.90 ± 0.21	31.0 ± 2.6
HDT	–	7.40 ± 0.17	12.3 ± 1.0
EP1	60	5.12 ± 0.56	>1000
EP2	75	8.84 ± 0.45	6.00 ± 0.43
EP3	48	4.14 ± 0.29	17.22 ± 0.08
EP4	34	7.24 ± 0.46	>1000

6.2.2 Investigation of Antitumor Activity on different human cancer cells

6.2.2.1 Cell viability on MDA-MB-231 breast cancer cells

Curcumin and the curcumin mimics were evaluated for their cytotoxic properties in human triple negative MDA-MB-231 breast cancer cells.

Interestingly, only curcumin and **EP4** suppressed metabolic activity (measured by MTT assay), in metastatic triple-negative MDA-MB-231 breast cancer cells with a mesenchymal-like phenotype (Figure 6.1).

The high activity of **EP4** (EC_{50} value of 4 μM in both cell lines) exceeds the potency of curcumin, which had EC_{50} values of 20 μM in MDA-MB-231. The other mimics investigated did not show any cytotoxic effects.

To determine the specific cell death pathway responsible for the observed cytotoxicity of **EP4**, curcumin and **EP4** were tested in combination with inhibitors of ferroptosis (Fer-1) and apoptosis (Q-VD). Consistent with the literature, the results showed that curcumin-induced cell death was partially attenuated by both Fer-1 and Q-VD, suggesting a mixed type of cell death (Figure 6.2). Meanwhile, the cytotoxic effects of **EP4** were mitigated by Q-VD and remained unaffected by Fer-1 (Figure 6.2). This suggests that **EP4**-induced cell death occurs primarily by apoptosis and is not mediated by ferroptosis.

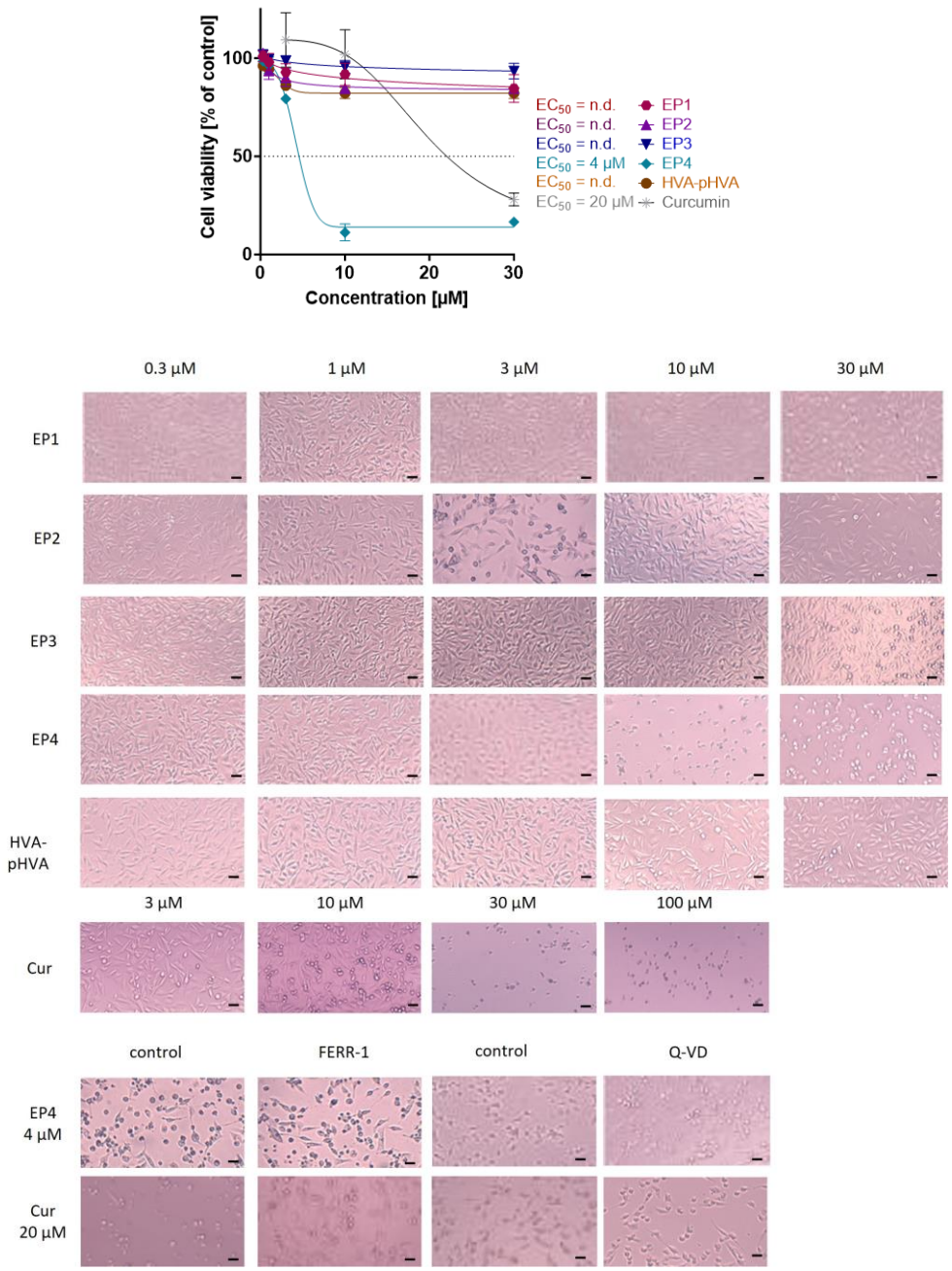

Figure 6.1 Cytotoxic effects of curcumin and curcumin mimics in human MDA-MB-231 breast cancer cells.

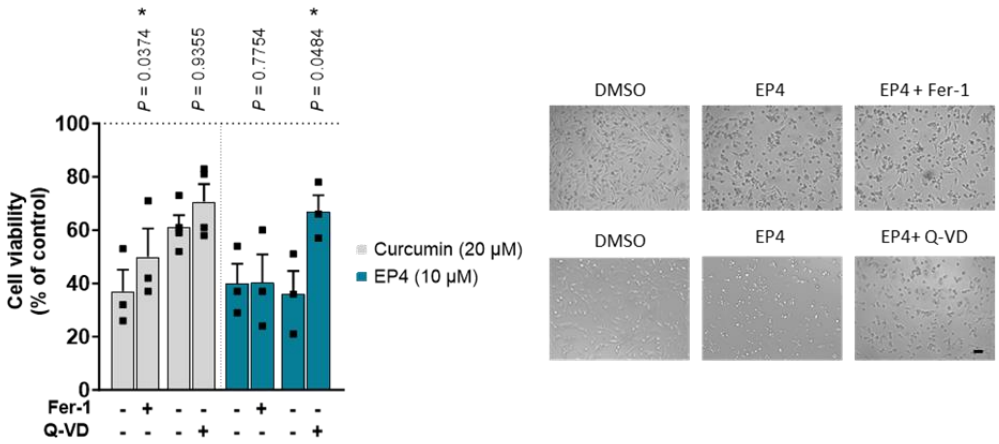

Figure 6.2 Curcumin induces both ferroptosis and apoptosis, whereas **EP4** only induces apoptosis.

6.2.2.2 Antiproliferative Effect on different human tumor cell lines

The antiproliferative effect of Ethyl Phosphonates (**EP**) were screened on different human tumor cell lines of unrelated histological origin. As healthy cell model human dermal fibroblasts (HDF) were chosen to determine the selectivity of action of the tested compounds towards cancer cells. The preliminary screening, performed by treating cells with 10 and 50 µM concentrations for 48 h, demonstrated that, all compounds have a relevant cytotoxic activity on the analysed cell lines except for **EP3** resulting inactive. The most potent effect is valuable on A375 cell line (Figure 6.3).

According to the data found on MDA-MB-231, **EP4** results the more selective compound. For this reason, it was considered for further deeply analyses dose–response curves were obtained and the corresponding IC_{50} values were calculated on all the cell lines tested. **EP4** showed a good activity with IC_{50} value in the range of 15- 35 µM and excellent selectivity with IC_{50} of 175 µM on HDF cells (Figure 6.4).

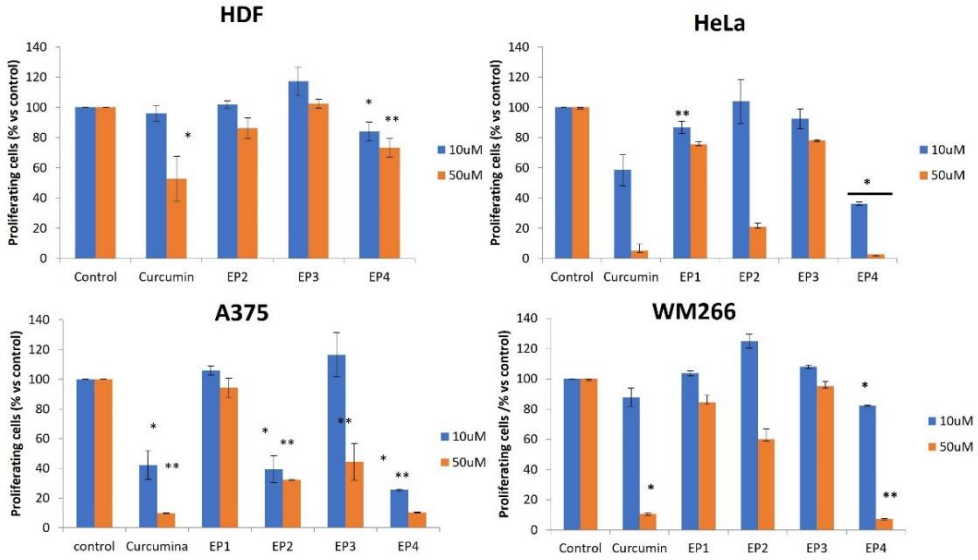

Figure 6.3 Effect of compounds on tumor and healthy cell proliferation. The cells were incubated in the presence of the compounds at 10 µM or 50 µM for 48 h at 37 °C. The proliferation was determined by MTT assay. The results are presented as the percentage of proliferating cells with respect to the control (vehicle-treated cells) and are expressed as means ± DS, * $p < 0.05$. **$p < 0.01$.

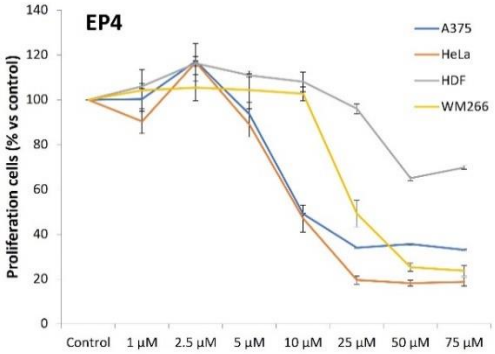

Cell lines	IC_{50} (µM) EP4	SD
A375	22	± 2.3
WM266	34	± 3.7
HeLa	14	± 5.7
HDF	175	± 80

Figure 6.4 Dose–response curves obtained using the indicated concentrations of **EP4** on different cell lines. The results are presented as the percentage of proliferating cells compared to the control (vehicle-treated cells) and are expressed as means ± SD of two independent experiments performed in triplicate, IC_{50} (µM) values (± SD) obtained after 48 h of incubation.

6.2.3 Investigation of EP4 on the Metastatic cell migration

Furthermore, it was also studied the ability of the most active compound **EP4** in inhibition of metastatic cell migration. Therefore, WM266 monolayers were scratched linearly and incubated with **EP4** at a concentration corresponding to half of its IC_{50} values. This choice was dictated by the need to avoid a high mortality of the cells assayed at 48 h, the end point of this assay. The concentrations chosen were 15 μM. The results obtained show that in the presence of compound, the wound healing was strongly delayed compared to the control (Figure 6.5), demonstrating that **EP4** is the effective substance on the inhibition of WM266 migration.

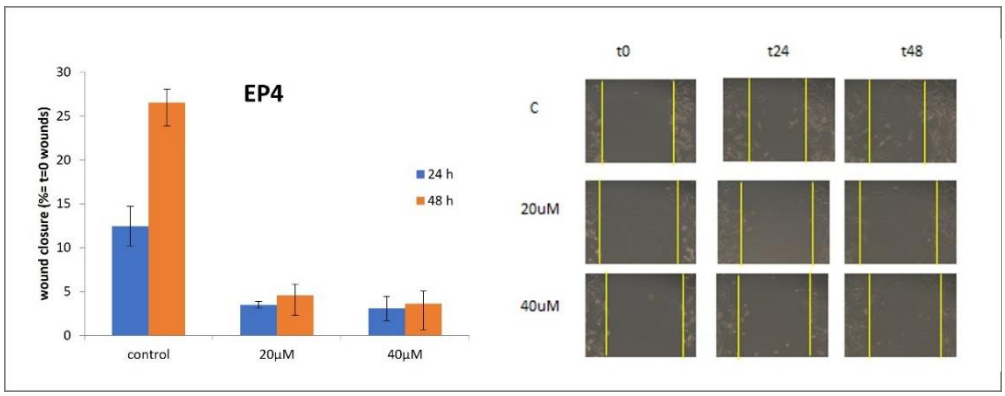

Figure 6.5 Cell wound healing assay. Effect of **EP4** on wound healing activity. WM266 cells were scratched and treated with **EP4** at the indicated concentrations. Each scratch area on the monolayer was photographed at 0, 24 and 48 h. Bars depict mean ± SE of three independent experiments.

6.2.4 Inhibition of RSL3-induced ferroptotic cell death

To assess the potential cytoprotective properties of curcumin derivatives against ferroptosis, all compounds were tested at concentrations of 3 and 30 µM, either alone or in combination with the glutathione peroxidase 4 (GPX4) inhibitor such as RSL3 (Figure 6.6). Of the mimics tested, **EP2** showed the most potent protective effects against RSL3-induced ferroptosis. It significantly inhibited ferroptotic cell death at a concentration of 3 µM and completely prevented ferroptosis at 30 µM. The curcumin derivatives **EP1** and **EP3** also showed small but significant protective effects at 30 µM, leading to an increase in cell viability of about 20%. Conversely, the two cytotoxic compounds, curcumin and **EP4**, did not exhibit cytoprotective effects at either 3 or 30 µM.

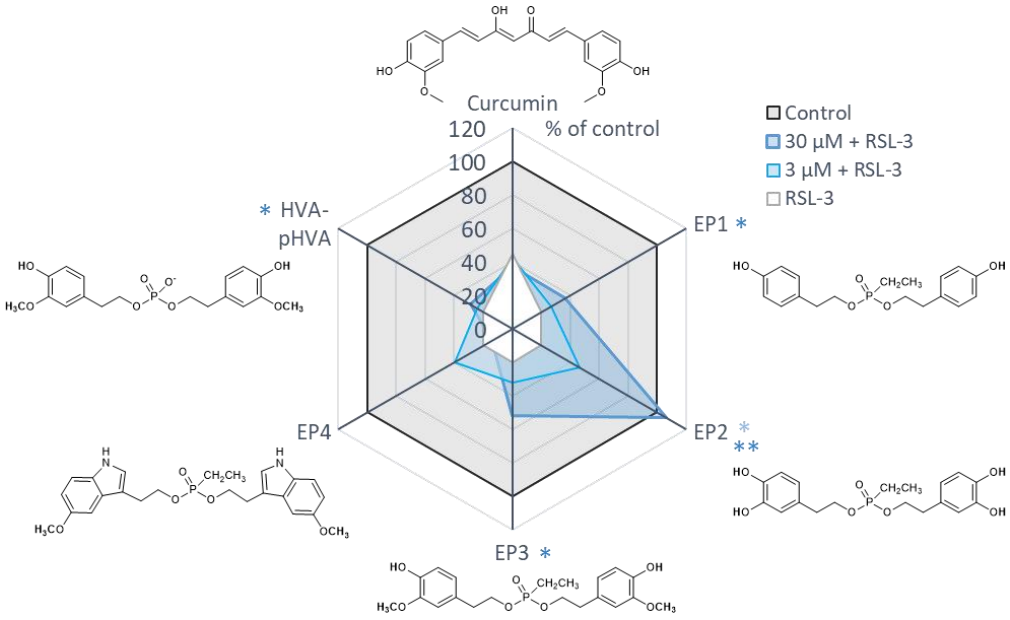

Figure 6.6 Protective effects of curcumin mimics against RSL3-induced ferroptosis.

6.3 Conclusions

This study reported the synthesis and an extensive biological investigation of new curcumin mimics named ethyl phosphonates (**EP1-EP4**). The synthetic approach was highly efficient employing orthogonal protection of hydroxyl groups.

In the light of reported apoptotic and ferroptotic activity of curcumin, we have explored both anticancer activities of new **EP** mimics. The mimics **EP2** and **EP4** resulted to be very interesting in different manners. **EP2** displayed strong antioxidant activity (DPPH assay) and potent inhibitory activity of ferroptosis as non-apoptotic cellular death.[11] Differently, **EP4** showed a very potent anticancer activity against different human cancer cell lines (HeLa, A375, WM266, MDA-MB-231) and no cytotoxicity on normal cells (HDF). Mechanistic investigation suggested that **EP4**-induced cell death occurs primarily by apoptosis.

In conclusion, **EP4** is the most effective against different type of cancers and **EP2** represents a potential candidate for neurodegenerative disorders.

6.4 Experimental Session

6.4.1 General Methods

All chemicals were purchased from Sigma–Aldrich (Milano, Italy). HPLC–grade ACN and MeOH were purchased from Carlo Erba Reagents and Sigma-Aldrich, respectively. Reactions were monitored by TLC (F254 precoated silica gel plates, Merck) and column chromatography (Merck Kieselgel 60, 70–230 mesh, Milano, Italy). HPLC analysis was performed with a Shimadzu LC–8A PLC system (Shimadzu Analytical and Measuring Instruments, Milano, Italy) equipped with a Shimadzu SCL–10A VP System control and a Shimadzu SPD–10A VP UV–Vis detector. Mass spectrometric analyses were performed on AB SCIEX TOF/TOF 5800 in positive or negative mode and Waters Micromass ZQ Instrument (Waters, Milano,

Italy) equipped with an electrospray source in positive mode. The NMR spectra were recorded at 25 °C on an NMR spectrometer Bruker DRX, Bruker Advance (Bruker Italia Srl, Milano, Italy) and INOVA-500 NMR instrument (Varian, Milan, Italy).

6.4.2 General Procedure for the Synthesis of EP1-EP4

For the synthesis of building blocks (**1.1**-**3.1**) see paragraph 4.4.2

1 mmol of compound **1.1** (**2.1**, **3.1** or **4**) was dissolved in 1.5 mL of DCM dry in presence of 2 mmol of TEA at 0 °C. Subsequentially 0.5 mmol of ethyl dichlorophosphate was added and the reaction was stirred at room temperature for 2 h, monitoring by TLC (hexane/EtOAc 60:40, v/v). The reaction was quenched with H_2O and extracted using H_2O/DCM. The combined organic phases were dried over anhydrous Na_2SO_4 and evaporated under reduced pressure. and then coarse purified by column chromatography eluted with EtOAc/hexane 80:20 (v/v).

0.24 mmol of protected compounds were then dissolved in 1 mL of THF and reacted with the complex TEA·3HF (2.5 equiv. for each TBDMS group) at room temperature for 2 h. The reaction was dried under reduced pressure and purified by column chromatography eluted with DCM/MeOH 95:5 (v/v) obtaining the final compounds **EP1-EP4** with yields 34 - 75%.

All compounds **EP1**-**EP4** were purified by RP-HPLC using a Phenomenex Gemini RP18 column (10-µm particle size, 21.20 mm × 250 mm i.d.) with a linear gradient of ACN in H_2O, from 20% to 100% over 30 minutes at a flow rate of 7 mL/min with detection at 280 and 260 nm. The identity of compounds **EP1**-**EP4**, with a final purity >95%, were confirmed by 1D and 2D NMR and MALDI-TOF analyses.

EP1 ^{1}H NMR (400 MHz, CD_3OD, 25 °C, δ ppm, *J* Hz): δ = 7.04 (4H, d, *J* = 8.36, H-3, H-3', H-5, H-5'); 6.73 (4H, d, *J* = 8.34, H-2, H-2'; H-6, H-6'); 4.06 (4H, m, H-8, H-8'); 2.82 (4H, t, *J* = 6.62, H-7, H-7'); 1.64 (2H, m, P($\underline{CH_2}CH_3$)); 1.01 (3H, m, P($CH_2\underline{CH_3}$)) ppm. ^{13}C NMR (100 MHz, CD_3OD, 25 °C, δ ppm): δ = 155.8; 129.7 (x2); 128.1; 114.9 (x2); 66.5 (d, J_{C-P} = 7.47 Hz); 35.6 (d, J_{C-P}= 6.27 Hz); 17.4 (d, J_{C-P} = 143.9 Hz); 5.10 (d, J_{C-P} = 6.64 Hz) ppm. ^{31}P NMR (161.98 MHz, CD_3OD, 25 °C, δ ppm): δ = 33.8 ppm. MALDI-MS (positive ions): m/z calculated for $C_{18}H_{23}O_5P$= 350.13; found: 351. 23 $[M+H]^+$, 373.24 $[M+Na]^+$, 389.21 $[M+K]^+$.

EP2 ^{1}H NMR (400 MHz, CD_3OD, 25 °C, δ ppm, *J* Hz): δ = 6.70 (2H, d, *J* = 7.95, H-5, H-5'); 6.67 (2H, d, *J* = 1.81, H-2, H-2'); 6.54 (2H, dd, *J* = 7.98, 1.60, H-6, H-6'); 4.06 (4H, m, H-8, H-8'); 2.77 (4H, t, *J* = 6.47, H-7, H-7'); 1.64 (2H, m, P($\underline{CH_2}CH_3$)); 1.02 (3H, m, P($CH_2\underline{CH_3}$)) ppm. ^{13}C NMR (100 MHz, CD_3OD, 25 °C, δ ppm): δ = 144.8; 143.6; 128.9; 120.0; 115.8; 115.0; 66.5 (d, J_{C-P} = 6.71 Hz); 35.9 (d, J_{C-P} = 6.59 Hz); 17.4 (d, J_{C-P} = 142.4 Hz); 5.1 (d, J_{C-P} = 6.50 Hz) ppm. ^{31}P NMR (161.98 MHz, CD_3OD, 25 °C, δ ppm): δ = 34.7 ppm. MALDI-MS (negative ions): m/z calculated for $C_{18}H_{23}O_7P$ = 382.12; found: 381. 13 $[M-H]^-$.

EP3 ^{1}H NMR (500 MHz, CD_3OD, 25 °C, δ ppm, *J* Hz): δ = 6.81 (2H, s, H-2, H-2'); 6.74 (2H, d, *J* = 8.23, H-5, H-5'); 6.65 (2H, d, *J* = 8.23, H-6, H-6'); 4.09 (4H, m, H-8, H-8'); 3.83 (6H, s, -OCH_3); 2.83 (4H, t, *J*= 6.85, H-7, H-7'); 1.65 (2H, m, P($\underline{CH_2}CH_3$)); 1.02 (3H, m, P($CH_2\underline{CH_3}$)) ppm. ^{13}C NMR (100 MHz, CD_3OD, 25 °C, δ ppm): δ = 147.5; 144.9; 128.9; 121.2; 114.8; 112.3; 66.5 (d, J_{C-P} = 7.12 Hz); 55.0; 36.0 (d, J_{C-P} = 6.41 Hz); 17.4 (d, J_{C-P} = 142.6 Hz); 5.1 (d, J_{C-P} = 6.27 Hz) ppm. ^{31}P NMR (161.98 MHz, CD_3OD, 25 °C, δ ppm): δ = 34.3 ppm. MALDI-MS (positive ions): m/z calculated for $C_{20}H_{27}O_7P$= 410.15; found: 433.28 $[M+Na]^+$, 449.25 $[M+K]^+$.

EP4 ^{1}H NMR (500 MHz, DMSO-d6, 25 °C, δ ppm, *J* Hz): δ = 10.7 (2H, s, NH); 7.23 (2H, d, *J* = 8.88, H-7, H-7'); 7.14 (2H, s, H-2, H-2'); 7.02 (2H, d, *J* = 1.63, H-4, H-4'); 6.72 (2H, dd, *J* = 8.76, 2.09, H-6, H-6'); 4.13 (4H, m, H-9, H-9'); 3.74 (6H, s, -

OCH_3); 2.99 (4H, t, J = 6.77, H-8, H-8'); 1.67 (2H, m, P($\underline{CH_2}CH_3$)); 0.96 (3H, m, P($CH_2\underline{CH_3}$)) ppm. ^{13}C NMR (100 MHz, CD_3OD, 25 °C, δ ppm): δ = 153.5; 131.2; 127.9; 124.3; 112.5; 111.6; 110.0; 100.5; 65.4 (d, J_{C-P}= 6.71 Hz); 55.8; 26.9 (d, J_{C-P} = 5.52 Hz); 18.2 (d, J_{C-P} = 142.0 Hz); 6.8 (d, J_{C-P} = 7.23 Hz) ppm. ^{31}P NMR (161.98 MHz, CD_3OD, 25 °C, δ ppm): δ = 33.4 ppm. MALDI-MS (negative ions): m/z calculated for $C_{24}H_{29}N_2O_5P$= 456.18; found: 455. 17 $[M-H]^-$.

6.4.3 DPPH assay

The DPPH solution (200 µM) was prepared in methanol and placed in the dark for 30 min before the analyses. The compounds were dissolved in MeOH to prepare the stock solutions 100 µM. DPPH solution was placed in cuvette (final concentration 50 µM), and the solutions of each compound (final concentration range 1 – 75 µM) were rapidly added and mixed into every test tube to reach a final volume of 500 µL. The reaction was followed by a spectrophotometric analysis continuously measuring the absorbance at λ = 517 nm for 30 min.

The percentage of inhibition (% inhibition) was calculated following the equation:

$$\%\ inhibition = \frac{A_{control} - A_{sample}}{A_{control}}\ x\ 100$$

The EC_{50} value (the inhibition concentration of a sample at 50% fall in absorbance of DPPH) was used to compare the DPPH scavenging activities.

6.4.4 ORAC assay

150 µL of the fluorescein solution (11.12 x 10^{-2} µM in phosphate buffer 0.75 mM, pH 7.4) was added into each well of a 96-well plate. Subsequently, 23 µL of buffer and 2 µL of stock solutions in DMSO of tested compounds were added to the wells to reach the final concentration range 1.25–20 µM. The plate was incubated for 30 min

at 37 °C and then 25 µL of AAPH (152.6 mM) was added to each well. Immediately, the fluorescence was recorded by a microplate reader for 2 h in 1 min steps at 37 °C (λ_{ecc} = 485 nm, λ_{em} = 528 nm).

6.4.5 Biological assays on human cancer cells

6.4.5.1 MDA-MB-231 cell line

Human triple negative MDA-MB-231 breast cancer cells and were obtained from the American Type Culture Collection (ATCC, Manassas, VA). MDA-MB-231 cells (2×10^4 cells/cm^2) were cultured in DMEM (glucose 4.5 g/L, Thermo Fisher Scientific, Waltham, MA) supplemented with 10% heat-inactivated fetal calf serum (Merck) and 1% penicillin-streptomycin solution (Thermo Fisher Scientific) at 37°C in a 5% CO_2 atmosphere. Cells were routinely tested for mycoplasma contamination using the MycoAlert™ PLUS Mycoplasma Detection Kit from Lonza (Basel, Switzerland). In addition, their morphology was examined regularly. MDA-MB-231 cells were seeded in triplicate in 96-well plates at a density of 20,000 cells per well in 100 µL of medium and allowed to attach for 24 h. Compounds were added with a final DMSO concentration of 0.5% and cells were incubated for a further 48 h. The pan-kinase inhibitor staurosporine (1 µM, Merck) was used as a reference compound. To identify the cell death programme, the apoptosis inhibitor Q-VD-Oph (50 µM, Merck) and the ferroptosis inhibitor ferrostatin-1 (10 µM, Cayman Chemicals, Ann Arbor, MI) were added to the medium 2 h before treatment with the cytotoxic compounds. For the MTT assay, 20 µl of 3-(4,5-dimethylthiazol-2-yl)-2,5-diphenyltetrazolium bromide (MTT, 5 mg/ml in PBS pH 7.4, sterile filtered, Merck) solution was added to each well and the cells were incubated for 1.5 h. The final vehicle (DMSO) concentration was adjusted to 0.5%. Then, 100 µl SDS solution (10% in 20 mM HCl, pH 4.5) was added and the plates were shaken at 130 rpm in the dark for 18-20 h. Absorbance was measured at 570 nm using a SpectraMax iD3 plate reader (Molecular Devices).

Absorbance values from ethanol-treated cells were used for background substraction, and cell viability was expressed as percentage relative to the DMSO control.An asymmetric sigmoidal (5 PL) curve fit was performed using GraphPad Prism 9. Microscopic images were captured just prior to the addition of MTT using a Motic AE31E microscope equipped with a Motic 10+ camera and Motic Image Plus 3.0 ML software with a 10x objective (Motic, Barcelona, Spain).

6.4.5.2 HeLa, A375, WM266 and HDF cell lines

Human adenocarcinoma (HeLa), Human melanoma (A375) and human normal dermal fibroblasts (HDF) were grown in DMEM with 10% fetal bovine serum (FBS), 1% glutamine, 100 U/mL penicillin, and 100 µg/mL streptomycin (Euroclone, Italy). Human metastatic melanoma cell line (WM266) was grown in RPMI with 10% fetal bovine serum (FBS), 1% glutamine, 100 U/mL penicillin, and 100 µg/mL streptomycin. The cells were maintained in humidified air containing 5% CO2 at 37 °C. Cell Proliferation Assay. HeLa, A375, WM266 and HDF cells were seeded at a density of 1.2*103 cells/100µL, WM266 and HDF at density of 2* 103 cells/100µL, on 96-well plates. Each molecule (10 or 50 µM) or DMSO as vehicle, were added to the cells. After 48 h incubation at 37 °C, cell viability was assessed by performing the 3-(4,5-dimethylthiazol-2-yl)-2,5- diphenyltetrazolium bromide (MTT, Sigma Aldrich, Italy) reduction inhibition assay. Cytotoxicity experiments were independently performed at least three times. Statistical significance was obtained by Student's t-test paired, two-sided. Data are expressed as means standard error (S.E.). P values<0.05 were statistically significant. All the experiments were performed at least in triplicate and repeated at least 3 times. The IC50 values were obtained by the Prism 6.01 software (GraphPad San Diego, CA, U.S.) by extrapolating them from the dose–response curves data.

6.4.6 Wound Healing assay

In vitro cell migration has been evaluated using the wound healing scratch assay. 6 x 10^5 WM266 cells were plated and grown to the confluence. Successively, the cells were linearly scratched with a pipette tip to generate the wound. Once the detached cells were removed, the molecule at indicated concentrations was added and the cells were incubated at 37 °C. After the scratch area was photographed at 0, 24, and 48 h^{12} using a phase optical microscope at 10X magnification (Zeiss) and the distance between the edges of the incisions was measured. Its mean value was determined as follows: wound closure (%) = 1x (wound width tx/wound width t0) X100. Bars depict mean ± SE of three independent experiments.

6.4.7 Inhibition of RSL3-induced ferroptotic cell death

The anti-ferroptotic properties of the compounds were evaluated in MDA-MB-231 cells. Cells were seeded in 96-well plates at a density of 20,000 cells per well in 100 µL medium. After incubation for . Cells were treated with vehicle (0.5% DMSO) or the compounds at 3 µM and 30 µM alone or in combination with RSL3 (0.3 µM, Cayman Chemicals).

Bibliogaphy

(1) Hatcher, H.; Planalp, R.; Cho, J.; Torti, F. M.; Torti, S. V. Curcumin: From Ancient Medicine to Current Clinical Trials. *Cellular and Molecular Life Sciences* **2008**, *65* (11), 1631–1652. https://doi.org/10.1007/s00018-008-7452-4.

(2) Shehzad, A.; Rehman, G.; Lee, Y. S. Curcumin in Inflammatory Diseases. *BioFactors* **2013**, *39* (1), 69–77. https://doi.org/10.1002/biof.1066.

(3) Sardjiman, S. S.; Reksohadiprodjo, M. S.; Hakim, L.; van der Goot, H.; Timmerman, H. 1,5-Diphenyl-1,4-Pentadiene-3-Ones and Cyclic Analogues as Antioxidative Agents. Synthesis and Structure-Activity Relationship. *European Journal of Medicinal Chemistry* **1997**, *32* (7–8), 625–630. https://doi.org/10.1016/S0223-5234(97)83288-6.

(4) Zhao, S.; Pi, C.; Ye, Y.; Zhao, L.; Wei, Y. Recent Advances of Analogues of Curcumin for Treatment of Cancer. *European Journal of Medicinal Chemistry* **2019**, *180* (319), 524–535. https://doi.org/10.1016/j.ejmech.2019.07.034.

(5) Tassano, E.; Alama, A.; Basso, A.; Dondo, G.; Galatini, A.; Riva, R.; Banfi, L. Conjugation of Hydroxytyrosol with Other Natural Phenolic Fragments: From Waste to Antioxidants and Antitumour Compounds. *European Journal of Organic Chemistry* **2015**, *2015* (30), 6710–6726. https://doi.org/10.1002/ejoc.201500931.

(6) Bernini, R.; Carastro, I.; Santoni, F.; Clemente, M. Synthesis of Lipophilic Esters of Tyrosol, Homovanillyl Alcohol and Hydroxytyrosol. *Antioxidants* **2019**, *8* (6), 174. https://doi.org/10.3390/antiox8060174.

(7) Kumar, S.; Raina, K.; Agarwal, C.; Agarwal, R. Silibinin Strongly Inhibits the Growth Kinetics of Colon Cancer Stem Cell-Enriched Spheroids by Modulating Interleukin 4/6-Mediated Survival Signals. *Oncotarget* **2014**, *5* (13), 4972–4989. https://doi.org/10.18632/oncotarget.2068.

(8) Chen, T.-C.; Chuang, J.-Y.; Ko, C.-Y.; Kao, T.-J.; Yang, P.-Y.; Yu, C.-H.; Liu, M.-S.; Hu, S.-L.; Tsai, Y.-T.; Chan, H.; Chang, W.-C.; Hsu, T.-I. AR Ubiquitination Induced by the Curcumin Analog Suppresses Growth of Temozolomide-Resistant Glioblastoma through Disrupting GPX4-Mediated Redox Homeostasis. *Redox Biology* **2020**, *30* (December 2019), 101413. https://doi.org/10.1016/j.redox.2019.101413.

(9) Li, R.; Zhang, J.; Zhou, Y.; Gao, Q.; Wang, R.; Fu, Y.; Zheng, L.; Yu, H. Transcriptome Investigation and In Vitro Verification of Curcumin-Induced HO-1 as a Feature of Ferroptosis in Breast Cancer Cells. *Oxidative Medicine and Cellular Longevity* **2020**, *2020*, 1–18. https://doi.org/10.1155/2020/3469840.

(10) de Souza Farias, S. A.; da Costa, K. S.; Martins, J. B. L. Analysis of Conformational, Structural, Magnetic, and Electronic Properties Related to

Antioxidant Activity: Revisiting Flavan, Anthocyanidin, Flavanone, Flavonol, Isoflavone, Flavone, and Flavan-3-Ol. *ACS Omega* **2021**, *6* (13), 8908–8918. https://doi.org/10.1021/acsomega.0c06156.

(11) Mehta, J.; Rayalam, S.; Wang, X. Cytoprotective Effects of Natural Compounds against Oxidative Stress. *Antioxidants* **2018**, *7* (10), 147. https://doi.org/10.3390/antiox7100147.

(12) Di Gaetano, S.; Pirone, L.; Galdadas, I.; Traboni, S.; Iadonisi, A.; Pedone, E.; Saviano, M.; Gervasio, F. L.; Capasso, D. Design, Synthesis, and Anticancer Activity of a Selenium-Containing Galectin-3 and Galectin-9N Inhibitor. *International Journal of Molecular Sciences* **2022**, *23* (5), 2581. https://doi.org/10.3390/ijms23052581.

Appendix: PhD Course Activity Summary

1 Publications (include submitted):

- Romanucci, V.; Giordano, M.; Pagano, R.; Agarwal, C.; Agarwal, R.; Zarrelli, A; Di Fabio, G. Solid-phase synthesis of curcumin mimics and their anticancer activity against human pancreatic, prostate, and colorectal cancer cell lines. *Bioorganic & Medicinal Chemistry* **2021**, *42* (March), 116249. https://doi.org/10.1016/j.bmc.2021.116249.

- Romanucci, V.; Giordano, M.; Pagano, R.; Zimbone, S.; Giuffrida, M.L.; Milardi, D.; Zarrelli, A; Di Fabio, G. Investigation on the solid-phase synthesis of silybin prodrugs and their timed-release. *Bioorganic & Medicinal Chemistry* **2021**, *50* (October), 116478. https://doi.org/10.1016/j.bmc.2021.116478.

- Romanucci, V.; Pagano, R.; Lembo, A.; Capasso, D.; Di Gaetano, S.; Zarrelli, A; Di Fabio, G. Phosphodiester Silybin Dimers Powerful Radical Scavengers: A Antiproliferative Activity on Different Cancer Cell Lines. *Molecules* **2022**, *27* (5), 1702. https://doi.org/10.3390/molecules27051702.

- Romanucci V.*, Pagano R.*, Kandhari K., Zarrelli A., Petrone M., Agarwal C., Agarwal R, Di Fabio G., "Synthesis of 7-O-Tyrosyl Silybin Derivatives as Novel Set of Potent Anti-Prostate Cancer Compounds", **2024**, submitted to *European Journal of Medicinal Chemistry.* (*These authors contributed equally to this work)

- Fortunato M. E., Pagano R., Romanucci V., Licenziato C., Zarrelli A., Di Serio M., Di Fabio G., Russo V. "Novel insights into acetylation kinetics in continuous flow milli-reactor for chemo-enzymatic separation of Silybin A/B", **2024**, submitted to *Chemical Engineering Journal*.

2 Attended Courses:

- Natural phenolic compounds: structure, reactivity and applications, Prof. Lucia Panzella
- Smart Drug Delivery Systems, Prof. Annalisa Guaragna
- Advanced Mass Spectrometry, Prof. Angela Amoresano
- Introduction to Data Analysis, Prof. Raffaele Velotta
- Synthetic Glycochemistry, Prof. Emiliano Bedini and Prof Alfonso Iadonisi
- Protein Engineering, Prof. Angela Duilio

3 Attended Seminars:

- Il mondo del lavoro oggi, 17/05/2021, Dott. Lorenza Moscarella
- I 5 errori del CV, 24/05/2021, Dott. Lorenza Moscarella
- Functional and Pathological Interactions of α-synuclein, 21/06/2021, Dott. Giuliana Fusco
- Il chimico: un'esperienza nell'industria, 10/01/2022, Dr. Vito Savino
- R&D in a big company, 21/01/2022, Dr. Andrea Di Matteo
- Protezioni dei contenitori metallici destinati ad uso alimentare, 14/04/2022, Dr. Biagio Leone
- A through the looking glass view of voltage-gated ion channel structure, 02/09/2022, Prof. Daniel Minor
- Academic publishing workshop: what to consider when publishing your research, 17/10/2022, Prof. Cristina De Castro and Dr. Inez van Korlaar.

- On discovery and sensitivity in (photo)catalysis, 05/09/2023, Prof. Frank Glorius
- Introduction to Small Angle X-ray Scattering, 20/09/2023, Dott. Andreas Keilbach

4 Attended congresses/schools/ communication:

- IV International Summer School of Natural Products, 06-08 July 2021.
  Oral communication: Combinatorial solid phase synthesis of new curcumin mimics: investigation of neuroprotective and anticancer activity
- XXVII Congresso Nazionale della Società Chimica Italiana, 14-23 September 2021.
  Oral communication: Phosphate-linked Silybin dimers: synthesis and investigation of biological activity.
- National Congress of the Division of Chemistry of Biological Systems, 20-22 June 2022.
  Oral communication: Silybin-tyrosol conjugates as promising Multitarget Ligands (MTLs) to contrast neurodegenerative diseases.
- International Symposium on Pathomechanisms of Amyloid Diseases" 25-27 August 2022.
  Poster communication: Silybin-Hydroxytyrosol Hybrids as MultiTarget Directed Ligands (MTDLs) to Contrast Alzheimer's Disease